ANALYSIS OF THE SEDIMENTARY AND GEOMORPHIC SIGNATURE OF RETREATING TIDEWATER GLACIERS IN WESTERN ANTARCTIC PENINSULA BAYS

A Dissertation Presented to

the Faculty of the Department of Earth and Atmospheric Sciences

University of Houston

In Partial Fulfillment

of the Requirements for the Degree

Doctor of Philosophy

in Geology

By

Yuribia Patricia Muñoz

May 2018

ANALYSIS OF THE SEDIMENTARY AND GEOMORPHIC SIGNATURE OF RETREATING TIDEWATER GLACIERS IN WESTERN ANTARCTIC PENINSULA BAYS

_____
Yuribia P. Muñoz

APPROVED:

_____
Dr. Julia S. Wellner
Chair of the Committee
Dept. Earth and Atmospheric Sciences
University of Houston

_____
Dr. Joel Saylor
Dept. Earth and Atmospheric Sciences
University of Houston

_____
Dr. Paul Mann
Dept. Earth and Atmospheric Sciences
University of Houston

_____
Dr. John B. Anderson
Dept. Earth, Environmental, and Planetary Sciences
Rice University

_____
Dean
College of Natural Sciences and Mathematics
University of Houston

ACKNOWLEDGEMENTS

My friends and lab mates with whom I have spent countless hours in the lab, in the field, and also having, much needed, fun away from my desk: Proma Bhattacharyya, Janet Kong, Delaney Robinson, Rachel Clark, Alicia Staszyc, Laurin Hardin Musso, Helena Manuel, and Reham Rafe. Jennifer Campo has been the most fun partner during fieldtrips and also a great help dealing with some stubborn software. Carolina Ramon-Dueñas has also been a dear partner in fieldtrips and in the lab, may we keep having ideas to publish!

Colleagues from other labs have also inspired me through their hard work and dedication: Dr. Rebecca Minzoni, Dr. Rodrigo Fernandez, Dr. Lauren Simkins, Lindsay Prothro, Ruthie Halberstadt, and Dr. Veronica Sanchez. I am definitely forgetting to include some people, but I really appreciate all the help throughout my years at UH.

And finally, my family that has supported me throughout the many years of school; mis queridas hermanas y por supuesto mi madre, porque gracias a ella todo esto ha sido posible.

ANALYSIS OF THE SEDIMENTARY AND GEOMORPHIC SIGNATURE OF RETREATING TIDEWATER GLACIERS IN WESTERN ANTARCTIC PENINSULA BAYS

An Abstract of a Dissertation

Presented to

the Faculty of the Department of Earth and Atmospheric Sciences

University of Houston

In Partial Fulfillment

of the Requirements for the Degree

Doctor of Philosophy

in Geology

By

Yuribia Patricia Muñoz

May 2018

ABSTRACT

The Antarctic Peninsula (AP) is the northernmost extent of the Antarctic continent. Due to the location of this small ice cap, it is being subjected to warming earlier than the Antarctic mainland and serves as a natural laboratory to study changes in glacial stability and the resulting sediment deposits. The AP is a rapidly changing area and assessing past responses to climate events in this region would enable us to predict more accurately future trends as climatic conditions fluctuate in the AP and in other areas in Antarctica.

Sediment analysis coupled with ^{210}Pb, ^{137}Cs, and radiocarbon dating, as well as multibeam swath bathymetry and shallow seismic (CHIRP) were used to study the modern surface sediment distribution in Flandres Bay, the geomorphic seafloor features in bays throughout the AP, and Holocene sediment cores from Flandres, Collins, and Beascochea bays.

In Flandres Bay, grain size coarsens from the inner to the outer bay. Discrete areas of the bay are affected differently by varying factors to distribute sediment; these factors include persistent fast sea ice, differential rates of primary productivity, and winnowing of fine grained sediments away from the bay.

The geomorphology found in the seafloor of western AP bays indicates that bay geometry exerts a control on the number and type of landform features found in the bays. We identified networks of channels carved in bedrock, likely produced by subglacial meltwater channels, which highlights the presence of subglacial meltwater production in the northern AP region, possibly through several glacial cycles.

Results from sediment core analysis from Collins Bay suggest deglaciation started before 9280 cal. yr B.P., while in Beascochea Bay deglaciation started much later, possibly around 5910 cal. yr B.P. A recent glacial advance was interpreted in the inner bay areas of Collins, Beascochea, and Flandres bays, roughly corresponding to the Little Ice Age. This conclusion is also supported by geomorphic features found in proximal bay areas which indicate a recent glacial advance. The modern glacial retreat is observed in most bays studied in the AP indicating a common forcing mechanism, likely the intrusion of warmer water melting the glacier fronts.

TABLE OF CONTENTS

LIST OF FIGURES

LIST OF TABLES

Chapter 1

INTRODUCTION

The Antarctic Peninsula (AP) is the northernmost extent of the Antarctic continent (Fig 1.1). The AP is a long (1200 km), thin (250 km) strip of land, with an average elevation of 500 m, but up to 2500 m. It is covered by an ice cap with varying thicknesses along the peninsula, up to 500 m in some areas. Due to the location of this small ice cap it is being subjected to warming before the Antarctic mainland and serves as a natural laboratory to study glacial stability, fluctuations in accumulation rates, and to measure the impact of global warming. Understanding the behavior and responses of the AP to climatic changes serves as an analogy to other rapidly changing systems in Antarctica, such as the West Antarctic Ice Sheet, and in the northern hemisphere.

The AP is heavily glaciated; the east side of the peninsula is characterized by the presence of ice shelves, and the western side of the peninsula by small glaciers that terminate in the ocean called "tidewater glaciers". These glaciers carry sediment varying in size (from clay to boulders) into the bays. These glacial systems are very sensitive to climatic changes and respond rapidly to fluctuations in the environment because they are thin compared to ice sheets, they have small drainage areas, and high accumulation rates (Anderson, 1999; Domack et al., 2005).

In the second chapter, we completed a detailed analysis of surface-sediment distribution in a bay in the western AP, Flandres Bay, in order to build a model of

modern day sediment-dispersal patterns coming from a retreating, tidewater glacier. The fjord is surrounded by numerous, small tidewater glaciers that drain the AP ice cap. Flandres Bay is protected from open sea conditions by Anvers Island and it is considered to have a dry subpolar climate, separating the warm, wet subpolar bays in the north from the dry, polar bays in the south. Cook et al. (2005) showed all the glaciers terminating in this fjord are retreating.
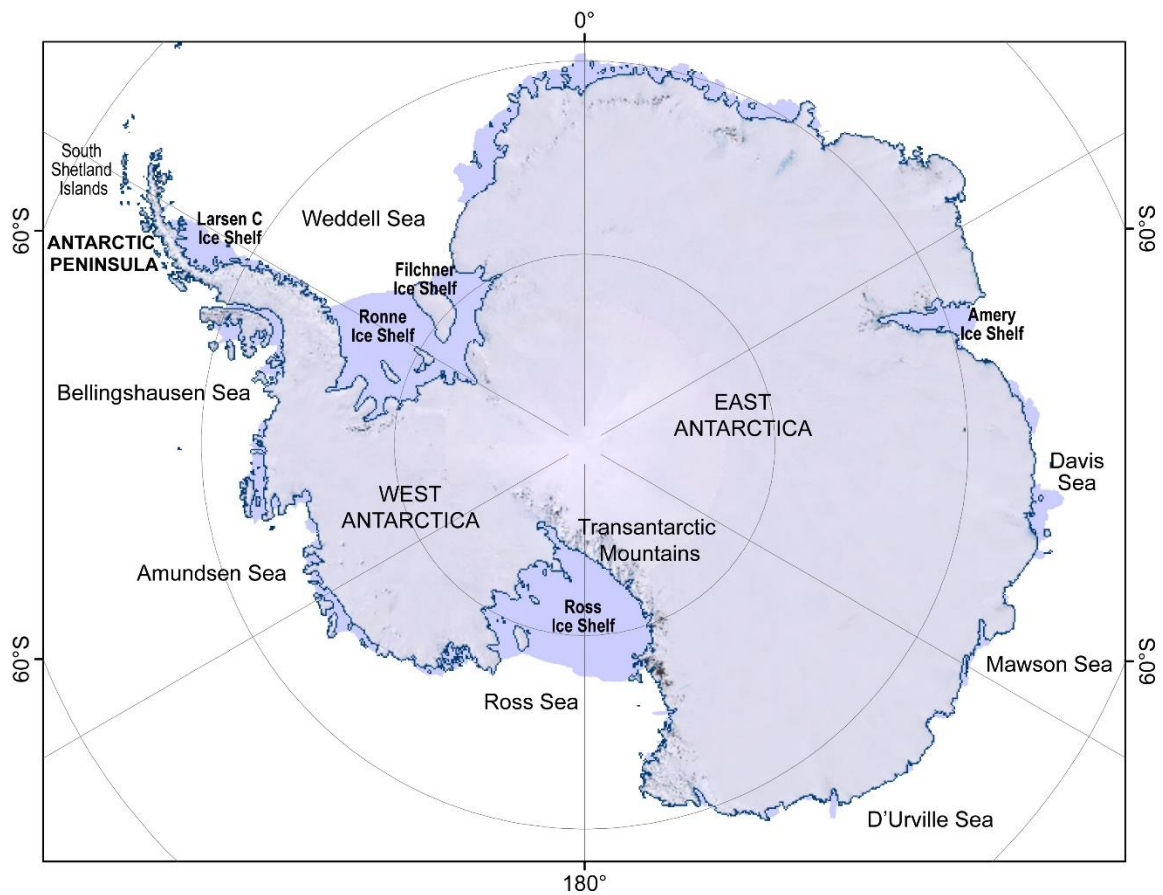
Figure 1.1 Polar projection map of Antarctica, completed using data from the Polar Geospatial Center and Bedmap2 (Fretwell et al., 2013). Blue line outlines the continent, light blue shade shows ice shelves.

In the third chapter, we mapped the geomorphology of several bays along a North-South transect in the western AP. Retreating ice leaves behind a distinct signature (facies) in the sedimentary record accumulating in the fjords as well as morphological features on the seafloor (Syvitski, 1989; Syvitski, 1991; Wellner et al., 2001; Anderson et al., 2002). A distinctive suite of subglacial geomorphic features that represent grounding of ice and subsequent retreat has been described in various studies from the Antarctic shelf (Wellner et al., 2001; Heroy & Anderson, 2005; Wellner et al., 2006). We focus on the marine features within the bays and present a model of geomorphic features. In addition, we look at the bay length and width, glacier drainage size flowing into the bays, seafloor lithology, and water depth in order to understand the controls of ice flow and retreat dynamics in these locations.

In the fourth chapter, we examine marine-sediment cores to reconstruct the deglaciation history and Holocene climatic events from three bays in the western Antarctic Peninsula. In total, 16 sediment cores were used for this study; four in Flandres Bay, four in Collins Bay, and eight in Beascochea Bay. Variations on lithology, sedimentary structures, magnetic susceptibility, density, pebble abundance, and grain size were paired with a ^{210}Pb-and-radiocarbon age model to interpret depositional environments. We compare our results to similar studies in other areas of the AP to evaluate changes in depositional environments resulting from climatic events during the Holocene, provide a regional context for the observed variations in the sediment record, and identify forcing mechanisms.

The purpose of this research is to understand the local variations in the AP, the environments of deposition, and analyze the products as well as the responses to climate variability. In order to fully interpret recently seen trends in the AP, it is necessary to distinguish between natural variability and abnormal fluctuations. Recognizing changes throughout the Holocene well-enough will give us the means necessary to make realistic predictions of future ice behavior.

Tectonic setting of the Antarctic Peninsula

The Antarctic Peninsula (AP) formed as a Mesozoic-Cenozoic magmatic arc, in response to the subduction of Pacific Ocean lithosphere beneath the supercontinent Gondwana (Barker et al., 1991; Grad et al., 2002). The subduction and arc magmatism ceased and the area developed into a passive margin (Henriet et al., 1992; Heroy and Anderson, 2005). Since then, glaciers have controlled sediment deposition in the area. The location of the fjords is guided by Mesozoic-Cenozoic faulting (Pudsey et al., 1994), while some of the northeast-southwest trending features in the AP are the result of back-arc extension (Gonzalez-Ferran, 1985). The Bransfield Strait separates the AP from the South Shetland Islands (Fig. 1.2). The Bransfield Strait is a back-arc basin formed in the late Oligocene-early Miocene. The rift today contains active volcanoes (Grad et al., 2002).

The AP is composed mainly of calc-alkaline Mesozoic-Cenozoic igneous rocks (Thomson et al., 1983). Jurassic and Cretaceous sedimentary and volcanic rocks rest on pre-Jurassic basement, intruded by plutons of the Andean intrusive suite (Hawkes, 1981).

Adie (1969) compiled a geologic map of the northern AP, unfortunately the area is

largely covered by ice (Fig. 1.3).
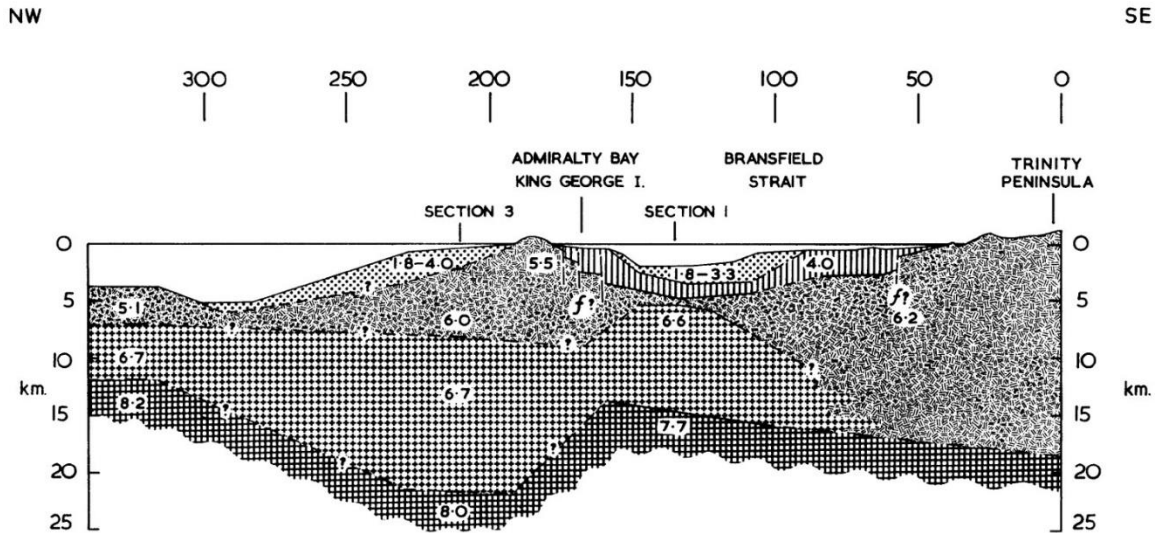
Figure 1.2 Generalized cross section from the northern AP (Trinity Peninsula) across the Bransfield Strait and into the South Shetland Islands. Numbers in the top show distance in kilometers. Numbers and patterns represent velocity (km/sec) ranges: 1.5-3.6 unconsolidated and consolidated sediments, 3.6-4.5 volcanic rocks and/or consolidated sediments, 4.5-6.3 acid igneous and/or metamorphic rocks, 6.5-6.9 basic igneous and/or metamorphic rocks, 7.6-8.2 mantle rocks (Ashcroft, 1972).

The continental shelf around Antarctica has a landward sloping profile, high

depths, and rugged topography likely due to the repeated advance of glaciers (Anderson,

1999). When the ice sheet advances from land into the continental shelf, it erodes older

strata in the inner shelf and carries it towards the outer shelf (Anderson, 1999). Several

small basins are present in the bays and in the inner continental shelf trapping

glacial/interglacial sediments. Overall, the morphology of the inner continental shelf has

been sculpted by glacial abrasion and plucking, and some areas like joints and faults have

been accentuated by glacial erosion (Domack et al., 2006).

Lithology legend:

Age	Unit
Quaternary	Volcanic rocks
Pliocene	Pecten conglomerate
Miocene	James Ross I. Volcanic group
Miocene	Seymour Island series
U. Tertiary	Volcanic rocks
L. Tertiary to U. Cretaceous	Andean Intrusive suite
L. to M. Campanian	Snow Hill Island series
U. Jurassic	Volcanic rocks
M. Jurassic	Sedimentary rocks
Carboniferous?	Trinity Peninsula series
L. Paleozoic	Intrusive/Volcanic rocks
Precambrian	Basement rocks

Joinville Island
Dundee Island
Pauiet I.
D'Urville Island
Andersson I.
Erebus and Terror Gulf
Snow Hill Island
Seymour I.
Many Jura
C. Wiman
C. Gage
Admiralty Sound
Vega Island
False I. Pt.
Lockyer I.
C. Foster
James Ross Island
Nygren Pt.
C. Longing
Larsen Inlet
Sobral Peninsula
C. Gordon
Rohss Bay
Persson I. Pt.
Channel
Gustav
Prince
Eagle I.
Duse Bay
Tabarin Peninsula
Fridtjof Sound
Hope Bay
C. Kinnes
Antarctic Sound
Hope I.
Bransfield I.
Gourdin I.
C. Legoupil
Huon Bay
C. Ducorps
TRINITY PENINSULA
DAVIS CO...
ORD...
C. Kjellman
Charcot Bay
C. Kater
Gilbert Strait
Tower I.
Bransf...
Deception I.

North Foreland
Ridley I.
C. Melville
Penguin I.
King George Bay
Martins Head
Admiralty Bay
King George Island
Round Pt.
Stigant Pt.
Nelson Strait
Duthoit Pt.
Nelson Island
Robert Pt.
Greenwich I.
Robert I.
C. Morris
Renier Pt.
McFarlane Strait
Mt. Friesland 1788
Barnard Pt.
South Bay
Williams Pt.
Desolation I.
Livingston Island
Hero Bay
Barclay Bay
C. Shirreff
Rugged I.
Morton Strait
Snow I.

0   20   40   60   Km
0   20   40   Miles

N

Figure 1.3 (previous page and this page) Geologic map of the northern Antarctic Peninsula and South Shetland Islands. White areas represent ice-covered land, black arrow points north. Andean Intrusive Suite includes: adamellite, diorite, granite, gabbro, granodiorite, quartz diorite, and tonalite. Modified from Adie (1969).

Chapter 2

LOCAL CONTROLS ON SEDIMENT ACCUMULATION AND DISTRIBUTION IN FLANDRES BAY: IMPLICATIONS FOR PALEOENVIRONMENTAL INTERPRETATIONS[1]

1. Introduction

Studies focusing on the analysis of the sedimentary facies in glacial marine environments, both in the northern and southern hemispheres, have resulted in a variety of conceptual models of sediment distribution (Anderson et al., 1980; Powell, 1981; Anderson et al., 1983; Elverhoi et al., 1983; Gilbert, 1983; Molnia, 1983; Elverhoi, 1984; Powell, 1984; Powell & Molnia, 1989; Syvitski, 1989; Domack & Ishman, 1993; Ishman & Domack, 1994; Powell & Domack, 1995; Anderson, 1999). Numerous proxies are taken into account when developing such models: lithology, grain size and texture, micromorphology, sedimentary structures, bedding contacts, stratigraphic relations, and biologic influence. The sediment deposits in these glaciated areas include diamictons, gravelly to sandy muds, turbidites, diatomaceous muds, and diatomaceous oozes. In nearly all models of sediment distribution, the coarser sediments are usually found closer

---

to the head of the fjord, near the ice front, and decrease in size towards the fjord mouth. Because primary productivity increases away from the glacier front, a higher biogenic component in the sediment is expected at the mouth of the bays. Paleoreconstructions of depositional environments in fjords and other glacial marine environments are based on observations and descriptions of sediment down-core as well as by our understanding of modern sediment distribution (e.g. Smith & Schafer, 1987; Kennedy & Anderson, 1989; Jennings & Weiner, 1996; Warner & Domack, 2002; Hillenbrand & Ehrmann, 2005; Heroy et al., 2008; Michalchuk et al., 2009; Milliken et al., 2009; Fernandez et al., 2011a; Anderson et al., 2011; Majewski et al., 2012; Cowan et al., 2014). Understanding sediment distribution is critical for studies reconstructing glacial and ice-sheet behavior based on paleo-records (e.g. Naish et al., 2009; Anderson et al., 2011; Fernandez et al., 2011b; Stokes et al., 2015).

Numerous factors control sedimentation in Antarctic fjords, including climate, seafloor topography, bay geometry, oceanographic regime, the presence of sea ice, the size of drainage areas, and proximity to sediment sources (Griffith & Anderson, 1989; Domack & McClennen, 1996; Ashley & Smith, 2000). In addition, the glacial behavior contributes and may ultimately provide the terrigenous output. Each of these contributes differently to the distribution of sediment along the bays. Characteristics of single bay systems are difficult to integrate and quantify since they can be widely variable, from the number of glaciers draining into a single bay to processes carrying and depositing sediment in and out of the bay. Nevertheless, they can have an enormous effect on the deposition and distribution of sediment, sometimes obscuring the trends that are expected

for given environments (Gilbert et al., 2002; Wölfl et al., 2014). Therefore, when applying any model of sediment distribution in a fjord environment, one must take into account how local variations of bay systems may be expressed in the sediment record. In this study, we analyze sediment grain size, lithology, and distribution in a bay in the West Antarctic Peninsula (AP). Using a dense collection of marine sediment cores, the known modern glacial climate of the region, oceanographic and bathymetric controls, we assess the general trends within these deposits and how local variations affect sediment distribution.
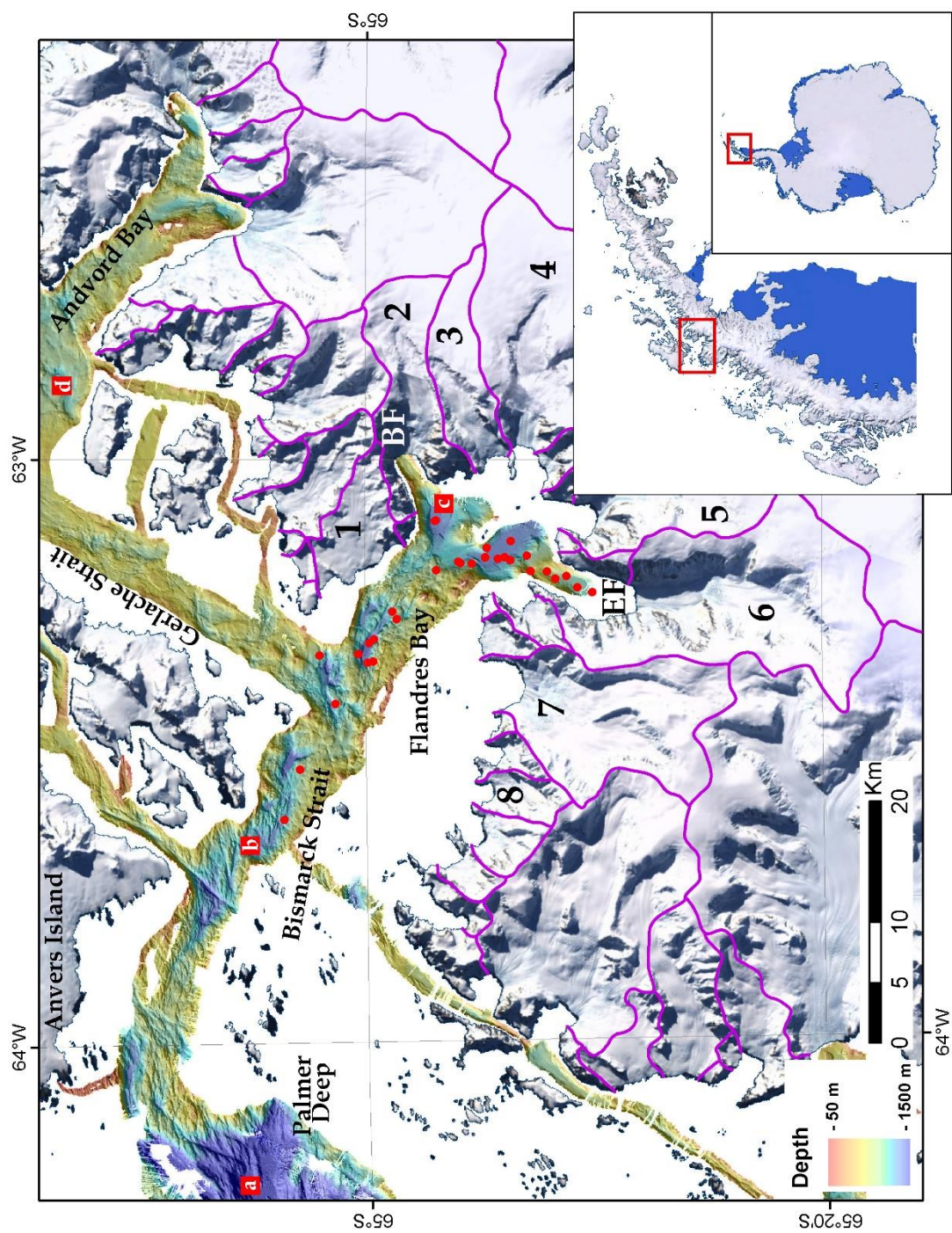
Figure 2.1 (previous page) Map of Flandres Bay, located in western Antarctic Peninsula. Insets show the location of the Antarctic Peninsula with respect to Antarctica and the location of the study area. Seafloor bathymetry mapped using multibeam swath bathymetry data from cruises NBP0201, NBP0502, NBP0602A, NBP0703, and NBP1001 to the Antarctic Peninsula. Red circles represent core locations. Glacial drainage basins of glaciers are outlined in purple (from Cook et al., 2014). Briand Fjord and Etienne Fjord are abbreviated as BF and EF. Numbers show glaciers draining into Flandres Bay: 1 Vogel Glacier, 2 Bolton Glacier, 3 Sayce Glacier, 4 Goodwin Glacier, 5 Archer Glacier, 6 Talbot Glacier, 7 Niepce Glacier, 8 unnamed glacier; letters in red squares show ^{210}Pb sedimentation rates: a, 1.71 mm/yr; b, 1.17 mm/yr; c, 2.8 mm/yr; d, 0.65 mm/yr (Isla et al., 2002; Isla et al., 2004; Boldt et al., 2013).

2. Study area

2.1. Background

The AP is heavily glaciated (Fig. 2.1); however, very different climate regimes characterize the eastern and western AP, even at the same latitude. In general, the eastern side is cooler, with extensive ice shelves, while the western side is warmer and wetter, with small tidewater glaciers draining into fjords and bays. According to Cook et al. (2014), the drainage areas of the tidewater glaciers in the AP average 130 km^2, but some can be over 6000 km^2. Tidewater glaciers are very sensitive to climatic changes and respond rapidly to fluctuations in the environment because they are thin compared to ice sheets, have small drainage areas and have high accumulation rates (Anderson, 1999). Rapid sediment accumulation in fjords results in a high-resolution sedimentary record that can be used as a tool to reconstruct local glacial behavior (Griffith & Anderson, 1989; Syvitski, 1989, 1991; Wellner et al., 2001; Anderson et al., 2002). The westerly winds increase summer warming in the AP by bringing warm, maritime air that lead to basal melt and loss of ice.

The prevailing westerlies drive surface waters around the continent towards the east creating the Antarctic Circumpolar Current (ACC). Temperatures in the Southern Ocean have risen 0.17 °C between the 1950s and the 1980s, mainly along the Antarctic Circumpolar Current (Gille, 2002), and especially near the western AP, where sea surface summer temperatures have risen more than 1 °C in the same time period (Meredith & King, 2005). Recent data suggest that the ACC has shifted south due to stronger westerly winds (Bi et al., 2002; Hall & Visbeck, 2002; Lubin et al., 2008). This in turn brings warmer water to fjords in the western AP. The presence of warmer water masses closer to the continent increases basal melting in glaciers and ice shelves (Domack et al., 2003; Rignot et al., 2008; Hellmer et al., 2012; Pritchard et al., 2012). In this case, the bathymetric morphology becomes critical since dense water masses would not override topographic highs, for example sills, in the ocean floor (Smith et al. 1999), which are characteristic of many fjords (Elverhoi et al., 1983; Skei, 1983).

2.2. Setting

Flandres Bay (65°3'S, 63°14'W) is located in the Danco Coast, north of the Graham Coast in the western side of the AP, south-east of Anvers Island (Fig. 2.1). The bay is about 30 km long and 20 km wide and it is surrounded by numerous small tidewater glaciers that drain the AP ice cap (Figs. 2.1, 2.2). The drainage size area of glaciers terminating into this bay varies in size from less than 10 km^2 to 215 km^2 (Cook et al., 2014). The head of the bay is characterized by a series of embayments where tidewater glaciers drain into the bay. The largest embayments are Briand Fjord in the northern

margin and Etienne Fjord in the southern margin (Fig. 2.1). Cook et al. (2005, 2014) measured glacier front retreat of various tidewater glaciers terminating in Flandres Bay, including Bolton Glacier, Sayce Glacier, Goodwin Glacier, Archer Glacier, Talbot Glacier, Niepce Glacier and an unnamed glacier (Figs. 2.1, 2.2). All of them show some degree of retreat, between 55 m (for Archer Glacier) and 607 m (for Talbot Glacier), measured from the 1940s to the early 2000s. However, no direct correlation was found between the size of the drainage area and the retreat distance (Cook et al., 2014).

Flandres Bay is protected from open ocean conditions by Anvers Island and has been classified as having a dry, subpolar climate (Griffith & Anderson, 1989; Boldt et al., 2013), separating the warm, wet subpolar bays in the north from the dry, polar bays in the south. Atmospheric temperatures vary from slightly above 0 °C in the summers to -8 °C to -11 °C in the winters (Domack & Ishman, 1993; King et al., 2003). However, atmospheric temperature records from Faraday/Vernadsky station (50 km south of Flandres Bay) show a warming of 5.7±1.6 °C/century, the highest for the AP area where the average warming is 3.7±1.6 °C/century (Vaughan et al., 2003). In situ observations at Faraday/Vernadsky station show that annual precipitation days have increased by 12.4 days/decade since the early 1950s (Turner et al., 2005), while in an ice core collected in the south-west AP, Thomas et al. (2008) calculated a doubling of snow accumulation since the 1850s.

In a map from the American Geographical Society published in 1969, compiled by R.J. Adie, no rock outcrops are identified in Flandres Bay. However, the exposed rocks in the surrounding areas, the south-eastern region of Anvers Island and the regions directly

across the AP, on the eastern side of the AP, are composed of Upper Jurassic volcanic rocks and Lower Tertiary to Upper Cretaceous Andean intrusive rocks (granite, granodiorite, and tonallite). It is likely that these same rock types underlie the glaciers that drain into Flandres Bay.

Flandres Bay is located eastward of the Bismarck Strait (Fig. 2.1), at the southern end of the Gerlache Strait that connects the Bransfield Strait in the north and the Bellingshausen Sea in the south. The western side of the AP receives incursions of Upper Circumpolar Deep Water, which brings oceanic, relatively warm (>1.5 °C), saline (34.3-34.8), nutrient-rich water to this area (Ishman & Domack, 1994; Domack et al., 2003). However, this water mass may experience modifications near the bays resulting from local conditions like sea-ice formation and meltwater from glaciers (Smith et al., 1999; Martinson et al., 2008; Allen et al., 2010).

Sea ice has a major influence in the AP glacial marine sedimentation, largely affecting primary productivity. The intrusion of the warm Upper Circumpolar Deep Water into the shelf in this area, combined with warming atmospheric temperatures in the western AP (Vaughan et al., 2003; Turner et al., 2013), influence sea-ice formation, thickness, and persistence through the seasons (Smith & Klinck, 2002; Stammerjohn et al., 2008, Stammerjohn et al., 2012). Stammerjohn et al. (2012) have reported that the ice season in the AP and the Bellingshausen Sea has been reduced by more than three months between 1979-1980 to 2010-2011. Considering this, an intriguing sea-ice behavior occurs in Etienne Fjord, where fast sea ice was directly observed to cover the entire fjord during the austral summers of 1988 (PD1988-III), 2002 (NBP0201), 2007

(NBP0703), and 2012 (NBP1203). Sea-ice thicknesses in Etienne Fjord have not been measured.

Results from ^{210}Pb analyses show that modern sediment accumulation rates in the western AP are highly variable (Fig. 2.1), for example, accumulation rates in the Gerlache Strait vary from 0.65 mm/yr to 3.1 mm/yr (Isla et al., 2002; Isla et al., 2004), but can be as high as 5.1 mm/yr (Harden et al., 1992). Whereas in the inner area of Flandres Bay accumulation rates are 2.8- 3 mm/yr (Boldt et al., 2013), and in the outer bay/Bismarck Strait the accumulation rate is 1.17 mm/yr (Isla et al., 2002; Isla et al., 2004). Further west, in the area around Palmer Deep, the measured ^{210}Pb accumulation rate is 1.71 mm/yr (Isla et al., 2002; Isla et al., 2004). Clearly, there is a high variability in sediment accumulation rates that are the result of a wide variety of processes influencing these different areas.

3. Methods

3.1. Multibeam swath bathymetry

Swath bathymetry data were collected onboard the RV/IB *Nathaniel B. Palmer* on multiple expeditions to Flandres Bay, including NBP0201, NBP0502, NBP0602A, NBP0703, and NBP1001. Multibeam soundings were collected in a swath perpendicular to the ship track using a Simrad EM120 12 kHz swath profiler hull-mounted with 191 beams. The data were corrected using sound-velocity and conductivity–temperature–depth profiles, then edited by the scientific party onboard. Maps were created in ArcGIS®, using a resolution of 20 m (Fig. 2.1).

3.2. Sediment cores

US Antarctic Program expeditions have collected a total of 41 cores from 1982 to 2007 in Flandres Bay (Table 2.1). Core types include grab samples, box cores, kasten cores, trigger cores, piston cores, and jumbo piston cores. They were described and logged onboard, including color (using a Munsell soil color chart), grain size and texture, laminations, dropstones, ice-rafted debris, fossil content, organic matter, and bioturbation. Additional observations were made in the national core repository, the Antarctic Research Facility at Florida State University in Tallahassee, Florida. For the purposes of this study, only the surface sediment, which represents modern sediments, was analyzed in each core. The list of all the cores included in this study is presented in Table 2.1. Fig. 2.2 shows the locations and names of the cores in Flandres Bay. Cores are separated in two groups; the first group includes the grab samples and short cores (box, trigger and kasten cores, 27 in total). These are more likely to preserve the sediment water interface because recovery of these cores involves a low-impact operation. The second group includes an additional 14 cores, piston and jumbo piston cores. Note that 10 of these cores were collected in the same location or very close to a grab sample or short core (Fig. 2.2 shows a small circle and a large circle representing the cores in the same location). The medium- to high-impact operation required to recover piston and jumbo piston cores makes them less likely to preserve the sediment–water interface. However, we include them in this study for completeness and to demonstrate that in almost all the cases (one is the exception) the short core sediment description and the long core

sediment description are very similar, resulting in the same sediment facies. This enables us to rely on findings where only a jumbo piston or piston core was collected and not a short core (which is the case in four sites in this study). Table 2.1 also shows which cores were sampled for grain size and smear slide counts of lithology. Grain size was measured using a Malvern Mastersizer 2000 Laser Particle Size Analyzer. Particle sizes between 0.02 µm and 2000 µm can be accurately measured using this instrument. The sediment was not treated to remove the biogenic component. The grain size percentiles from the Laser Particle Size Analyzer were separated into clay (<4 µm), fine silt (4-24 µm), medium silt (24-44 µm), coarse silt (44-63 µm), and sand (>63 µm). Mean, skewness, kurtosis, and sorting were calculated using the formulas of Folk & Ward (1957). Pebbles were not described quantitatively; instead, descriptive terms are included for each sediment sample: abundant, common, scattered, and none observed in the sample. Published cruise reports from the Deep Freeze operation DF85 and NBP0703 include smear-slide counts of percentage abundance of lithologic constituents of sediment in cores. Smear slides were made for cores that did not have this information using the same procedure as described in these cruise reports (Cassidy et al., 1984; Bryan, 1992a, 1992b; Hovan & Janecek, 1994a, 1994b). The abundance of quartz, clay, diatoms, feldspar, mica, heavy minerals, and hornblende on the smear slide was quantitatively recorded using a petrographic microscope with a capacity for 900X magnification. The constituents were counted in a transect using a grid over the entire smear slide so that all grains sampled were reported. Facies were created based on grain size, lithology and, pebbles found in the sediment.
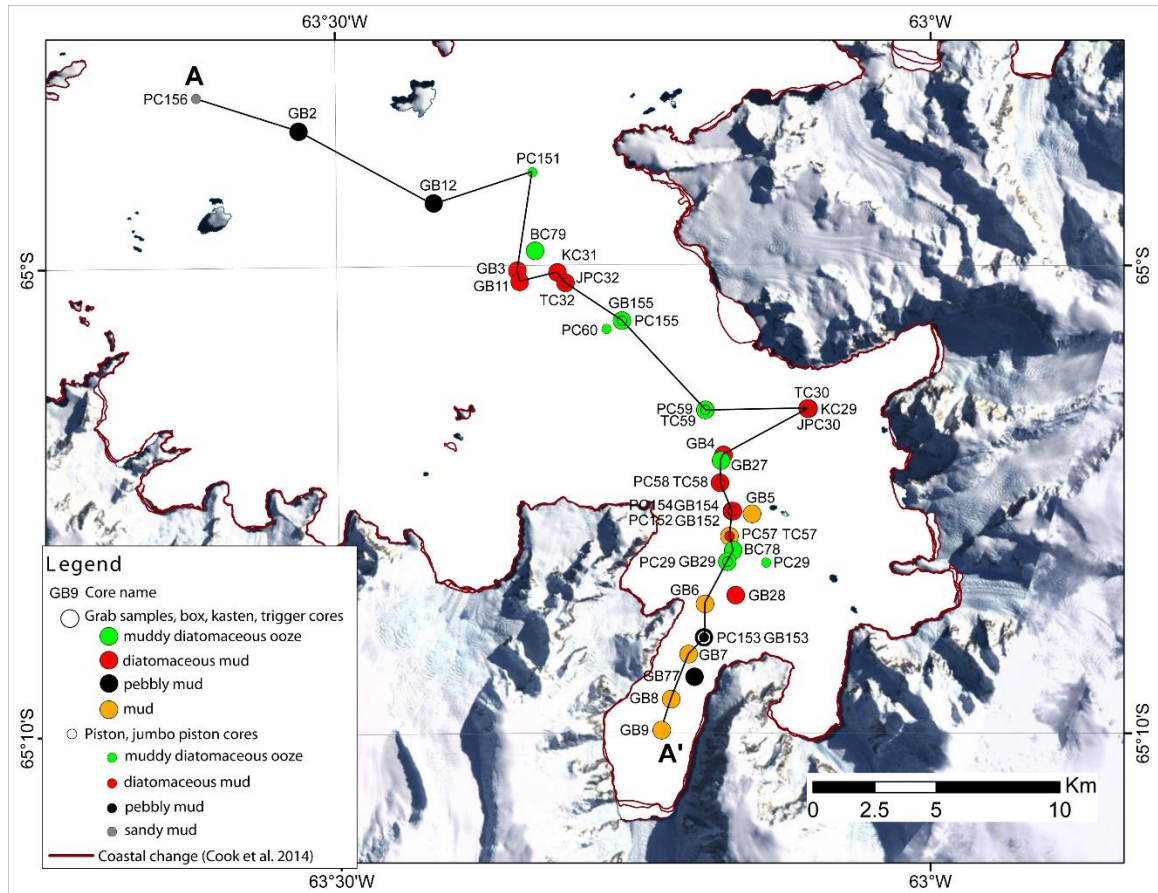
Figure 2.2 (previous page) Grab samples and cores collected in Flandres Bay: grab sample (GB), box core (BC), kasten core (KC), trigger core (TC), piston core (PC), and jumbo piston core (JPC). Some cores were collected in pairs (one grab sample and one piston core for example); therefore, a small circle and a large circle are in the same location. Names of each core correspond to core identification numbers in Table 2.1. The profiles line A–A' is presented in Fig. 2.6. Maroon outlines show glacier front change as measured by Cook et al. (2014).

4. Results

4.1. Bathymetry

The seafloor topography of Flandres Bay is very rugged with the exception of deep basins, which have a flat bottom and very gentle slopes (Fig. 2.1). Slope maps of the bathymetry show lower relief areas in the inner bay and parts of the Gerlache Strait, and highly rugged topography in the outer bay (appendix A, Fig. A.2). The inner bay is

19

separated from the outer bay by a sill, an elongated, transverse ridge, with an average depth of 350 m. The inner bay is composed of two low relief basins, one with an area of about 2000 km^2 and the other approximately 7000 km^2, both over 700 m deep. Etienne Fjord, located in the southern margin of Flandres Bay, has only been partially surveyed. At its center, it is characterized by an extensive, flat basin, approximately 500 m deep. Etienne Fjord is separated from the Flandres inner bay by a shallow sill, approximately 290 m deep. Briand Fjord, located on the northern margin of Flandres Bay, exhibits a distinct morphology compared to Etienne Fjord. A shallow sill (about 270 m of water depth) is also present in Briand Fjord, separating it from the main inner bay area. The depths in Briand Fjord do not vary drastically; the deepest point located in the center of the fjord is only 360 m deep. The flanks of the fjord were found to have low relief and be relatively shallow too.

Outer Flandres Bay is characterized by a more rugged bathymetry with several small basins with flat bottoms. These basins range in area between 750 km^2 and 1200 km^2 and are elongated, nearly parallel along the axis of the bay. The regions towards the Bismarck Strait, in the west end of Flandres Bay, deepen and increase in ruggedness while the regions towards the Gerlache Strait, north-east of Flandres Bay, shallow and flatten (Fig. 2.1).
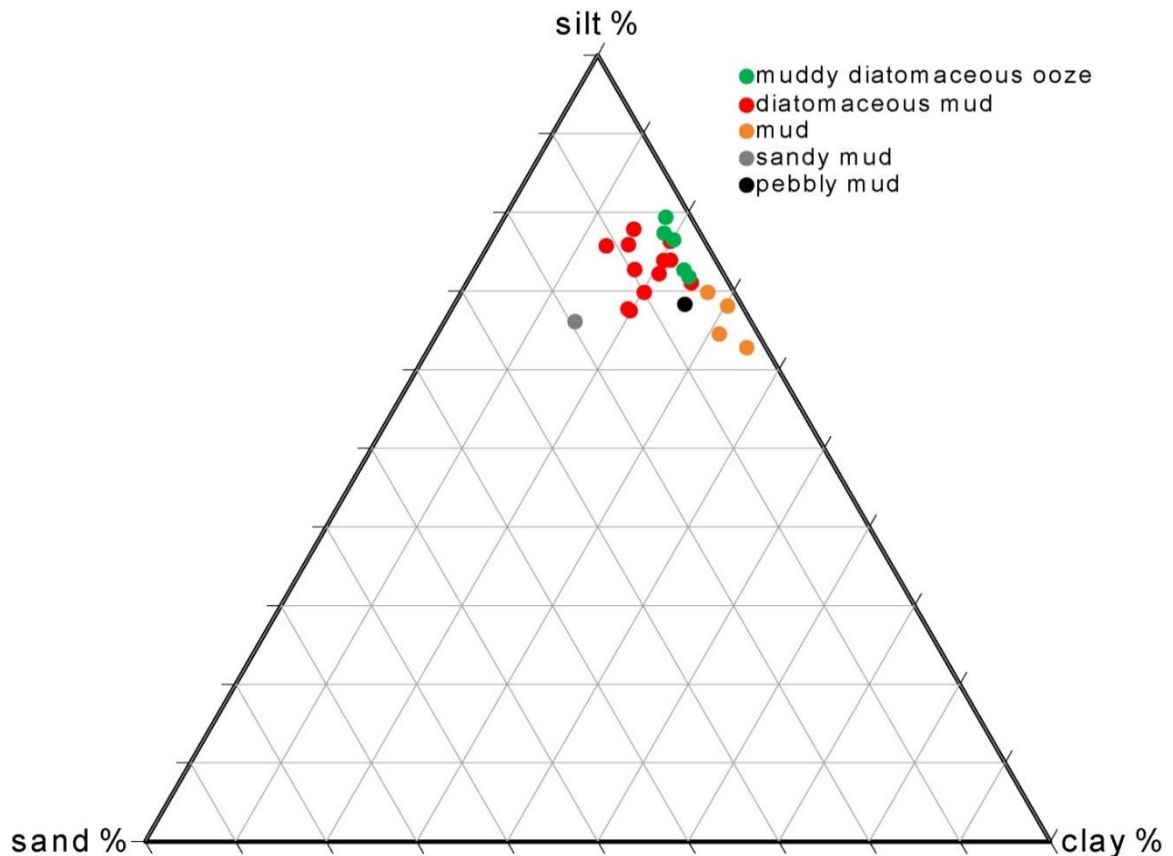
Figure 2.3 Ternary diagram of samples collected in Flandres Bay. Comparison of sand–silt–clay percent composition of the sedimentary facies in Flandres Bay. Ternary diagram shows measured sediment samples in Table 2.1. Facies are well grouped indicating homogeneity. Muddy diatomaceous ooze and diatomaceous mud overlap but they are distinguished by their diatom content. Plotted using TRI-PLOT software by Graham & Midgley (2000).

4.2. Surface sediment description

4.2.1. Sediment texture and lithology

Surface sediment samples were analyzed for grain size and lithology content (Table 2.1). Silt size (4-63 µm) is the dominant grain size with 63-79%, clay (<4 µm) follows with 13-35% and sand (>63 µm) is the lowest constituent, with 2-19% (Figs. 2.3, 2.4). Within the silt size range (4-63 µm), fine silt (4-24 µm) has 44-63% of the total grains in the sample, while medium silt (24-44 µm) composes 6-18%, and coarse silt (44-63 µm)

21

only 2-8% of the total grains measured per sample. The distributions of grain size along

Flandres Bay are shown in the maps in Fig. 2.4. Quartz, diatoms, clay minerals, and

heavy minerals make up the majority of the lithology found in the samples, although

minor amounts of feldspar, mica, and hornblende were also found. Of the total grains in

the sediment sample, quartz grains constitute 26-66%, diatoms varied widely between 1%

and 60%, clay minerals were 10-43%, and heavy minerals were 0-16%. Feldspar, mica,

and hornblende compose less than 5% of the total grains in the sediment samples. Maps

presenting the amounts of clay minerals, diatoms, heavy minerals, and quartz found in the

smear slides are shown in Fig. 2.5. In order to determine sediment sources throughout

Flandres Bay, changes in sediment lithology and grain size were studied in relation to

water depth (shallow to deep) and in relation to distance along the fjord axis (head to

mouth). For the purposes of this study, the head of the bay is in Etienne Fjord, where

samples were collected closest to the ice front, while the Bismarck Strait represents the

mouth of the bay, which is the farthest from the ice front and in semi-open water

conditions. The calculated mean, skewness, kurtosis, and sorting were also studied using

these relations. A slight increase in the mean and mode of the grain size was found from

the inner to the outer bay as well as with increasing depth. Skewness, kurtosis, and

sorting are relatively stable in the inner and outer bay and at all water depths (appendix

A, Figs. A.5, A.6).

Table 2.1 List of cores collected in Flandres Bay. X mark signifies grain size measurement and lithology counts completed in a sample, the results are shown in Figs. 2.3-2.6

Ship	Cruise	Core ID	Core Type	Latitude	Longitude	Water depth (m)	Core length (cm)	Grain size measurement	Lithology counts	Pebbles	Sediment facies
Glacier	DF82	GB152	grab sample	-65.088	-63.168	689	0			scattered	diatomaceous mud
Glacier	DF82	GB153	grab sample	-65.133	-63.192	351	0			abundant	pebbly mud
Glacier	DF82	GB154	grab sample	-65.088	-63.167	689	0			scattered	diatomaceous mud
Glacier	DF82	GB155	grab sample	-65.02	-63.26	437	0			scattered	muddy diatomaceous ooze
Glacier	DF85	TC57	trigger core	-65.097	-63.17	650	15		X	scattered	mud
Glacier	DF85	TC58	trigger core	-65.078	-63.178	439	16		X	common	diatomaceous mud
Glacier	DF85	TC59	trigger core	-65.052	-63.19	384	13		X	common	muddy diatomaceous ooze
Glacier	DF86	GB77	grab sample	-65.147	-63.2	448	0			abundant	pebbly mud
Glacier	DF86	BC78	box core	-65.102	-63.167	650	37			none	muddy diatomaceous ooze
Glacier	DF86	BC79	box core	-64.995	-63.333	494	36			none	muddy diatomaceous ooze
Polar Duke	PD88-III	GB27	grab sample	-65.07	-63.177	585	0			none	muddy diatomaceous ooze
Polar Duke	PD88-III	GB28	grab sample	-65.118	-63.165	467	0			none	diatomaceous mud
Polar Duke	PD88-III	GB29	grab sample	-65.106	-63.172	620	0			none	muddy diatomaceous ooze
Polar Duke	PD90-VII	GB2	Smith-McIntyre grab	-64.952	-63.531	460	0			abundant	pebbly mud
Polar Duke	PD90-VII	GB3	Smith-McIntyre grab	-65.002	-63.348	500	0	X	X	none	diatomaceous mud
Polar Duke	PD90-VII	GB4	Smith-McIntyre grab	-65.068	-63.175	580	0	X	X	none	diatomaceous mud
Polar Duke	PD90-VII	GB5	Smith-McIntyre grab	-65.089	-63.151	530	0	X	X	none	mud
Polar Duke	PD90-VII	GB6	Smith-McIntyre grab	-65.121	-63.191	171	0	X	X	none	mud
Polar Duke	PD90-VII	GB7	Smith-McIntyre grab	-65.139	-63.205	408	0	X	X	none	mud
Polar Duke	PD90-VII	GB8	Smith-McIntyre grab	-65.155	-63.22	493	0	X	X	none	mud
Polar Duke	PD90-VII	GB9	Smith-McIntyre grab	-65.166	-63.228	490	0	X	X	none	mud
Polar Duke	PD90-VII	GB11	Smith-McIntyre grab	-65.006	-63.346	445	0	X	X	abundant	diatomaceous mud
Polar Duke	PD90-VII	GB12	Smith-McIntyre grab	-64.978	-63.418	440	0			abundant	pebbly mud
Palmer	NBP0703	KC29	kasten core	-65.0516	-63.1031	684	188	X	X	common	diatomaceous mud
Palmer	NBP0703	TC30	trigger core	-65.0515	-63.1038	684	94	X	X	scattered	diatomaceous mud
Palmer	NBP0703	KC31	kasten core	-65.0028	-63.3144	723	266	X	X	scattered	diatomaceous mud
Palmer	NBP0703	TC32	trigger core	-65.0065	-63.3075	713	137	X	X	scattered	diatomaceous mud
total short cores and grab samples:		27						12	15		
Glacier	DF82	PC151	piston core	-64.967	-63.335	360	286	X	X	scattered	muddy diatomaceous ooze
Glacier	DF82	PC152	piston core	-65.088	-63.168	689	210	X	X	scattered	diatomaceous mud
Glacier	DF82	PC153	piston core	-65.133	-63.192	351	46	X	X	abundant	pebbly mud
Glacier	DF82	PC154	piston core	-65.088	-63.167	689	229	X	X	common	diatomaceous mud
Glacier	DF82	PC155	piston core	-65.02	-63.26	437	280	X	X	scattered	muddy diatomaceous ooze
Glacier	DF82	PC156	piston core	-64.94	-63.617	608	264	X	X	scattered	sandy mud
Glacier	DF85	PC57	piston core	-65.097	-63.17	650	246		X	common	diatomaceous mud
Glacier	DF85	PC58	piston core	-65.078	-63.178	439	175		X	common	diatomaceous mud
Glacier	DF85	PC59	piston core	-65.052	-63.19	384	423	X	X	common	muddy diatomaceous ooze
Glacier	DF85	PC60	piston core	-65.023	-63.273	448	262			common	muddy diatomaceous ooze
Polar Duke	PD88-III	PC29	piston core	-65.106	-63.172	620	191	X	X	scattered	muddy diatomaceous ooze
Palmer	NBP0201	PC29	piston core	-65.1065	-63.1391	670	196	X	X	scattered	muddy diatomaceous ooze
Palmer	NBP0703	JPC30	jumbo piston core	-65.0515	-63.1038	684	572.5	X	X	scattered	diatomaceous mud
Palmer	NBP0703	JPC32	jumbo piston core	-65.0065	-63.3075	713	666	X	X	none	diatomaceous mud
total (all cores):		41						23	28		

Core sample locations vary between 171 m water depth (in the distal part of Etienne Fjord) and 723 m water depth (in the distal part of Briand Fjord) (Table 2.1). There is a general trend of increasing grain size as water depth increases (Fig. 2.6). The relative percentage of sand grains increases from 3% in the shallowest depth to 10-12% in the deepest sample location; clay size decreases from 27% to 17% from shallowest to deepest sampled area; and while total silt (4-63 μm) remains constant, the fine silt (4-24 μm) component also decreases with depth. Lithologic components remain relatively constant with water depth (Fig. 2.6).

There is a general trend of increasing grain size away from the head of the fjord (Figs. 2.4, 2.6). In almost all the samples, percent sand increases (from 2% to 19%) and percent clay decreases (from 35% to 14%) away from the head of the bay (Fig. 2.4). Total silt (4-63 μm) remains relatively constant but coarse (44-63 μm) and medium (24-44 μm) silt increase from the head to the fjord mouth (Figs. 2.4, 2.6). The percent of diatoms increases towards the middle of the bay (from 1% in the fjord head to 60% in mid-Flandres Bay) and then decreases again in the outer bay (Fig. 2.5). Etienne Fjord has the least amount of diatoms; percentages decrease to 1.4% of the total sediment (Fig. 2.6). Clay minerals were found throughout the bay in, approximately, the same amounts with no apparent change from head to mouth. Percent quartz has a general decrease away from the fjord head, the highest values were found in Etienne Fjord (52-66% quartz) (Figs. 2.5, 2.6).
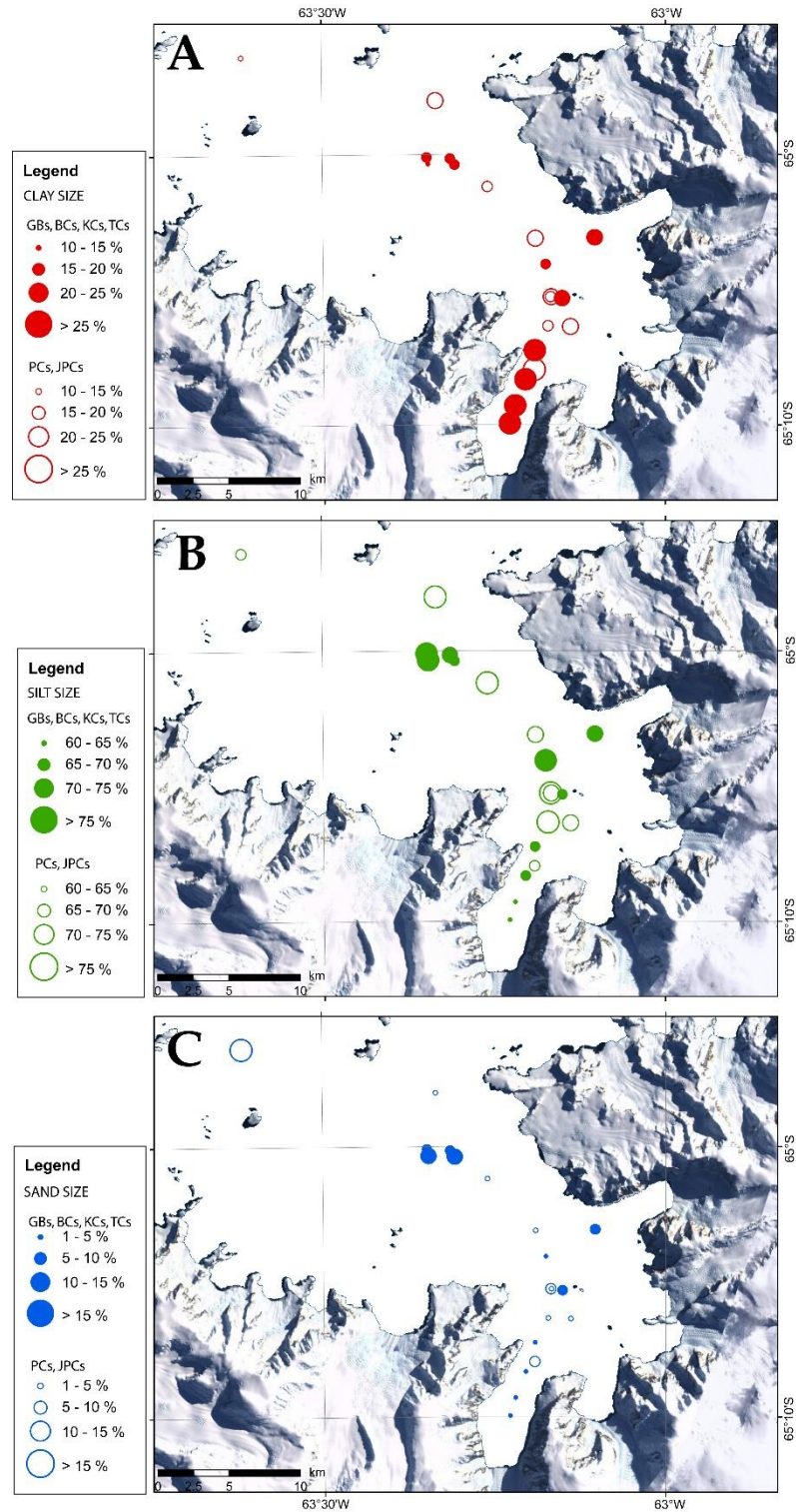
Figure 2.4 Distribution maps of percent grain size along Flandres Bay: (A) clay, (B) total silt, and (C) sand percentages per sample. Solid circles represent grab samples (GB), box cores (BC), kasten cores (KC), or trigger cores (TC). Open circles represent piston cores (PC) or jumbo piston cores (JPC). Sampled cores are listed in Table 2.1.

25
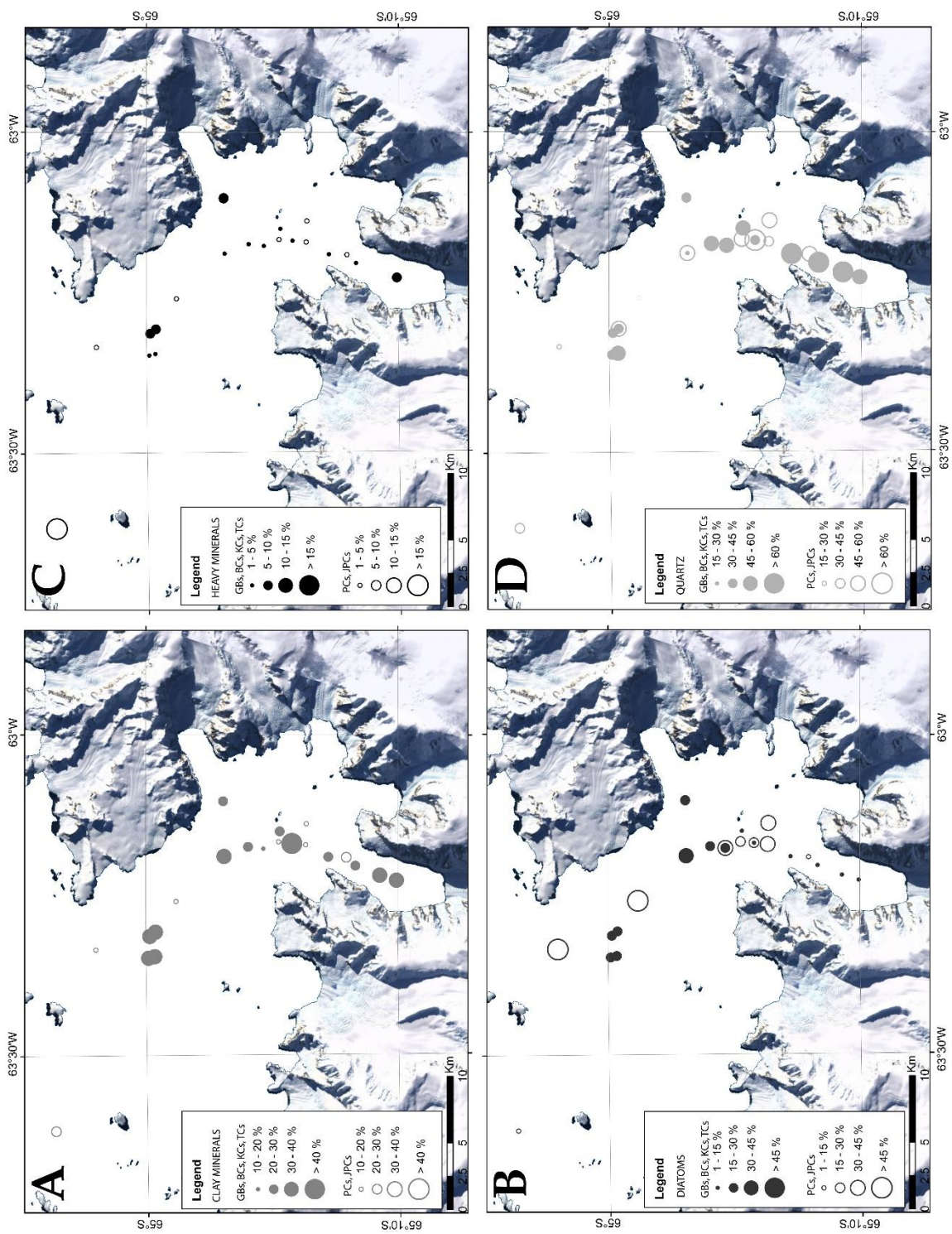
Figure 2.5 (previous page) Distribution maps of percent lithology along Flandres Bay: (A) clay minerals, (B) diatoms, (C) heavy minerals, and (D) quartz percentages per sample. Solid circles represent grab samples (GB), box cores (BC), kasten cores (KC) or trigger cores (TC). Open circles represent piston cores (PC) or jumbo piston cores (JPC). Sampled cores are listed in Table 2.1.

4.2.2. Sediment facies and distribution

Five sediment facies (Table 2.2) are defined using results from grain size and lithological analysis: (1) muddy diatomaceous ooze, containing >30% diatoms with a mixture of clay and silt <70%, <15% sand, and none to common pebbles; (2) diatomaceous mud, containing between 15% and 30% diatoms, a mixture of clay and silt >70%, <15% sand, and none to common pebbles; (3) pebbly mud, <15% diatoms, a mixture of clay and silt >70%, <15% sand, and abundant pebbles of varying sizes; (4) sandy mud, <15% diatoms, a mixture of clay and silt >70%, between 15% and 30% sand, and scattered pebbles of varying sizes; and (5) mud, <15% diatoms, a mixture of clay and silt >70%, <15% sand, and none to common pebbles.

Table 2.2 Definitions of sediment facies used in this study

Facies	% Diatoms	% Mud (clay and silt)	% Sand	Pebbles
Muddy diatomaceous ooze	>30	<70	<15	None to common
Diatomaceous mud	15-30	>70	<15	None to common
Pebbly mud	<15	>70	<15	Abundant
Sandy mud	<15	>70	15-30	Scattered
Mud	<15	>70	<15	None to common

Muddy diatomaceous ooze was found in the northern outer bay (towards the Gerlache Strait) and in the middle of the bay. Diatomaceous mud covers the basins in the inner and outer bay. Sandy/pebbly mud was found in samples in the outer bay (in Bismarck Strait) and in the distal part of Etienne Fjord (inner bay). Mud was only found in samples collected in the central and distal regions of Etienne Fjord (Figs. 2.2, 2.7, and 2.8).
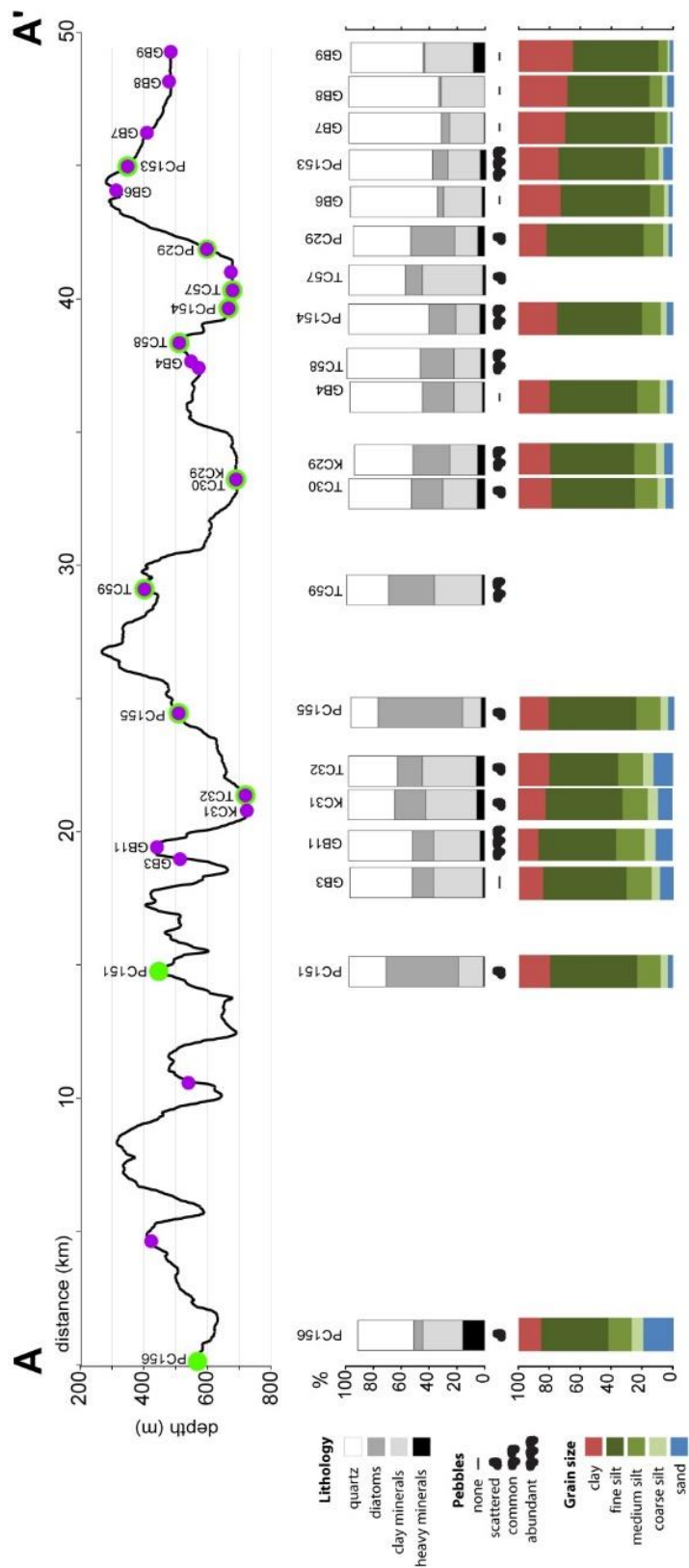
Figure 2.6 Profile line A–A' along Flandres Bay, location in Fig. 2.2. The circles in the profile line represent sampled cores with their resulting percent lithology, percent grain size, and pebbles. Name of each core is also shown. Purple circles represent grab samples (GB), box cores (BC), kasten cores (KC) or trigger cores (TC). Green circles represent piston cores (PC) or jumbo piston cores (JPC). Notice that not all sampled cores are shown in this figure, only cores in the profile line A-A'.

29

5. Discussion

5.1. Glacier front retreat and ice cover

The glaciers in Flandres Bay analyzed by Cook et al. (2005, 2014) are Bolton Glacier (which drains into Briand Fjord), Talbot Glacier (which drains into Etienne Fjord), Sayce Glacier, Goodwin Glacier, Archer Glacier, Niepce Glacier, and an unnamed glacier (Fig. 2.1). Although in varying amounts, all of these glaciers show retreat; the largest retreat corresponds to Talbot Glacier which shows a glacier front retreat of 607 m from 1968 to 1997 and the shortest is Archer Glacier with 55 m of glacier front retreat in the same time span (Fig. 2.2, data from complimentary material of Cook et al., 2005; Cook et al., 2014). These two glaciers are next to each other, have similar drainage basin areas, and are exposed to the same atmospheric temperatures; therefore, the different rates of retreat suggest that other factors influence glacier front retreat besides atmospheric temperature. Six sediment samples have been collected in Etienne Fjord, where the highest glacier ice-front retreat has taken place: one piston core during DF82 (that recovered pebbly mud facies); one grab sample during DF86 (that recovered pebbly mud facies); and four Smith-McIntyre grab samples during PD90-VII (which recovered mud facies) (Figs. 2.2, 2.6, 2.7). Although the recovery of these sediments took place over a multi-year span of time, there is no evidence pointing to a fundamental change in sediment facies; the retreat rate of Talbot Glacier is 20 m/yr in average (607 m, measured from 1968 to 1997) and the core locations are approximately between 4 km and 9 km away from the glacier ice front; therefore, there is a high likelihood that the sediments are representative of the same depositional conditions over

the eight-year span of time that passed between the first sediment sample collected

(1982) and the last (1990). In addition, PC153, collected in 1982, is composed of a single

sediment facies; pebbly mud throughout the entire core length, 46 cm (Cassidy et al.,

1984), which suggests that the sedimentary environment has remained unchanged for a

long time. However, there are no age constrains or sediment accumulation rates available

for sediments from Etienne Fjord and no sediment samples have been collected in this

area since 1990. The mud was sampled in the middle of the fjord, a deep and flat basin.

The lithology of the analyzed samples in Etienne Fjord is composed of >50% quartz,

between 20% and 35% clay and less than 6% diatoms (Figs. 2.5, 2.6). Particle size is

dominated by fine silt (4-24 μm), 53 -58%, and clay, 25 -35% (Figs. 2.4, 2.6). This

lithology and grain size are characteristic of suspended sediment delivered by meltwater

plumes (Syvitski & Murray, 1981; Elverhoi et al., 1983; Ó Cofaigh & Dowdeswell,

2001). The sediment collected in the middle of the fjord (approximately 500 m deep) had

scattered to no pebbles, which may be an indication that no ice rafting or downslope

sediment redistribution has occurred in this area (Fig. 2.6). Fast sea ice has been observed

to cover Etienne Fjord entirely, especially during the austral summers when cruises

PD1988-III (1988), NBP0201 (2002), NBP0703 (2007), and NBP1202 (2012) visited the

area. The low biogenic content in the sediment could be the result of continuous ice cover

in the fjord since permanent sea-ice results in lower biogenic productivity (Leventer et

al., 1996). However, the lack of data on sediment and organic fluxes makes this

assumption is difficult to assess. The only cruise that has successfully sampled the middle

of Etienne Fjord was PD90-VII (1990). The distal area of Etienne Fjord (with a depth of

approximately 290 m) is covered by pebbly mud (Figs. 2.2, 2.7).

31
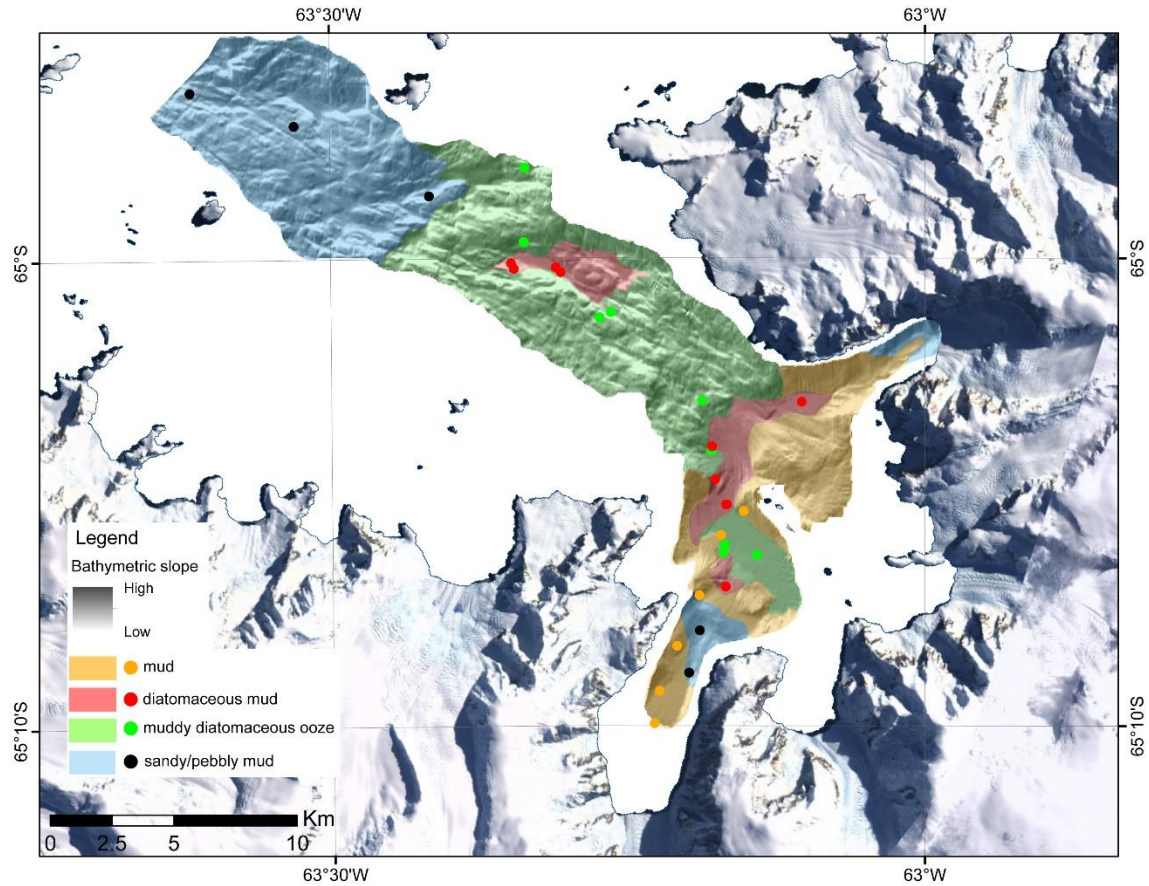
Figure 2.7 Sediment distribution in Flandres Bay draped over swath bathymetric data indicating bottom roughness.

The sediment facies found in Etienne Fjord do not follow the typical sediment distribution for a glaciated fjord environment. These models propose that coarser grains are found close to the ice front and particles decrease in size distally. Additionally, the biogenic component should increase away from the ice front. Although the fjord has scattered sediment samples, the sediment in the middle of the fjord is homogeneous mud, with low (< 6%) sand size particles, a very low (< 6%) biogenic component, and no pebbles (Figs. 2.6, 2.7). The pebbly mud is found only in the outer area of Etienne Fjord. No samples have been collected in the proximal area to the ice front. Unarguably, these

32

sedimentary facies are the result of different depositional processes active in this fjord. Persistent fast-sea ice possibly plays an important role in the distribution and lithology of the sediment in the fjord. Additionally, due to the current state of retreat of Talbot Glacier, it can be assumed that meltwater plumes are common and the most likely source of fine mud deposited in the middle of Etienne Fjord (Fig. 2.8). Interestingly, the fine mud deprived from significant biogenic matter and lacking pebbles is similar to a "null zone" interpreted to deposit under an ice shelf away from basal debris (Domack et al., 1999). The "null zone" unit ranges between 15 cm to 40 cm in thickness and it is described as laminated, with very little sand, and no pebbles.

5.2. Primary production

The middle of Flandres inner bay is characterized by the highest percentage of diatoms (from 39% to 60% of the total grains in the sample) and silt (4-63 μm) particles, in particular fine silt (4-24 μm), which is 50 -60% of the total grains in the sample (Figs. 2.4, 2.5, 2.6). In a study in Palmer Deep, an adjacent basin to Flandres Bay (Fig. 2.1), Warner and Domack (2002) found that the fine to medium silt-sized particles were mostly of biogenic origin (*Chaetoceros* spores, which are about 5-8 µm in size). Using this and other lines of evidence, they concluded that particle size can be used to represent depositional environments. In this case, the silt particles were likely to represent biogenic sedimentation. Although no biogenic flux data has been published for Flandres Bay, Isla et al. (2002; 2004) reported high primary productivity in the Gerlache Strait area. We therefore suggest that the main sediment source in this part of the bay is, in fact, biogenic

productivity. The combination of relatively warm water, low salinity (Leventer et al., 1996), meltwater, and reduced sea ice (Allen et al., 2010) increase biogenic productivity. This may be the case in Flandres Bay if warm Upper Circumpolar Deep Water ($> 1.5°$ C) from the Bellingshausen Sea flows into the Bismarck Strait and possibly into Flandres Bay. Increased meltwater from retreating glaciers (Cook et al., 2005) and decreased sea-ice cover in the region (Stammerjohn et al., 2012) may contribute to enhance high primary production rates. Although we argue for increased meltwater in Etienne Fjord, we estimate the water carries an excess of suspended sediment, which combined with persistent sea-ice cover, results in minor diatom productivity.

5.3. Ocean currents

Some areas in the western Antarctic Peninsula do not have high biogenic accumulation because the material is likely re-suspended or carried by strong currents to adjacent areas. This may be the case in outer Flandres Bay (along the Bismarck Strait), where Isla et al. (2002; 2004) measured high primary production rates but found low percentages of biogenics in the accumulated sediment. They show percentages of dry weight of sand and found similar results to ours, sand size increases from 1% to 29% from Palmer Deep to Bismarck Strait and into the Gerlache Strait. Sand size then decreases to 5% from the Gerlache Strait out into the Bransfield Strait, suggesting stronger currents in the southern area of the Gerlache Strait, close to Flandres Bay. They conclude that this sediment composition is the result of lateral transport of the biogenic component. The water flowing north towards the Gerlache Strait must be strong enough
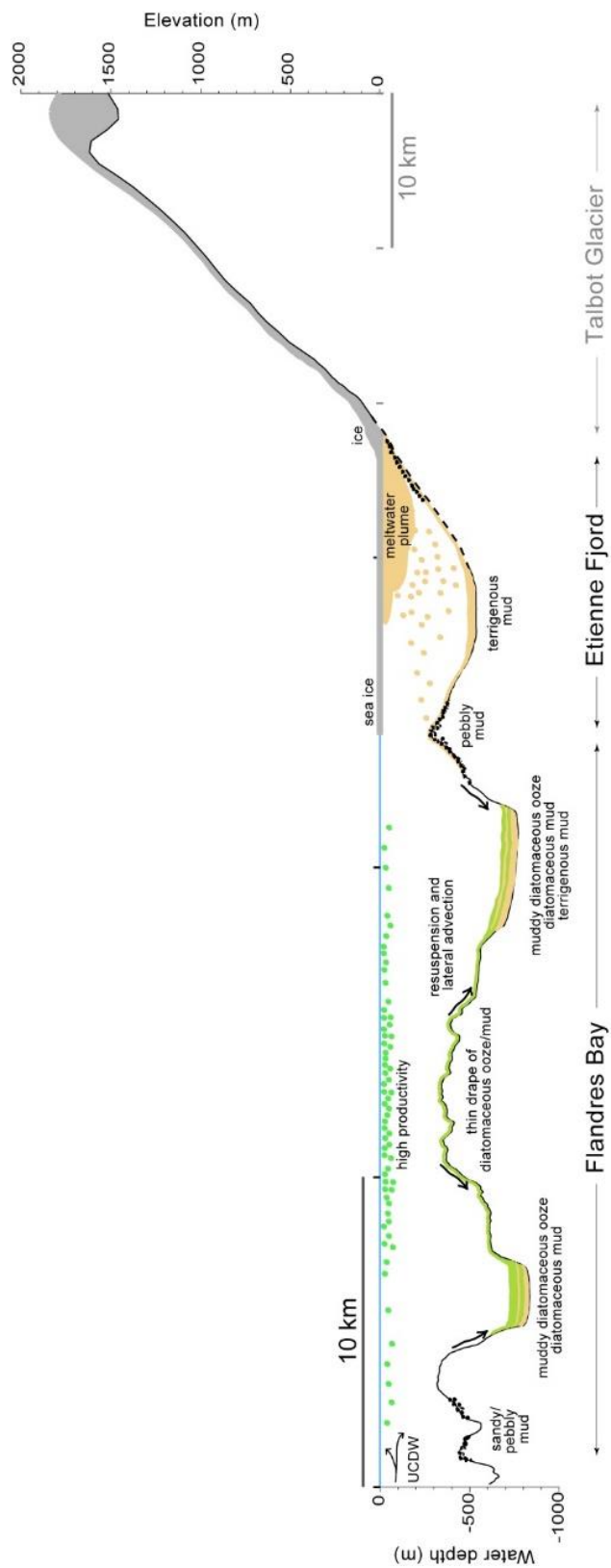
Figure 2.8 Cartoon showing sediment processes in Flandres Bay. Note different horizontal scale used in Talbot Glacier (elevation for Talbot Glacier from Cook et al., 2014).

35

to carry clay and fine silt-sized particles, leaving behind lag deposits of coarser material. The cores collected in the outer bay are characterized by higher sand percentages, low diatom percentages, and abundant pebbles (Figs. 2.4, 2.5, 2.6). As such, it is likely that these deposits are the result of winnowing of the fine grains and sediment re-suspension events. Additional observations of sediment deposits down core, including grain size, sorting, skewness, and kurtosis would further corroborate our conclusions. In addition, analyses using shallow seismic data would be helpful if we assume sediment is being carried and deposited downstream, most likely in the northern Gerlache Strait. However, this approach requires a more thorough study that would account for the glacial retreat history, the sediment flux, and the interaction of water currents in this area.

5.4. Comparison to similar studies

Sediment characteristics, accumulation, and distribution varies with climate, sea-floor topography, bay geometry, size of drainage basins, oceanographic regime, and distance to glacier front. In a study of Andvord Bay, just north of Flandres Bay (Fig. 2.1), Griffith & Anderson (1989) describe the inner bay as composed of sandy diatomaceous mud with scattered pebbles and the outer bay as muddy diatomaceous ooze with scattered pebbles, which decrease in abundance towards the mouth of the bay. Another study in the same bay (Domack & Ishman, 1993) describes a terrigenous facies (sandy muds to muddy sands) close to glaciers and a biosiliceous facies (pebbly muds with high organic carbon and opaline silica) in the center and towards the mouth of the bay. Sediment distribution is controlled by bay geometry and oceanographic controls while sediment

input is controlled by climate and drainage basin. Both studies found sand-rich mud deposits for the inner bay and diatom-rich mud deposits for the outer bay.

In Flandres Bay, grain size increases from head to mouth, while the highest percentage of biogenics is found in the middle of the bay (Figs. 2.4, 2.5). Oozes occur away from glaciers but inside the bay and into Gerlache Strait, which suggests high productivity in these areas that are likely protected from open water conditions and from strong currents. However, because there are no sediment flux analyses for this bay and no published studies on the activity of ocean currents inside the bay we cannot discard the possibility that these oozes are the result of downstream deposition of material from the outer bay. Sandy/pebbly sediment is present in both the outer and inner bay, although these possibly result from different processes. In the outer bay, this type of sediment is probably the result of strong currents that carry the finer particles northwards, into the Gerlache Strait, or towards the Palmer Deep area. Whereas in Etienne Fjord (inner bay), the sandy/pebbly sediment is likely part of a grounding zone area that formed when glaciers were expanded, in Briand Fjord the same type of sediments results from active deposition of a modern retreating glacier. Figure 2.8 shows a schematic representation of the various sediment distribution processes that take place in a modern environment like Flandres Bay. We estimate that thicker sediment deposits exist in the middle to outer bay due to longer open marine conditions, which would result in thinner deposits towards the inner bay. An additional analysis of shallow seismic data is necessary to confirm these assumptions.

An unexpected finding in a proximal setting, the middle of Etienne Fjord, is mud with the least percentage of biogenics and scattered to no pebbles because the glacier that feeds into Etienne Fjord (Talbot Glacier) has undergone the highest retreat of all glaciers studied in Flandres Bay (Cook et al., 2005; 2014). A recent study by Wölfl et al. (2014) in a fjord in King George Island, northern AP, found the same general trend of sediment distribution as our findings in Flandres Bay, an increase in grain size down-fjord, which was explained by an increase in energy conditions away from the bay head. We propose that the dominance of fine-grained sediment in the inner part of Etienne Fjord is a signal of the rapidly retreating ice. Further studies should assess the most proximal deposits of both retreating and advancing, or stable, ice to determine if the fine-grained deposits are truly a signal of rapid retreat, not just distance. However, there is a possibility that the anomalies found in this study may be a result of modern rapid retreat, and not a common event in the sediment record in AP fjords. If we assume that sediment has accumulated in fjord basins continuously since ice started retreating to modern positions, this would result in a very high sediment accumulation, which would eventually change the bathymetry of the fjords. Instead of having a rugged bathymetry, common in bedrock, the seafloor would be smoother, with large sediment deposits filling the basins. If this is the case, then the sediment delivered from retreating glaciers would deposit further down-fjord. In addition, ocean currents would have a higher likelihood of flowing into these areas and removing the finer particles, which would result in winnowed deposits. We propose modern fjord deposits have a greater marine influence, and less glacial influence. Although sediment input is controlled by climate and drainage basin, the marine processes play the main role regarding the distribution of the sediment.

6. Conclusions

This study presents an analysis of surface sediment in Flandres Bay. The sediment facies found in this study contrasts with other studies that suggest terrigenous deposits occur predominantly in the inner bay while biogenic deposits in the outer bay. In our study, grain size coarsens from inner to outer Flandres Bay. Sediments sampled in the head of the bay have the highest clay component whereas samples collected in the mouth of the bay have the highest sand component. Our findings suggest that discrete areas of the bay are affected differently by varying factors to distribute sediment; these factors include persistent fast sea ice, differential rates of primary productivity, and winnowing of fine grained sediments away from the bay. This variability is reflected in the accumulated deposits and must be considered when analyzing sediments down core. Additional factors such as fjord geometry, sediment flux, water currents, and glacial retreat history may also play a role in the sediment yield and distribution in Flandres Bay and in other bays in the AP. Further analysis on sedimentation rates, seafloor bathymetry, the role of meltwater, and glacier velocities will add to the understanding of the sediment distribution patterns found in this bay. The anomalies found in this study may reflect modern warming trends in the western AP and if so, then similar patterns should be found in other bays in this region. Our study emphasizes the need to understand how local signatures are reflected in the sediment record, how much variability there is among similar environments/bays, and whether or not this variability obscures regional patterns.

Chapter 3

SEAFLOOR GEOMORPHOLOGY OF WESTERN ANTARCTIC PENINSULA BAYS: A SIGNATURE OF ICE FLOW BEHAVIOR[2]

1. Introduction

While warming temperatures in the Antarctic Peninsula (AP) have resulted in the retreat of 90% of the regional glaciers (Cook et al., 2014) and the collapse of ice shelves (Morris & Vaughan, 2003; Cook & Vaughan, 2010), recent studies have shown that since the late 1990s this region is currently experiencing a cooling trend (Turner et al., 2016). The AP is a dynamic region that serves as a natural laboratory to study ice flow and the resulting sediment deposits. As the ice retreats, it leaves behind glacial geomorphic features on the seafloor; these submarine landforms have been mapped in glaciated environments in Antarctica (Anderson et al., 2001; Wellner et al., 2001; Evans et al., 2004; Heroy & Anderson, 2005; Wellner et al., 2006; Larter et al., 2009; Livingstone et al., 2013; Hodgson et al., 2014), southern Chile (Dowdeswell & Vasquez, 2013), North America (Dowdeswell et al., 2016) and northern Europe (Ottesen et al., 2005; Ottesen & Dowdeswell, 2006; Ottesen & Dowdeswell, 2009; Dowdeswell et al., 2010) giving insight into the glacial history of each region. Several seafloor features have been mapped

west of the AP on the continental slope and continental shelf (Dowdeswell et al., 2004; Graham & Smith, 2012; Gales et al., 2013), the South Shetland Islands (Milliken et al., 2009; Simms et al., 2011), South Georgia Island (Hodgson et al., 2014; Graham et al., 2017), Bransfield Strait (Canals et al., 2000; Canals et al., 2002), Gerlache Strait (Evans et al., 2004), south of Anvers Island (Domack et al., 2006) and Marguerite Bay (Ó Cofaigh et al., 2002; Anderson & Fretwell, 2008; Livingstone et al., 2013). However, the seafloor geomorphology in western AP bays has not been described in detail, except for a few locations (Garcia et al., 2016; Munoz & Wellner, 2016; Wölfl et al., 2016). Although most of the data we present are publicly available, this is the first instance, to our knowledge, that a detailed description of the seafloor geomorphology of a large number of western AP fjords has been completed.

We combine multibeam swath bathymetry data collected during seven cruises to the Antarctic Peninsula. The multibeam bathymetry data presented in this study expose geomorphic features formed during past ice flow in several bays in the western Antarctic Peninsula, the South Shetland Islands, and Anvers Island (Fig. 3.1). We focus this study on four bays throughout the AP: Maxwell Bay, located on King George Island (KGI), north of the AP; Hope Bay, located on the northernmost tip of the AP known as the Trinity Peninsula; Lapeyrère Bay, on Anvers Island, west of the AP; and finally, Beascochea Bay, located in the Graham Land Coast of the western AP (Fig. 3.1). Data from additional bays throughout the AP (found in appendix B) have been integrated in the results section to support this investigation. The glacial seafloor features reveal flow
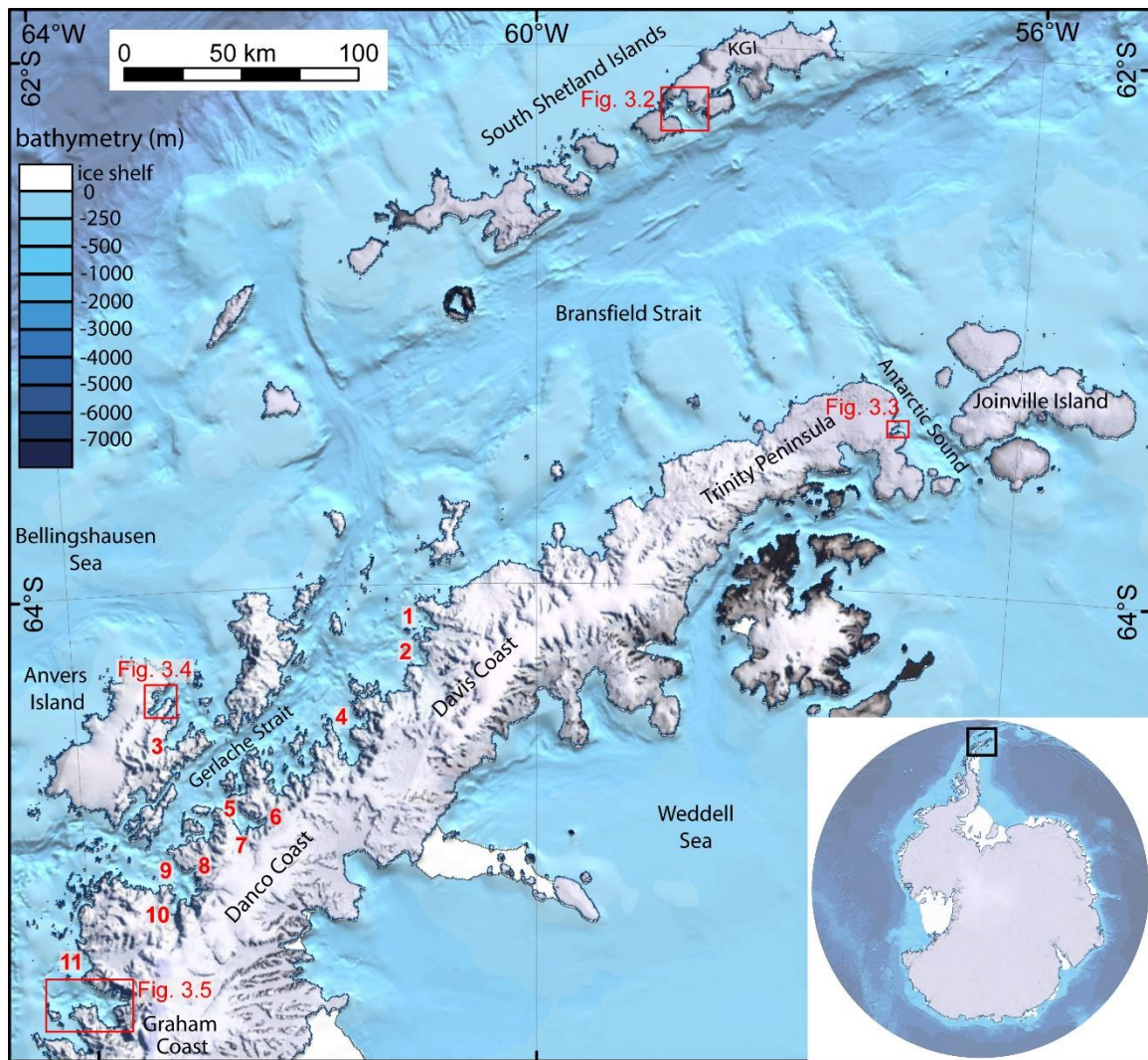
Figure 3.1 Map of the northern Antarctic Peninsula (AP) and South Shetland Islands, red boxes indicate Figures 3.2-3.5. Inset shows the location of the AP in Antarctica. KGI: King George Island, 1 Cierva Cove, 2 Brialmont Cove, 3 Fournier Bay, 4 Charlotte Bay, 5 Andvord Bay, 6 Moser Glacier 7 Lester Cove, 8 Briand Fjord, 9 Flandres Bay, 10 Etienne Fjord, 11 Collins Bay. Individual maps of bays 1-11 found in appendix B. AP map from Polar Geospatial Center, bathymetry and inset from IBCSO (Arndt et al., 2013).

behavior of grounded ice; structures formed in a deformable sedimentary substrate likely

represent subglacial conditions shortly before ice decoupling from the seafloor, and

structures in bedrock likely formed over several glacial-interglacial cycles (Wellner et al.,

2001; Campo et al., 2017). We map the glacial landforms and analyze local variables including bay length and width, glacier drainage size flowing into the bays, seafloor lithology, and water depth in order to understand the controls of ice flow and retreat dynamics in these locations.

2. Study area

The AP is the northernmost extent of the Antarctic continent. The AP is a long (~1200 km), thin (~250 km) strip of mountains of up to 3500 m in elevation. The geological setting of the AP is characterized by Cenozoic tectonic extension and active volcanism (Griffith & Anderson, 1989). Glacial ice flow over crystalline bedrock has preferentially eroded over joints and faults, accentuating their appearance (Domack et al., 2006). The predominant rock types are metamorphic and intrusive and extrusive igneous rocks (Griffith and Anderson, 1989). Ice covers about 80% of the AP, where ice thickness ranges between 400 to 800 m (Fretwell et al., 2013) and averages about 500 m. The ice cap covering Anvers Island reaches up to 600 m, similar to the western AP (Ashley and Smith, 2000), while in King George Island, the ice cap is only 150-200 m thick (Simms et al., 2011).

The high peaks of the AP form a topographic barrier to the westerly winds resulting in a warmer, wetter western AP, and a cooler, dryer eastern AP (Ó Cofaigh et al., 2014). The climate in Hope Bay (northern AP, Fig. 3.1) is cold, dry semi-polar (Pereira et al., 2013). Annual air temperature at Esperanza Research Station (located in Hope Bay) range between -30.6° C and 11.8° C, with an average of -5.1° C, and an annual

precipitation of 250 mm measured between 1952 and 2010 (Pereira et al., 2013; Schaefer et al., 2016). In contrast, the western AP receives an average of 1100 mm/yr, measured between 1997 and 2006 (Thomas et al., 2008), and up to 2900 mm/yr in some bays (Fernandez et al., 2016). Annual air temperatures in the western AP vary between slightly above 0° C in the summers to -8° to -11° C in the winters (King et al., 2003). Sea ice covers the bays seasonally, but most areas are sea-ice free during the summers (Domack & Ishman, 1993). The islands experience a maritime climate. KGI has a temperate to sub-polar glacial setting (Yoon et al., 2004), with little changes in air temperature throughout the year (average of -1.8° C, minimum of -5.7° C in July, and maximum of 2° C in January). Mean annual precipitation is about 1200 mm on the higher elevations, but much less in areas like Potter Cove where precipitation data indicate an annual average of 524 mm (Lee et al., 2008; KOPRI, 2014; Moon et al., 2015; Fernandez et al., 2016). In Anvers Island (west of the AP, Fig. 3.1), summer air temperatures reach up to 6-7.5° C, while in the winter the average is -5° C (Ashley & Smith, 2000). Precipitation in Anvers Island is on average approximately 1200 mm annually (Griffith & Anderson, 1989; Ashley & Smith, 2000) and up to 2000 mm/yr in Lapeyrère Bay, northern Anvers Island (Fernandez et al., 2016).
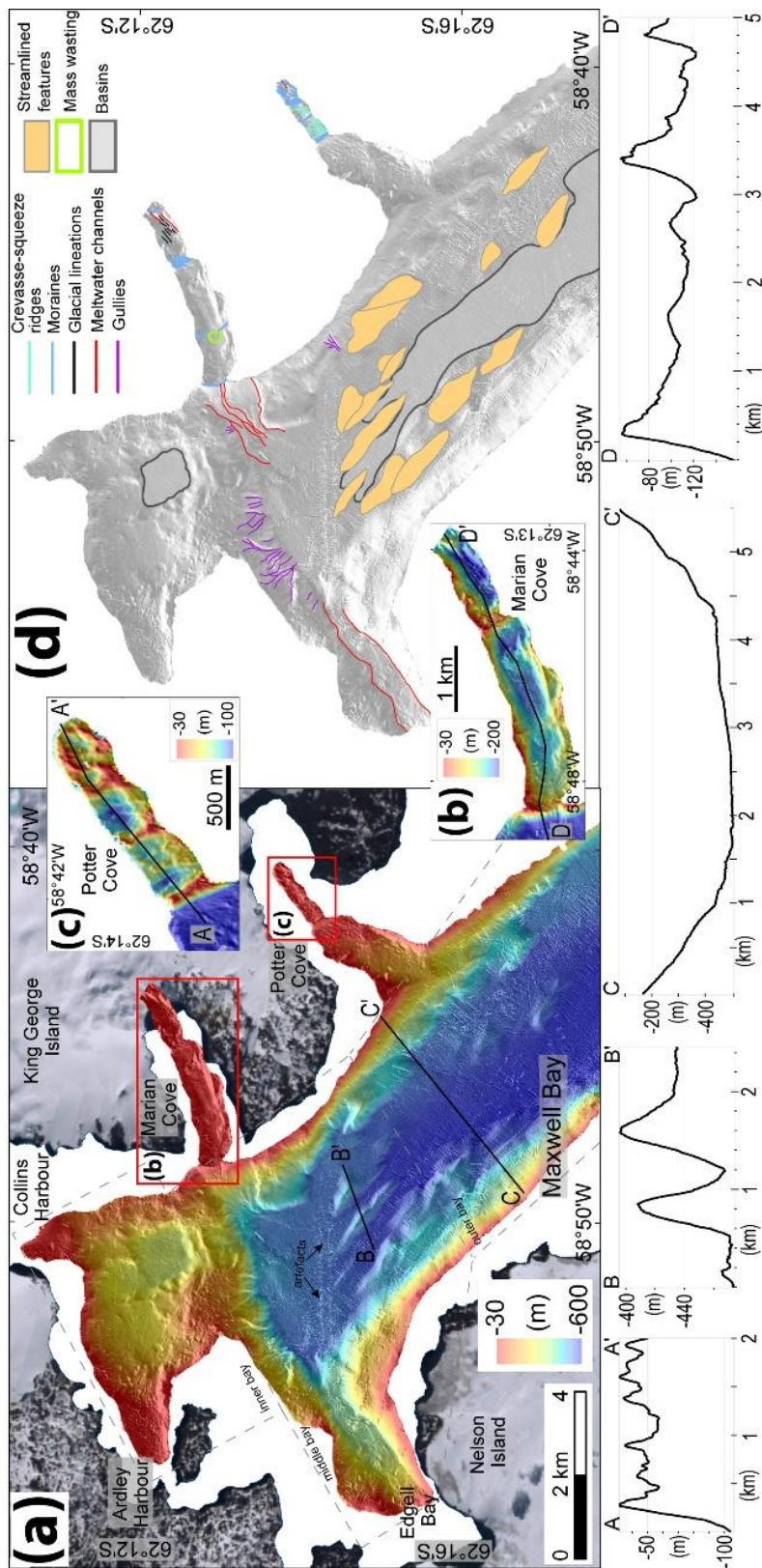
Figure 3.2 Multibeam swath bathymetry of Maxwell Bay (a), Marian Cove (b), and Potter Cove (c), vertical exaggeration is 5x in all images. (d) Interpretation of geomorphic features with hillshade as background. Cross sections A-A' and D-D' show transverse ridges in Potter Cove (c) and Marian Cove (b) respectively, B-B' shows elongated ridges in the bay, C-C' shows the U-shaped fjord valley.

45

2.1 Maxwell Bay

Maxwell Bay (62°13.7'S, 58°50.9'W) (Fig. 3.2) is located in the western end of King George Island. Maxwell Bay is about 15 km long, between 6-15 km wide, and has an approximate area of 140 km^2. Maxwell Bay has several embayments: Edgell Bay, Ardley Harbor, Collins Harbor, Marian Cove (Fig. 3.2b), and Potter Cove (Fig. 3.2c). Water depths vary widely from 35 m in the inner bay to 500 m in the outer bay. The outer bay is U-shaped (Fig. 3.2, C-C'), with tens of meters of sediment cover (Milliken et al., 2009; Fernandez et al., 2015). The glacier catchment area around Maxwell Bay is about 92 km^2, separated into four discrete glaciers. Collins Harbor, at the north end of Maxwell Bay, has a sediment accumulation rate of 5.5 mm/yr (Boldt et al., 2013).

Marian Cove (62°12.8'S, 58°46.1'W) (Fig. 3.2b) is an elongated bay in northeastern Maxwell Bay. The bay is approximately 4 km long and between 1-1.5 km wide, with an approximate area of 5 km^2. A single tidewater glacier (with a catchment area of about 15 km^2) drains directly into the bay. This glacier retreated about 1.7 km between 1956 and 2013 (Lee et al., 2008; Moon et al., 2015). Large meltwater and sediment influx into the bay occur in the summer months (Moon et al., 2015). Sediment accumulation rates vary between 5.2 and 6.6 mm/yr in Marian Cove (Boldt et al., 2013).

Potter Cove (62°13.9'S, 58°41.2'W) (Fig. 3.2c) is an elongated bay in southeastern Maxwell Bay. Potter Cove is approximately 4 km long and between 1 km wide in the bay head and 2.5 km wide in the bay mouth, approximately 7 km^2 in total area, and with water depths ranging between 25-150 m. Fourcade Glacier drains directly into this bay, however most of it terminates on land. The glacier catchment area is about 20 km^2. Ice

front retreat of Fourcade Glacier has been approximately 1 km in Potter Cove between 1956 and 2008 (Wölfl et al., 2016), with a greater retreat of grounded ice in the tidewater part of the glacier and much less on the land-based grounded ice (Ruckamp et al., 2011). Meltwater discharges are common in Potter Cove, especially during the summer (Wölfl et al., 2014), with sediment accumulation rates in outer Potter Cove of 1.6 mm/yr (Boldt et al., 2013).

2.2 Hope Bay

Hope Bay (63°24.4'S, 57°2.8'W) (Fig. 3.3) is located along the northernmost tip of the Antarctic Peninsula, draining into the Antarctic Sound. The bay is 6 km long, and between 800 m wide in the bay head and 3 km wide in the bay mouth; the bay area is about 11.5 km^2. Water depths in Hope Bay vary between 50-320 m. Two large glaciers drain directly into the bay; Depot Glacier (catchment area of 7 km^2) and Arena Glacier (catchment area of 16 km^2). In addition, three unnamed glaciers (each with an average area of 3 km^2) also discharge into Hope Bay. Boldt et al. (2013) measured a sediment accumulation rate of 3 mm/yr in Hope Bay.
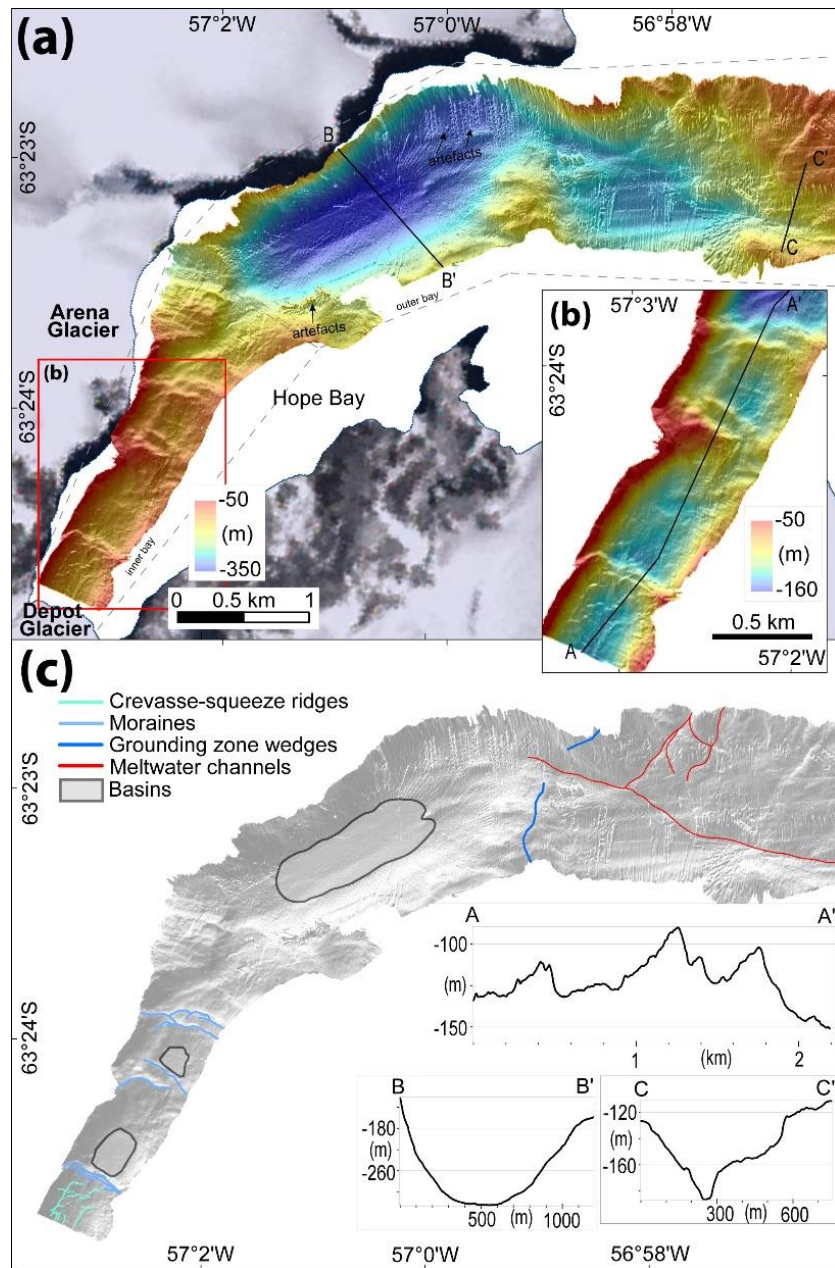
Figure 3.3 Multibeam swath bathymetry of Hope Bay (a), the inner bay area (b), and interpretation of geomorphic features with hillshade as background (c). Transverse ridges can be seen in A-A', the U-shaped fjord valley is seen in B-B', and a meltwater channel in the outer bay (C-C'). Vertical exaggeration is 3x in all images.

2.3 Lapeyrère Bay

Lapeyrère Bay (64°25.3'S, 63°17'W) (Fig. 3.4) is located in northeastern Anvers Island. Lapeyrère Bay is a narrow, elongated bay with water depths varying from 250-740 m. The bay is 11 km long, 2 km wide in the bay head and 3.5 km in the bay mouth, with an overall bay area of 32 km^2. One large glacier, Iliad Glacier (catchment area of 234 km^2), drains into the bay, in addition to other smaller glaciers around the perimeter of the bay, each with an average catchment area of 6 km^2. Sediment accumulation rates in Lapeyrère Bay are 2.2-3.2 mm/yr (Boldt et al., 2013).

2.4 Beascochea Bay

Beascochea Bay (65°31'S, 63°52.2'W) (Fig. 3.5) is the southernmost bay presented in this study. It is an elongated bay with several embayments in the bay head, three of them described below. Each one of the described embayments has a large glacier draining directly into it. None of the coves are named and therefore, for the purposes of this paper, we use the name of the glacier to identify the cove; Lever Glacier cove, Funk Glacier cove, and Cadman Glacier cove. Beascochea Bay is approximately 24 km long, 6-13 km wide, with an approximate bay area of 235 km^2. Several glaciers drain into this bay along its perimeter; their individual catchment area varies between 1-28 km^2. Sediment accumulation rates in Beascochea Bay vary between 2.2 and 7 mm/yr (Boldt et al., 2013).
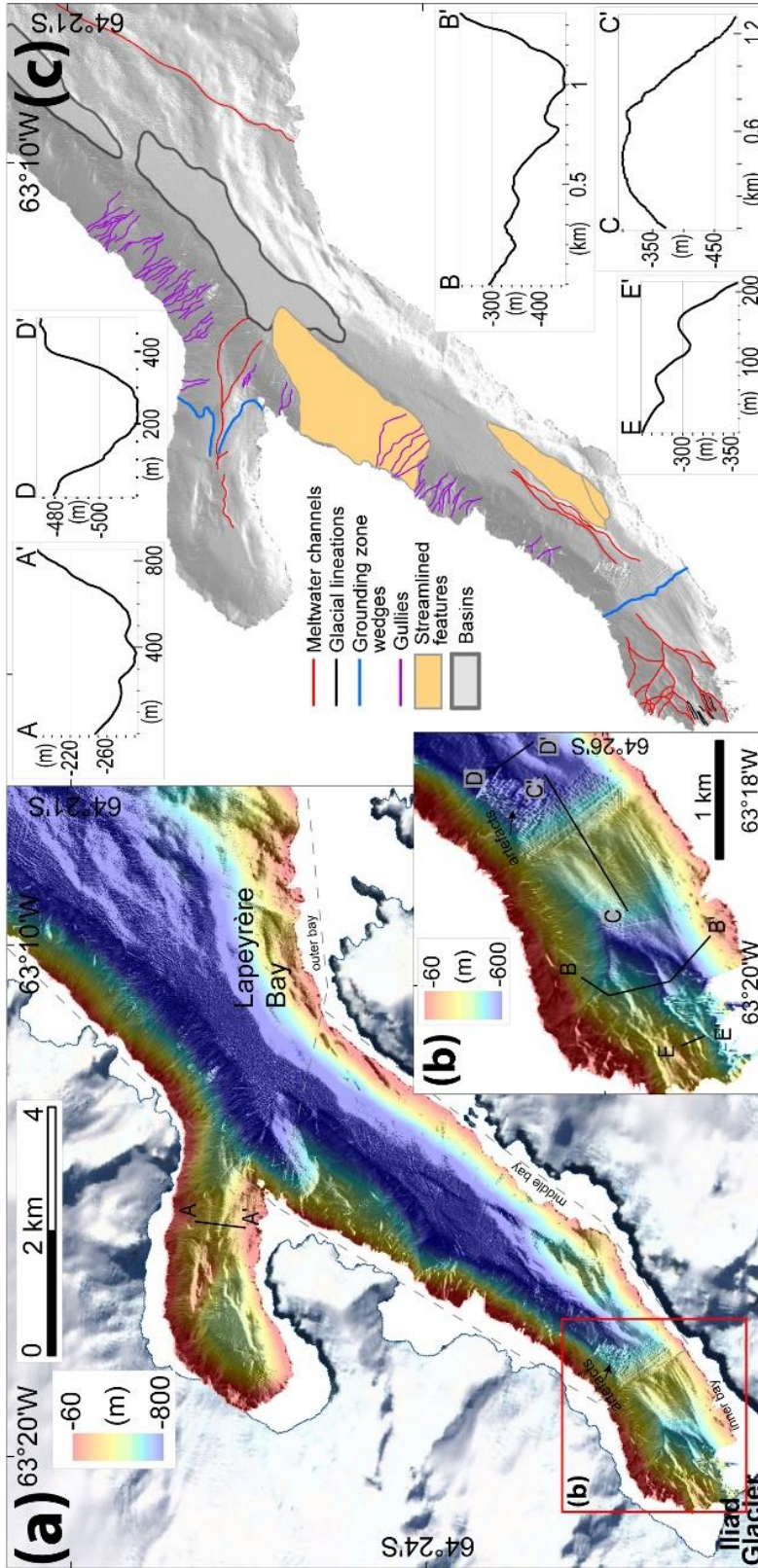
Figure 3.4 Multibeam swath bathymetry of Lapeyrère Bay (a), the inner bay area (b), and the interpretation of geomorphic features with hillshade as background (c). Cross section A-A', B-B', and D-D' show meltwater channels around the bay, C-C' shows the grounding zone wedge in the inner bay, and E-E' show glacial lineations in the inner bay area. Vertical exaggeration is 5x in (a) and 3x in (b).

Lever Glacier cove (65°30.7'S, 63°43.4'W) (Fig. 3.5b) is an elongated bay, 6 km long and 3 km wide, with a total bay area of about 16 km^2. The largest glacier draining into this cove is Lever Glacier (catchment area of 177 km^2), other glaciers draining into the bay are much smaller (individual average area is about 4 km^2). Funk Glacier cove (65°34.8'S, 63°45.4'W) (Fig. 3.5c) is an elongated bay, 4 km long and 2 km wide, with a total bay area of about 8 km^2. A large glacier drains directly into this cove, Funk Glacier, with a surface area of 158 km^2. Another small glacier, with a surface area of 3 km^2, also flows into the cove. During the late 1960s, this cove was covered by ice (Cook et al., 2014). Although it is unclear whether the ice cover was grounded ice or permanent sea ice, the fact that this area has alternated between ice-free and ice-covered since the late 1960s suggests fast sea ice cover and not grounded ice. Cadman Glacier cove (65°36.7'S, 63°48.7'W) (Fig. 3.5c) is the smallest cove surveyed in Beascochea Bay; it is 3 km long and 3 km wide, the total bay area is about 9 km^2. One large glacier drains directly into this cove, Cadman Glacier, with a surface area of 307 km^2.
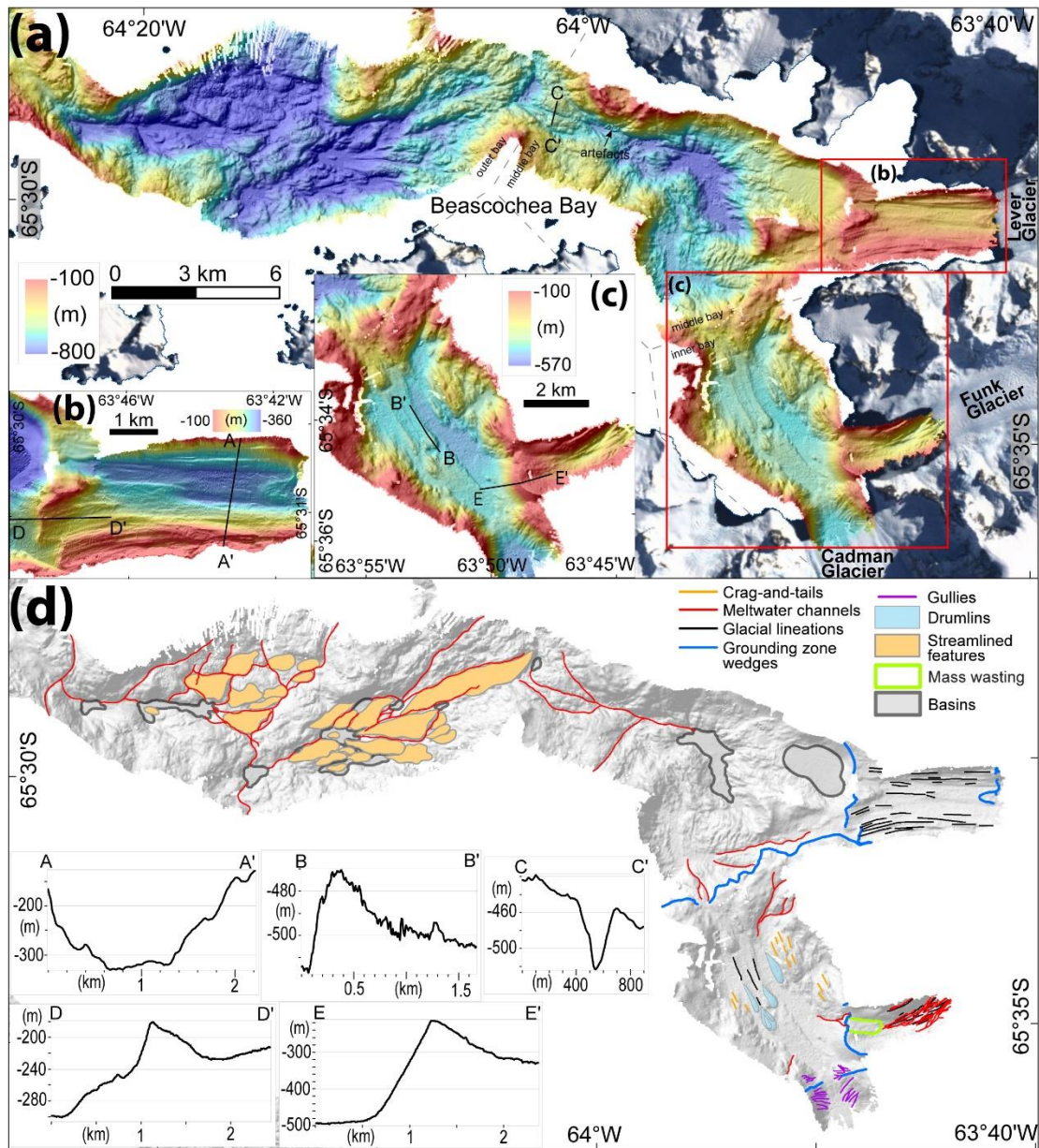
Figure 3.5 Multibeam swath bathymetry of Beascochea Bay (a), Lever Glacier cove (b), the inner bay area (c), and the interpretation of geomorphic features with hillshade as background (d). A-A' shows glacial lineations in Lever Glacier cove, B-B' show a drumlin in the inner bay area, C-C' show the cross-section profile of a meltwater channel, D-D' and E-E' show large transverse ridges. Vertical exaggeration is 3x in all images.

52

3. Methods

Multibeam swath bathymetry data were collected on multiple research expeditions to the western AP aboard the RV/IB *Nathaniel B. Palmer* (NBP0201, NBP0502, NBP0602A, NBP0703, NBP1001, and NBP1203) and the RV/IB *Araon* (ARA1304). Multibeam soundings were collected in a swath perpendicular to the ship track using a hull-mounted Kongsberg EM120 multibeam echo-sounder, with a swath of 191 beams, operating at a frequency of 12 kHz on the NBP cruises and Kongsberg EM122, with a swath of 432 beams, operating at a frequency of 12 kHz on the ARA cruise. These data sets were merged using CARIS HIPS & SIPS where the survey data were manually edited to remove anomalous readings and gridded to create relief maps. Grids were created per bay at resolutions of 25 m and in some cases 10 m. Here we show the optimal resolution of the data, which in most cases is the 25-m grid. These grids were then imported into ArcGIS 10 where hillshade effect was created with a z-factor >1 to simulate vertical exaggeration. This compilation of bathymetry in addition to other data sets have recently been published in Boldt et al. (2013) and Lavoie et al. (2015). In addition to mapping the submarine landforms, we compare them to the local physiographic variables of each bay including latitude, area, length, width, glacier catchment area, and the seafloor lithology based on CHIRP results, to understand controls on ice flow behavior. High resolution shallow sub-bottom CHIRP profiles were collected during NBP0703 throughout the study area. The data were collected using a hull-mounted Knudsen 320B/R with a frequency of 3.5 kHz and have been interpreted using SMT Kingdom software. CHIRP sonar provides a vertical resolution of about 1 m and

can image unconsolidated sediments up to 100 m below the seafloor. The CHIRP data were used to identify seafloor lithology (sediment type or bedrock) and the thickness of sedimentary units.

4. Bathymetry Results

We describe the seafloor landforms identified in the bays of the western AP. Fig. 3.6 shows some of these individual landforms mapped on the seafloor and Table 3.1 lists the criteria for identification in this study. The interpreted CHIRP facies are shown in Fig. 3.7. Maps of interpreted seafloor features throughout individual bays are shown in Figures 3.2-3.5 and in the supplementary material (appendix B). In addition, data tables in the supplementary material (appendix B) show the bay location, length, width, area, number of glaciers in each bay, total glacier catchment area, and the submarine landforms found in each bay.

4.1 Maxwell Bay

The seafloor in northern Maxwell Bay (Fig. 3.2), near Collins Harbor and Ardley Harbor, is a large, shallow platform with water depths up to 280 m. Water depths increase rapidly to >400 m in the middle of the bay, where gullies and channels that cut into the seafloor can be found. Meltwater channels (1-4 km long, 10-30 m wide, and 1-2 m deep) are present on the seafloor from Edgell Bay and from Marian Cove, trending towards the middle of Maxwell Bay. Large promontories are located between King George Island and

Nelson Island. A few elongated hills, parallel to the bay axis, are present in the middle of the bay (Fig. 3.2, B-B'). These seamounts range in length 1-2.5 km, maximum width of 200-800 m and a maximum height of 10-50 m. Sediment thickness in the outer bay are in excess of 100 m (Milliken et al., 2009), and therefore other features carved by flowing ice in this area, if any, are buried. Simms et al. (2011) described a large sediment fan at the mouth of Maxwell Bay, draining out of the bay into the Bransfield Strait. The fan has a sediment thickness of up to 1000 m and it is located in water depths between 400 and 1400 m.

Table 3.1 Geomorphic features mapped and criteria for identification

Glacial landform	Defining characteristics	Dimensions min-max (meters) length, width, height	Formation interpretation	Example
Crevasse squeeze ridge	Small, short ridges, cross cutting each other or isolated	30-300, 10-30, 1-3	Depositional, form in crevassed glacier terminus	Fig. 3.6g
Moraine	Transverse ridge, found individually or amalgamated	250-1000, 100-300, 8-30	Depositional, form in front of glacier terminus during short episode of ice stability	Fig. 3.6g
Grounding zone wedge	Transverse ridge, wedge shaped, steep distal and gentler proximal side	800-8000, 80-2500, 10-130	Depositional, form in front of glacier terminus during long episode of ice stability	Fig. 3.6e
Glacial lineation	Elongated, symmetric, parallel to semi-parallel ridge (to one another and to bay length)	80-2700, 5-200, 1-20	Depositional or erosional, form by ice ploughing	Fig. 3.6a
Drumlin	Tear-drop shaped with tail, formed in deformable sediment	500-1200, 60-380, 5-30	Depositional or erosional, form in glacigenic sediment	Fig. 3.6c
Crag-and-tail	Tear-drop shaped or large bedrock protrusion with tail, parallel to semi-parallel (to one another and to bay length)	130-900, 40-300, 2-28	Depositional or erosional, form in till or bedrock	Fig. 3.6d
Streamlined feature	Elongated hill formed in bedrock, symmetric to asymmetric	260-5000, 130-1200, 8-220	Erosional, in bedrock	Fig. 3.6b
Meltwater channel	Linear to sinous channels, formed in bedrock or sedimentary unit, found individually or in networks, abrupt initiation and termination points	270-7000, 8-800, 1-120	Erosional, in bedrock or sedimentary units	Fig. 3.6d
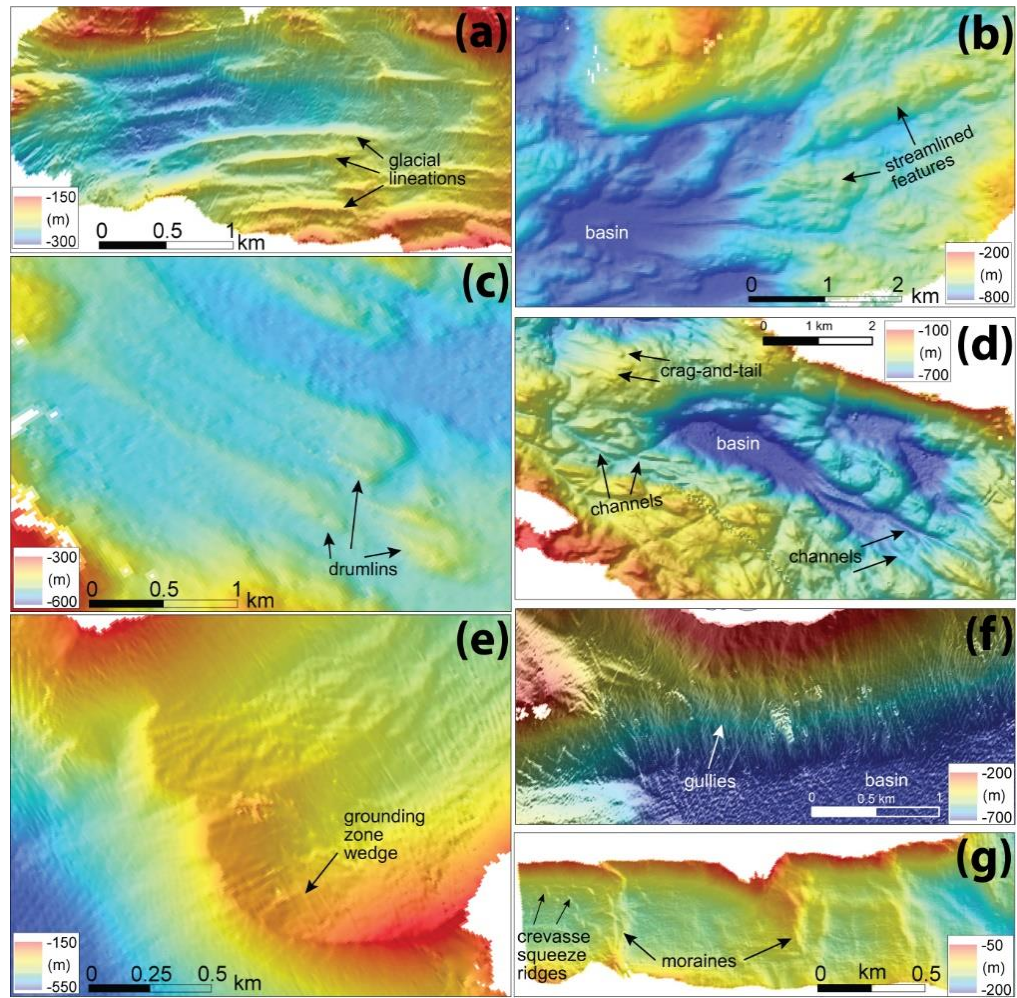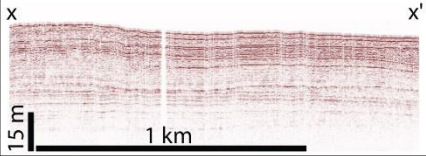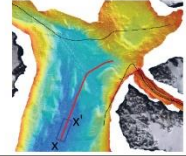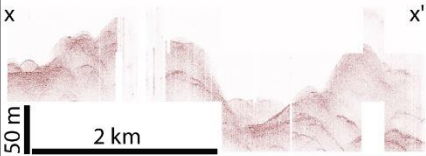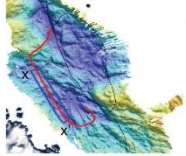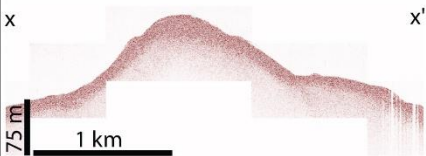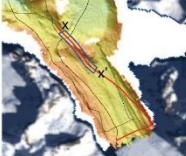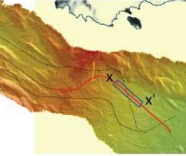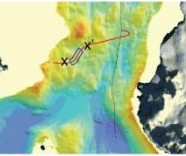
Figure 3.6 Seafloor landforms found in the bays of the western Antarctic Peninsula: (a) glacial lineations, (b) streamlined features and basin, (c) drumlins, (d) crag-and-tails, meltwater channels, and basin, (e) grounding zone wedge, (f) gullies and basin, (g) moraines and crevasse squeeze ridges.

The seafloor topography of Marian Cove (Fig. 3.2b) is characterized by transverse ridges in the bay (Fig. 3.2, D-D'). Three major transverse ridges divide the bay into a proximal, middle, and outer basin. The proximal basin is the deepest, up to 135 m depth compared to 120 m and 110 in the middle and outer basin, respectively. The outer, most distal transverse ridge separates Marian Cove from Maxwell Bay. This feature is at least

650 m long, 200 m wide, and 20 m high. Although this feature is found across the width of the bay, water depth varies along the ridge crest from 40 m in the north to 70 m in the south. The middle ridge (approximately 1 km long, 100 m wide, and 8 m high) appears breached, with a possible slope-failure deposit located on the west side of the ridge. Unfortunately, the resolution of the data is not clear enough to fully resolve this feature. However, the deposits have a fan shape and the water depths are shallower in this area indicating a likely mass wasting deposit. The inner, most proximal ridge (approximately 500 m long, 300 m wide, and between 20-30 m high) is wider than the other two and it could possibly be an amalgamation of more than one ridge. The data show hints of other, smaller ridges across the bay, located between the larger ridges, but these are not resolved due to the low resolution of the data. The inner (most proximal) basin seafloor shows elongated (80-340 m long), narrow hills (10-35 m wide, 1-2 m high), parallel to the bay axis, unevenly-spaced. Lastly, a topographic high, about 250 m long, 200 m wide, and 15 m high is located on the eastern end of the surveyed area, close to the modern ice front where a meltwater channel is identified. This feature is about 430 m long, 20 m wide, and 2 m deep.

Potter Cove (Fig. 3.2c) is separated from Maxwell Bay by a shallow sill, approximately 130 m wide and 12 m high. The seafloor geomorphology in Potter Cove is characterized by numerous transverse features (Fig. 3.2, A-A'). Although the multibeam survey covers a small portion of the bay (Fig. 3.2a), transverse ridges across the bay are abundant in the data set. We have classified the transverse ridges into two sets: 1) continuous ridges across the width of the surveyed area, individual ridges symmetrical in

cross-section profile, approximately 300-400 m long, 100-160 m wide, and 10-14 m high, and 2) semi-continuous ridges, semi-transverse to the cove, some cross-cutting each other, in which individual ridges are approximately 50-300 m long, 15-30 m wide, and 1-3 m high, with jagged crests and symmetrical cross-section profiles, located between the larger transverse ridges. Unlike the discrete transverse ridges in the mouth of the bay, ridges proximal to the head of the bay are arcuate and breached by a meltwater channel (280 m long, 8 m wide, and about 1 m deep).

Facies	Description	Interpretation	CHIRP example	Multibeam example
1	Acoustically layered, parallel reflectors	Glaciomarine sediments infilling basins	15 m / 1 km	
2	Bowtie or hummocky, chaotic reflectors	Bedrock	50 m / 2 km	
3	Strong surface, little to no acoustic penetration	Till and/or bedrock	75 m / 1 km	
4	Thin, acoustically semi-transparent drape, overlying a strong reflector	Thin, fine-grained sediment cover	25 m / 200 m	
5	Weak reflector, mound shape	Slump, debris flow deposits	25 m / 300 m	

Localized examples:
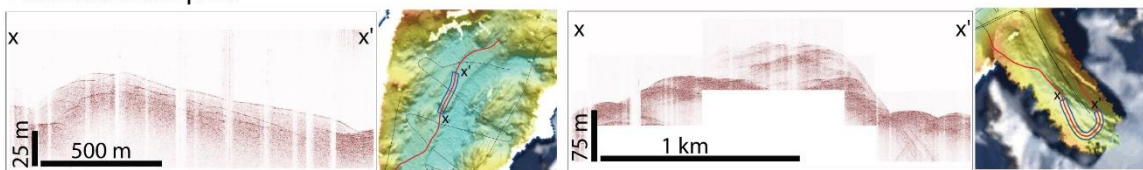
(a) Asymmetric wedge with reflectors: thin sediment cover, drumlin

(b) Stacked sediment packages: channel-glacial lineation pair, near ice front

Figure 3.7 CHIRP facies showing seafloor lithology. Five facies were identified throughout the bay, in addition, two localized examples of features are shown: (a) drumlin and (b) glacial lineations near the modern ice front. The blue rectangle in multibeam example shows the location of the CHIRP example shown.

4.2 Hope Bay

The seafloor in inner Hope Bay (Fig. 3.3) is characterized by several transverse ridges (Fig. 3.3b, A-A'), while the outer bay is characterized by a large, deep basin (Fig. 3.3, B-B'). Three sets of transverse ridges are present in the inner bay. Each one of these sets of ridges appears as a composite feature of more than one ridge stacked on or near one another. The most distal set of transverse ridges is at least 630 m long across inner Hope Bay, approximately 200 m wide, and 15 m high. The next set is 560 m long, with a width of up to 300 m and height ranging 10-20 m. The most proximal set of ridges measure 500 m long, 160 m wide, and 10 m high. The location of the proximal ridges matches the ice extent mapped in the late 1950s (from Cook et al., 2014), which suggests ice was grounded at this site forming the transverse ridges. The seafloor between the proximal set of transverse ridges and the modern ice front is covered by a series of discrete, arcuate-shaped ridges, some cross-cutting each other. The individual ridges are on average 30 m long (but up to 260 m in one case), 10-25 m wide, and 1-3 m high. These features have a symmetrical cross-section profile. Two large promontories separate the inner bay from the outer bay; immediately followed by a large (2 km^2 area) flat-bottomed basin. The outer bay is separated from the Antarctic Sound by a transverse bathymetric high, only partially surveyed, which is cut through by a meltwater channel (50 m deep, 300 m wide) that trends towards the Antarctic Sound (Fig. 3.3, C-C').

4.3 Lapeyrère Bay

The seafloor in front of Iliad Glacier in Lapeyrère Bay (Fig. 3.4b) is characterized by poorly-defined, elongated features (Fig. 3.4, E-E') and numerous meltwater channels (Fig. 3.4, B-B'). The elongated features are symmetrical, approximately 180-300 m long, 40 m wide, and 10 m high. The meltwater channels trend from the ice front margin towards the middle of the inner Lapeyrère Bay, separated from the middle and outer bay by a large transverse ridge (Fig. 3.4, C-C'). The meltwater channel lengths vary between 1.2 km and 2.5 km, channel widths are up to 200 m, and channel depths are 10-30 m. The transverse ridge is located 2.5 km from the Iliad Glacier front. The ridge is approximately 3 km long and 60 m high; width varies along the ridge, from 500 m near the bay walls to 2500 m in the middle of the inner bay. The ridge has an asymmetrical cross-section profile (Fig. 3.4, C-C'), with a gentle slope on the proximal side and steeper slope on the distal side. A long (5 km) meltwater channel emerges from the distal side of the transverse ridge and trends towards the middle of the bay (Fig. 3.4, D-D'). The channel is wide (300 m), with steep walls and a flat base 30 m deep. An elongated ridge is present in the middle bay, parallel to the bay axis. The ridge is about 2.2 km long, up to 400 m wide, and 220 m high. The seafloor in the middle and outer Lapeyrère Bay is smooth and gently dipping towards the outer bay. Abundant slope failures are observed on the steep walls of the fjord. A small, unnamed embayment (5 km long, 2 km wide) is located on northwestern Lapeyrère Bay. An unnamed glacier, with a catchment area of 57 km^2, drains into this unnamed embayment. A sinuous ridge, transverse to ice flow, now breached by meltwater channels and slope failures (Fig. 3.4, A-A'), is present in the

61

embayment mouth. The transverse ridge has an asymmetrical cross-section profile, it is 2.5 km long, 100 m wide, and up to 70 m high.

4.4 Beascochea Bay

The inner bay area (Fig. 3.5c), at the convergence of Cadman and Funk glaciers, is separated from the middle bay by an elongated feature, transverse to the bay length. The ridge is about 8 km long, 220 m high, and up 1 km wide. Some areas along this mount are rugged, possibly indicating bedrock. The features present in inner Beascochea Bay are drumlins, glacial lineations, and crag-and-tail landforms. Drumlins are tear-drop shaped, 600-1400 m long, 200-380 m wide, and 20-30 m high. The steep lee side points towards Cadman Glacier and the gentler, stoss side points towards the transverse ridge (Fig. 3.5, B-B'). CHIRP data shows these are sedimentary features (Fig. 3.7a). The drumlins are immediately followed by glacial lineations, located at the gentler end of the drumlins. These elongated landforms are 240-2600 m long, 30-170 m wide, and 2-10 m high. Crag-and-tail landforms are located peripherally to the drumlins and lineations, along the bay walls. These elongated features are 200-500 m long, 60-120 m wide, and 10-15 m high, and formed by a bedrock knob with a tail of sediment. Middle Beascochea Bay is characterized by a rugged seafloor with linear meltwater channels (Fig. 3.5, C-C') and large (2.5 km^2), deep (240 m) flat-bottomed basins. The meltwater channels have a V-shaped cross-sectional profile, cut into bedrock, and vary in depth (15-60 m), width (80-200 m), and length (200-2000 m). Some of these long, straight channels may be preferentially eroding joints and faults, similar to other areas along the AP shelf (Domack

et al., 2006). The bathymetry in outer Beascochea Bay is also rugged, but this region is characterized by an anastomosing network of meltwater channels cutting through bedrock and flowing between elongated mounts, with a few small (<1 km^2 area), deep (50-100 m depth), flat-bottomed basins located between the mounts. Water depths in this area vary between 600-800 m. The meltwater channels vary in depth (20-50 m), width (140-250 m), and length (100-3000 m), some with a V-shaped channel cross-section profiles and others with a U-shaped, flat-bottomed profiles. The channels have abrupt initiation points but terminate, generally, into the small basins that connect to other channels. Channel orientations vary from parallel to oblique to bay axis. The elongated mounts are asymmetric, carved in bedrock, with varying length (260-5000 m), width (210-1000 m), and height (15-90 m).

Lever Glacier cove is separated from middle Beascochea Bay by a transverse ridge (Fig. 3.5, D-D'). This feature has been partially surveyed but shows a wedge-shaped cross-sectional profile, steep distal side and gentler proximal side. The ridge is at least 5 km long, up to 1.5 km wide, and between 70 and 180 m high. Another transverse ridge is located less than 1 km from the modern ice front of Lever Glacier. The ridge was only surveyed in the northern area of the cove but it is likely present across the bay, next to the modern glacier front. It is sinuous (about 2.5 km long, 20 m high) with a prominent knob in the middle of the cove. This knob coincides with the deepest area in the cove, enhancing it further in the bathymetry. The seafloor of this cove is covered by glacial lineations (Fig. 3.5, A-A'), present from the proximal to the distal transverse ridges. The lineations are semi-parallel to the axis of the cove, individual features have a symmetric cross-sectional profile, and vary in length (400-1400 m), width (100-150 m), and heights

(5-10 m), as well as the distance between the ridge crests (90-260 m). Although water depths within the cove vary from 120-320 m, the glacial lineations are present throughout the cove regardless of water depth (Fig. 3.5b). In the CHIRP dataset, the lineations are characterized by a strong surface with no internal reflectors, which likely indicates till (Fig. 3.7).

Funk Glacier cove and inner Beascochea Bay are separated by a large (2.3 km long, 800-1000 m wide, 60-150 high), wedge-shaped transverse ridge (Fig. 3.5, E-E'). The eastern (proximal) side of the ridge is covered by a 20-m high, 1.4-km long feature that resembles a mass wasting deposit. However, this feature could also be the result of meltwater deposition generated when the ice was grounded nearby. Higher resolution multibeam data are needed to better characterize this feature and sediment analysis to interpret its depositional origin. Several glacial lineations are present on the seafloor and can be traced from the middle of the cove to the modern front of Funk Glacier. Individual features have a symmetrical cross-sectional profile, are parallel to one another, and have varying height (5-20 m), width (40-100 m), and length (160-700 m). Unlike the lineations in Lever Glacier cove, the subsurface of these landforms resembles an amalgamation or stacked sediment packages (Fig. 3.7b), most likely recently reworked till. A network of meltwater channels originates near the ice front and trend towards the middle of the fjord. Channel depths vary (6-20 m), as well as widths (30-200 m), and lengths (70-1200 m).

In Cadman Glacier cove we identify large promontories (up to 300 m high) on each side of the cove mouth, separating the cove from inner Beascochea Bay (Fig. 3.5c).

Abundant slope failures are present on the sides of the promontories. The middle of the cove has a flat basin with water depths down to 550 m.

5. Discussion

5.1 Distribution and interpretation of seafloor features

We have described numerous seafloor features in four bays in the western AP (additional bays are shown in appendix B). Many of the bays show similar landform distributions and therefore we propose a schematic model representative of an assemblage of submarine landforms in bays from the western AP (Fig. 3.8). This spatial distribution of landforms, from the modern ice front to the outer bay area, results from combining the geomorphology of all the bays presented. The inner bay is characterized by glacial lineations, straight meltwater channels, and in some cases moraines and crevasse squeeze ridges. The inner bay and middle bay are typically separated by a transverse ridge. The middle bay is characterized by deep, flat-bottomed basins and, in some examples, drumlinoid features (drumlins and/or crag-and-tails), with the stoss end pointing towards the outer bay. In most cases, the middle and outer bay are separated by another, likely larger, transverse ridge, which is immediately followed by large, asymmetrical, streamlined (elongated) features and meltwater channels in the outer bay. Although some seafloor features are common, we recognize there is some variation between the bays and within the bays themselves (Fig. 3.9).
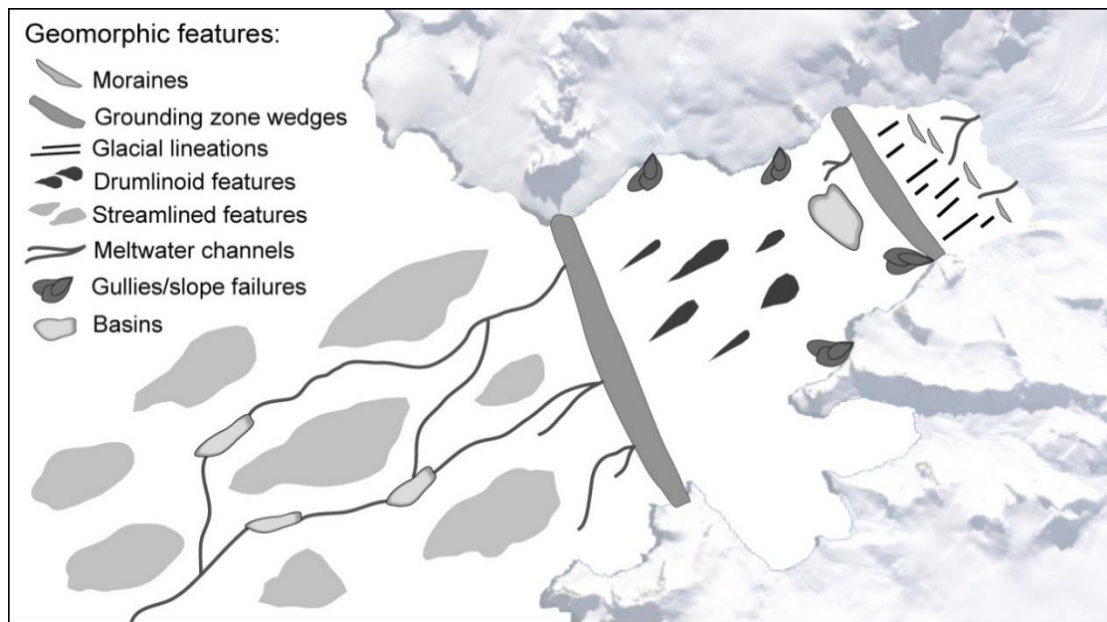
Figure 3.8 Schematic map view model showing the various geomorphic features found in the seafloor of glaciated bays in the western Antarctic Peninsula.

Models showing geomorphic features have been presented largely for the continental shelf in Antarctica (Wellner et al., 2001; Canals et al., 2002; Evans et al., 2004; Dowdeswell et al., 2008; Graham et al., 2009), and therefore our model differs from them since we show landforms focused in the confined bay areas. Our proposed schematic model is similar to other models of landform assemblages presented for glaciated environments in Svalbard (Ottesen & Dowdeswell, 2009) and Greenland (Dowdeswell et al., 2016). However, unlike the Ottesen & Dowdeswell (2009) model for restricted areas like fjords where the seafloor is dominated by landforms transverse to ice flow, our findings in AP fjords show a combination of landforms parallel and transverse to ice flow (Fig. 3.8). In addition, AP fjords show evidence of subglacial meltwater flow in the form of channels carved in bedrock. Figure 3.9 shows the distribution of submarine landforms

per bay compared to the area of the bay and the combined catchment area of the glaciers draining into each bay (also shown in appendix B tables). These features were likely formed during the final ice retreat phase throughout the AP bays during the Last Glacial Maximum. However, features carved in bedrock (e.g. meltwater channels, streamlined features) are likely the result of multiple cycles of glaciation in the bays, similar to other areas on the Antarctic continental shelf (Ó Cofaigh et al., 2005; Anderson and Fretwell, 2008; Graham et al., 2009; Livingstone et al., 2013). The submarine landforms are classified into three categories based on their depositional environment and sedimentary processes forming them: 1) subglacial landforms, 2) ice-marginal landforms, and 3) recent sediment reworking throughout the bays.

Figure 3.9 Comparing bay area, glacier catchment area, and submarine features found in bays. Bays are listed from northernmost (Marian Cove) to southernmost (Cadman Glacier Cove). The number of symbols in the chart is a representation of the number of geomorphic features found in each bay; one symbol: 1-10 features; two symbols: 11-20 features; three symbols: 21-30 features; and four symbols: >30 features found at that location.

68

5.1.1. Subglacial landforms

Elongated, parallel ridges: glacial lineations

Elongated ridges parallel to bay axis are interpreted as glacial lineations (Fig. 3.6a). In this study, lineations vary in length (between 80 m and 2.7 km long), width (between 5 and 200 m), and height (between 1 and 20 m high). Glacial lineations typically occur in groups in the inner bay (Fig. 3.2b, 3.4b, 3.5b-c), while in some cases lineations are also present in the middle bay area (appendix B Fig. B1). Glacial lineations form under flowing ice over a thin deformation till layer; most glacial lineation heights in this study are less than 10 m. The lineations are parallel to the former ice flow direction. In CHIRP, some lineations have a strong surface with no internal reflectors, while others are formed by stacked sediment packages of reworked sediment (Fig. 3.7).

Teardrop-shaped ridges in sediment: drumlins

Streamlined, teardrop-shaped ridges formed in deformable sediment are interpreted as drumlins (Fig. 3.6c). The stoss side indicates ice flow direction towards the bay mouth. Drumlins are covered by parallel acoustically laminated sediment (Fig. 3.7a). These features are observed in Beascochea Bay (Fig. 3.5d) and Andvord Bay (appendix B, Figs. B.1, B.4), both very large bays (Fig. 3.9). In both examples, the drumlins occur in an area of ice flow convergence from two large drainage systems. This convergence may result in flow acceleration, which would explain the formation of the drumlins (Wellner et al., 2001; 2006; Larter et al., 2009).

Teardrop-shaped ridges in bedrock: crag-and-tails

Streamlined, teardrop ridges formed in bedrock with a sediment tail are interpreted as crag-and-tails (Fig. 3.6d). These features are present in Beascochea Bay (Fig. 3.5d) and Andvord Bay (appendix B Figs. B1, B4), where they are associated with drumlins and glacial lineations. Crag-and-tail features are also present in Brialmont Cove, Flandres Bay, and Collins Bay, all broad bays (Fig. 3.9). These features vary in length (130-900 m), width (40-300 m), and height (2-28 m), but are in general smaller than drumlins and shorter than glacial lineations. Crag-and -tails are parallel to ice flow direction in the bays.

Elongated, asymmetrical ridges in bedrock: streamlined features

Large, elongated streamlined features are found in the outer bays carved in bedrock (Fig. 3.6b), as shown by the bowtie or hummocky reflections in the CHIRP data (Fig. 3.7). Actively flowing ice carved them in bedrock, most likely over multiple glaciation events (Anderson & Fretwell, 2008; Graham et al., 2009; Livingstone et al., 2013). These features are typically not symmetrical and in some areas are more elongated closer to the bay mouth and become stubbier away from the bay (Fig. 3.5d). Elongation at the bay mouth may indicate faster ice flow at those locations and then later deceleration as the ice reaches a larger, open area to flow outside of the confined bay (Bradwell et al., 2008).

Subglacial meltwater channels

Subglacial meltwater channels (Fig. 3.6d) have been carved into crystalline bedrock, in the inner bay areas (Fig. 3.4b) and in the outer bay areas (Fig. 3.5b, c). In addition,

channels are more frequent in the southern bays. The meltwater channels mapped in this study area indicate a complex network of flow, with short straight and anastomosing channels. Similar meltwater channels have been mapped in other Antarctic regions with crystalline bedrock (Lowe & Anderson, 2002; Anderson & Fretwell, 2008; Livingstone et al., 2013; Nitsche et al., 2013), and likely also formed through multiple glaciation events. The presence of these channels highlights the production of subglacial meltwater in the northern AP region, previously only identified in southern AP areas (Dowdeswell et al., 2004; Anderson & Fretwell, 2008; Livingstone et al., 2013).

Basin fill from subglacial sediment deposition

Several meltwater channels are associated with small flat-bottomed basins (Fig. 3.5d, 3.6d), similar to those found in other areas in the Antarctic continental shelf, interpreted as palaeo-subglacial lakes (Kuhn et al., 2017). Flat-bottomed basins have acoustically parallel sediment fill (Fig. 3.7). Subglacial sediment deposition occurs through subglacial meltwater flow and through tidal pumping, close to the grounding line (Domack, 1990; Domack et al., 2006).

5.1.2. Ice-marginal landforms

Large transverse ridges: grounding zone wedges

Large, transverse sedimentary ridges, usually formed at narrow locations in the bay perimeter are interpreted as grounding zone wedges (GZW) (Fig. 3.6e). These landforms are characterized by a strong surface with no internal reflectors (Fig. 3.7). GZW are

depositional features, formed during stillstand periods during a general ice retreat, when sediment is carried to the grounding line through bed deformation and basal melting (Alley et al., 1989; Anderson, 1999; Dowdeswell et al., 2008; Batchelor & Dowdeswell, 2015). Most of the GZW observed in the western AP bays are asymmetric, with a steep slope distal and gentler slope proximal to the ice front (Figs. 3.4, 3.5). The geometry of these transverse ridges is similar to much larger GZW in the Ross Sea (Halberstadt et al., 2016) and the Weddell Sea (Campo et al., 2017). The size of the GZW has been correlated with the length of ice stability (Alley et al., 2007; Dowdeswell & Vasquez, 2013; Batchelor & Dowdeswell., 2015), a larger GZW imply a longer period of ice stability.

Small transverse ridges: moraines

Moraines are small sedimentary ridges that can be transverse to the bay axis or arcuate, forming a lunate shape across the bay (Figs. 3.6g, 3.2, 3.3). These transverse ridges can form through various processes including melting out of basal and englacial debris-rich ice, ice push, dumping of supraglacial debris, and lodgement (Powell, 1981; Powell & Domack, 1995; Batchelor & Dowdeswell, 2015). The moraines are interpreted to form during ice retreat, but unlike the GZW, the duration of the stillstand is much shorter, and possibly more frequent (Ottesen et al., 2005; Batchelor & Dowdeswell, 2015).

Small ridges in networks: crevasse squeeze ridges

Small ridges, cross cutting each other, forming a network are interpreted as crevasse squeeze ridges (Figs. 3.6g). These only occur in two bays (Fig. 3.2, 3.3), in proximal settings with shallow water depths (<120 m). Crevasse squeeze ridges are not a common feature in Antarctica, however they have been observed in the Amundsen Sea embayment (Klages et al., 2013). These landforms have been reported in Iceland (Bennett & Glasser, 2009) and Svalbard (Ottesen & Dowdeswell, 2006, 2009) occurring either as symmetrical, low ridges, or as rhombohedral ridges, about 5 m high, found on the ice proximal margin of moraines. These ridges form by squeezing till in crevasses formed at the base of grounded ice, and they indicate ice stagnation followed by a rapid uncoupling from the seafloor (Powell & Domack, 1995; Ottesen & Dowdeswell, 2006; Bennett & Glasser, 2009). The preservation of these features indicates that no further ice front re-advance has occurred over them.

5.1.3. Recent sediment reworking throughout the bays

Slope failures: mass wasting and gullies

Slope failures occur in transverse ridges (either moraines or GZW) that result in the formation of a large fan-shaped feature in the bays (Figs. 3.2, 3.5). These features are not common in these bays but they are observed in the inner bay areas. Lobes are between 200-1200 m long and 300-500 m wide. The characteristic steep walls of the glacial valleys have gullies (Fig. 3.6f) throughout the perimeter of the bays, although in some bays gullies are more abundant than in others (Figs. 3.9, 3.10).

Proglacial meltwater channels

Straight, long, wide channels, carved in soft sediment, are interpreted as a modern erosional feature (Fig. 3.4b). These channels are differentiated from the subglacial meltwater channels by their linear channel axis. Although some are slightly sinuous, they do not form complex flow networks, some are observed in low numbers or even isolated in a bay (Fig. 3.4b). These types of channels are common in Chilean bays (Dowdeswell & Vasquez, 2013) and northern hemisphere fjords (Syvitski et al., 1987; Bennett & Glasser, 2009) where they form by dense sediment flows or turbidity currents resulting from glacifluvial meltwater or slope failures (Syvitsky et al., 1987; Dowdeswell & Vasquez, 2013).

Basin fill from turbid meltwater and rainout

The proglacial channels carry sediment flows from bathymetric high regions to deep basins (Fig. 3.6 b, d, f), where sediment of varying sizes is deposited in layers, forming the acoustically laminated basin fill (Fig. 3.7). In addition, hemipelagic processes (Powell & Domack, 1995; Ó Cofaigh & Dowdeswell, 2001; Domack et al., 2006) and meltwater plumes originating at the glacier terminus (Domack et al., 1994; Domack et al., 2006) contribute to sediment deposition in basins. Sediment reworking processes have likely been occurring since grounded ice started retreating, however, the recent warming period in the AP area may have contributed to an increase in meltwater production which may have resulted in larger sediment reworking.
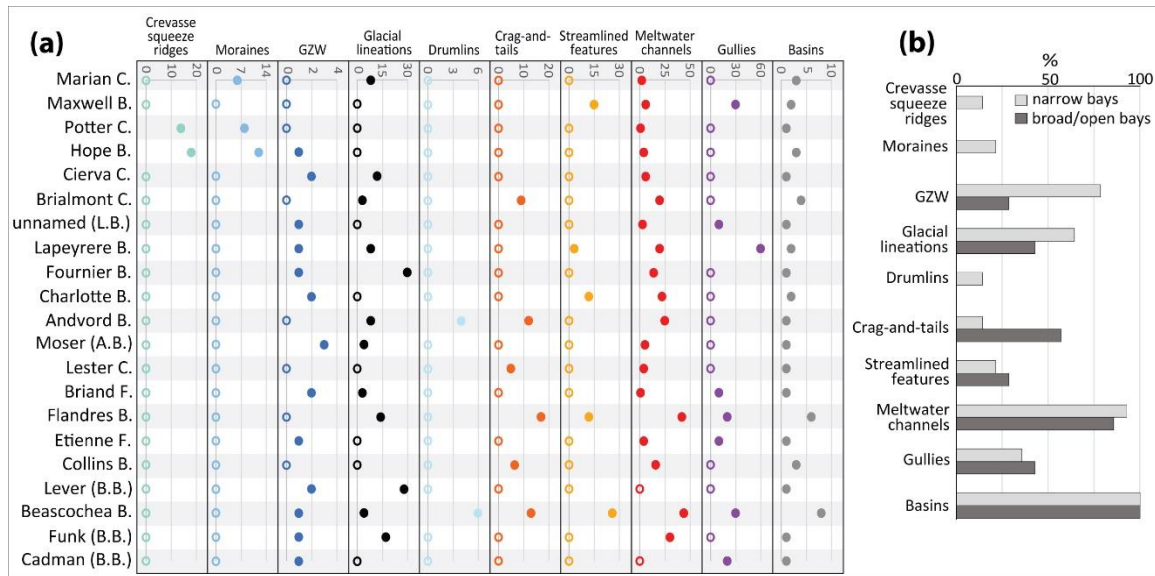
Figure 3.10 (a) Number of features found in the bays, open circles represent zero; the bays are listed from northernmost to southernmost latitude; C.: cove, B.: bay, F.: fjord, L.B.: Lapeyrère Bay, A.B.: Andvord Bay, B.B.: Beascochea Bay. (b) Percent of narrow (light grey) and broad/open bays (dark grey) in which the listed geomorphic features are found.

5.2 Observations on ice flow dynamics

There is a variable spatial distribution of the submarine landforms presented in this study (Fig. 3.1). Although, we present a generic model representative of the geomorphology in the western AP bays (Fig. 8), it is clear that not all the features are present in all the bays and therefore we examined the local conditions in order to understand ice flow in the western AP.

5.2.1. Latitude and temperature gradient

Although there are some latitudinal differences between the bays observed, Marian Cove (62°12'S) at the north and Cadman Glacier cove (65°36'S) at the south, we did not find a direct correlation between latitude and the number of features found in the bays

75

(Fig. 3.11a). However, the number of glacial lineations and meltwater channels increased towards the southern AP (Figs. 3.9 and 3.10). In addition, the complexity of the meltwater channel flow networks increased towards the south AP.

In northern locations in our study area, the seafloor has a lower relief, e.g., Maxwell Bay (Fig. 3.2) and Hope Bay (Fig. 3.3). Although there are some bathymetric highs, the seafloor appears smoother overall. In comparison, the southern bays have a more rugged seafloor, with very high differences in relief, e.g., Flandres Bay (appendix B, Fig. B.6) and Beascochea Bay (Fig. 3.5). The deep basins with flat bottoms in Flandres Bay and Beascochea Bay contrast with the variable relief around them. We attribute these differences in seafloor roughness to a higher sediment cover in the northern areas compared to the southern areas. The increased sediment cover is related to higher sediment accumulation rates, documented in Maxwell Bay by Milliken et al. (2009) and Boldt et al. (2013). Thus the smooth seafloor is likely due to burial of glacial features. The smooth seafloor cover in Maxwell Bay has more resemblance with Chilean fjords (e.g. Dowdeswell & Vasquez, 2013) and bays in South Georgia (e.g., Hodgson et al., 2014) than it does with other AP bays.
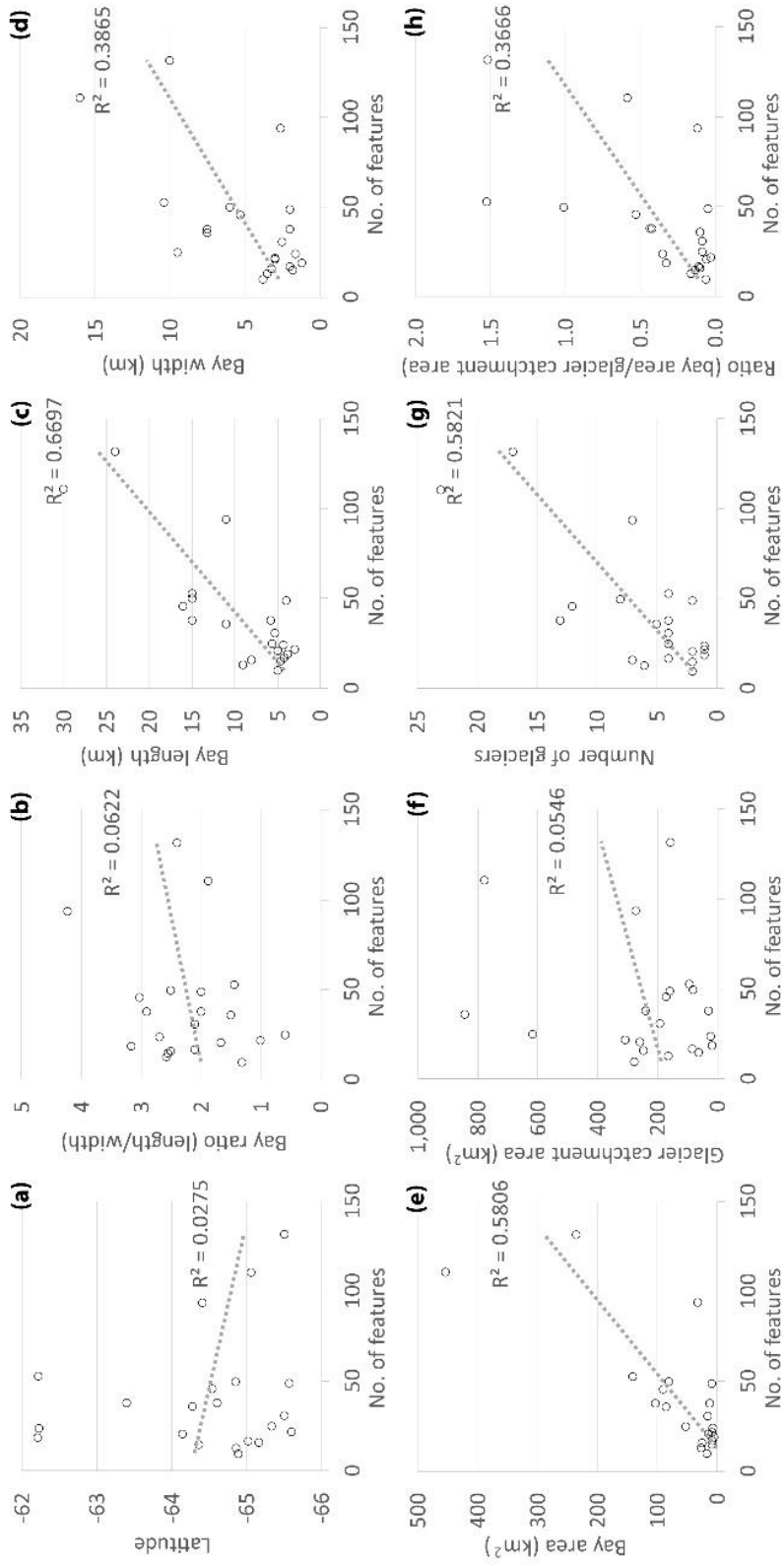
Figure 3.11 Graphs showing number of overall features found in the study areas as they relate to latitude (a), bay ratio (b), bay length (c), bay width (d), bay area (e), glacier catchment area (f), number of glaciers (g), and the ratio of bay area to glacier catchment area (h).

5.2.2. Bay area and glacier drainage area

One of the apparent variables in this comparison is the size of the bay area and the catchment area of the glaciers draining into any particular bay (Fig. 3.9). A reasonable assumption is that a larger drainage area would likely result in larger amounts of sediment and meltwater delivered to the seafloor, which could potentially form more seafloor features as ice flows in the bay. We compared bay area and glacier catchment area (total combined area of the glaciers draining into each bay) to the number of features mapped in the bays. We found a relatively high correlation between the bay area and the number of features (Fig. 3.11e), and a very poor correlation with total glacier catchment area (Fig. 3.11f). Larger bays have, on average, more submarine landforms, but a larger drainage area does not result in more submarine landforms in the bay. This conclusion implies that landform formation is complex and not directly dependent on the amount of ice flow into the bays.

When comparing glacier catchment areas to the type of features found (Fig. 3.9), the smaller drainage areas are correlated with the smaller size features, e.g. moraines, which are not found in bays with larger catchment drainage areas. This suggests that smaller fluctuations in the ice flow (that would result in the formation of smaller landforms) would not be apparent in larger glacial systems. Therefore, we conclude that the size of the bays, and not the size of the catchment area, dictates the number of features that form in the seafloor, but smaller glacier catchment areas are able to preserve evidence of small fluctuations in ice flow. This conclusion is consistent with results from Bourgeois Fjord and Blind Bay (Garcia et al., 2016), near Marguerite Bay in the southern AP, where an

inverse relation between drainage basin size and retreat of the glacier terminus was found. Similarly, Fox and Cooper (1998) measured the largest size reduction on the smaller ice bodies in the AP.

5.2.3. Geometry of bays

Since there is a large degree of variability regarding size of the bays (Fig. 3.9), we additionally analysed the bay length, bay width, and bay ratio (length/width). Bays with ratios lower than 1 were classified as open bays, ratios between 1 and 2 were classified as broad bays, and ratios higher than 2 were classified as narrow bays. We refer to this classification as the geometry of the bays. This geometry was compared to the type (and number) of features found in each observed bay (Fig. 3.10b). Because most bays in our study area were classified as narrow, we use "percentage of bays" as a way to normalize the results. Therefore, we refer to the percentage of narrow (or combined broad and open) bays where certain feature was identified; for example, Fig. 3.10(b) shows that 78% of the narrow bays have GZW, while only 28% of the broad/open bays have this same type of feature.

In Fig. 3.10(b) we note that crevasse squeeze ridges, moraines and drumlins occur only in narrow bays; GZW and glacial lineations occur mostly in narrow bays; crag-and-tails occur mostly in broad/open bays; and streamlined features, gullies/slope failures, meltwater channels, and basins tend occur all bays regardless of the bay geometry. In addition, we compared bay length, bay width, and bay ratio to the number of features

mapped (Fig. 3.11 b-d). We see that both, bay length and width, have a high correlation with the number of features found in the bay.

From these observations, we conclude that the geometry of the bay dictates the types of features that form. Narrower bays tend to form transverse features, like moraines and GZW, which form during periods of ice stabilization (Anderson, 1999; Alley et al., 2007; Dowdeswell et al., 2008; Dowdeswell & Vasquez, 2013; Batchelor & Dowdeswell., 2015). The width of the glacial valley has been suggested to play an important role for glacial flow (O'Neel et al., 2005; Joughin et al., 2008; Robel et al., 2017). Similarly, widths of ice-stream troughs, along with water depth, control ice flow by increasing the lateral resistance (Whillans & van deer Veen, 1997; Jamieson et al., 2012). Lateral drag increases as the width narrows which may lead to ice stabilization that could result in transverse features, based on the amount of sediment flux and duration of the still-stand (Howat & Domack, 2003; Dowdeswell & Vasquez, 2013). Transverse-to-flow features in the Ross Sea and Weddell Sea (Halberstadt et al., 2016; Campo et al., 2017) are larger than the GZW and moraines identified in this study and are the result of a much larger ice flow system. Therefore, width may play a major role in confined flow, e.g., fjords and bays.

5.3. Comparison to other glaciated regions

Similar assemblages of submarine landforms are found in bays of Greenland (Dowdeswell et al., 2016) and, to a lesser extent, in Svalbard (Ottesen & Dowdeswell, 2009). In Greenland, Dowdeswell et al. (2016) observed lineations near the modern ice

front followed by a LIA moraine with channels flowing towards a deep basin in the middle of the fjord, and streamlined features in the outer fjord areas. In Svalbard, several transverse retreat moraines and a larger LIA moraine ridge characterize the inner bay, followed by drumlinoid features in the middle to outer bay and larger transverse ridges in the outer fjord (Ottesen & Dowdeswell, 2009). Because Svalbard experiences higher sedimentation rates, compared to the AP, it is possible that some of the features seemingly not present may actually be covered.

Bays in South Georgia, an island northeast of the AP, also show some similarities to west AP bays; a shallower inner bay, followed by a moraine and a deep basin towards the outer bay (Hodgson et al., 2014). However, many of the bays in South Georgia have smooth seafloors, which indicates any other older features (if any) are likely buried. Dowdeswell and Vasquez (2013) mapped the geomorphology of some bays near the Southern Patagonian Ice Cap in Chile, and they show less similarities to western AP bays in general. Bays in Chile are dominated by meltwater production that is reworking and redistributing the sediment, draping the seafloor, creating a smooth cover throughout (Dowdeswell & Vasquez, 2013). Much less meltwater production and sediment reworking, along with relatively less sediment cover in the western AP bays, has enabled us to map submarine landforms in detail.

5.4. Possible late Holocene glacial advance

The seafloor in the ice proximal area in several of the bays presented in this study is characterized by a proximal transverse ridge, in most cases with glacial lineations, located

a few kilometers from the modern ice front; Marian Cove (Fig. 3.12b), Hope Bay (Fig.

3.12c), Lapeyrère Bay (Fig. 3.12d), Fournier Bay (Fig. 3.12e), Moser Glacier cove (Fig.

3.12f), Briand Fjord (Fig. 3.12g), Lever Glacier cove (Fig. 3.12h), and Funk Glacier cove

(Fig. 3.12i) show these features. We propose these proximal features are associated with a

LIA glacial advance. Similar sets of features (an ice proximal transverse ridge followed

by either smaller transverse ridges or elongated ridges parallel to the modern ice front) in

the inner bays have also been observed in Chile (Dowdeswell & Vasquez, 2013),

Greenland (Dowdeswell et al., 2016), and Svalbard (Ottesen et al., 2005; Ottesen &

Dowdeswell, 2009) and have been interpreted as LIA landforms. In Antarctica, there has

been less published research associating geomorphology and the LIA. Christ et al. (2014)

observed these same set of features in the ice proximal region of Barilari Bay (Fig. 3.12j)

and referred to them as a "fluted grounding zone wedge". They suggest a cooling and

glacial advance between 1220 A.D. and 1868 A.D. (Christ et al., 2014) based on

sedimentological analysis and ^{210}Pb and radiocarbon dates. Garcia et al. (2016) describe

the geomorphology of a western AP fjord near Marguerite Bay, south of our study area.

They show transverse, crescent-shape, and longitudinal ridges ("morainic" landforms),

along with elongated ridges, semi parallel to the fjord length in the inner bay. Although

they do not present any sedimentological analysis or dating, they interpret these inner

features as a result of LIA glacial advance in this fjord because these submarine

landforms appear pristine, with no evidence of a subsequent glacier advance, relatively

recent, and are located only a few kilometers from the modern ice front. In Potter Cove

(Fig. 3.2c), transverse moraines in the inner cove are likely associated with LIA advance

(Wölfl et al., 2016), but no dating was conducted on those features. In the neighboring

Maxwell Bay (Fig. 3.2), no sedimentological evidence was found of LIA advance

(Milliken et al., 2009), which may indicate that if there was any LIA advance in the

western AP bays, only smaller systems (narrow bays) and/or shallow bays would record

and preserve any geomorphic evidence, as suggested by our observations above. The LIA

event has been reported in western AP bays and the South Shetland Island by several

authors (Domack et al., 1995; Shevenell et al., 1996; Domack et al., 2001; Domack et al.,

2003; Hall, 2007; Hass et al., 2010; Monien et al., 2011; Simms et al., 2012) but it may be

a more widespread event throughout the AP than previously assumed. However, it is

worth noting that LIA interpretations by those authors were based on sedimentological or

terrestrial analysis that included results from dating techniques. Our interpretations are

based only on geomorphology and therefore chronology assessments are necessary to

support this argument. Another possibility is that some of these features are younger than

LIA. Cook et al. (2014) mapped the glacier front of several bays in the AP and some of

the glacier front lines coincide with the location of transverse landforms (Fig. 3.12c, g, h)

in small bays. To our knowledge, no sediment samples have been collected from any of

these proximal locations and thus no chronometric data have been completed to verify the

ages of these transverse features.

(a)

(d)
(e)
(f)
(g)
(h)
(i)
(j)

Grounding zone wedge
Glacial lineations

-100
Water depth
(m)
-1500

0   20   40   80
km

(j)
64°30'W

65°58'S

66°S

64°40'W   0   1   2   4
km

-150
(m)
-650
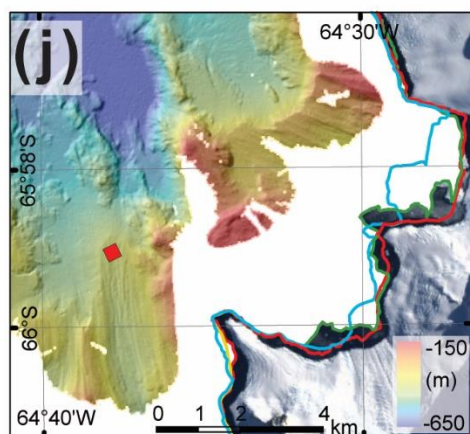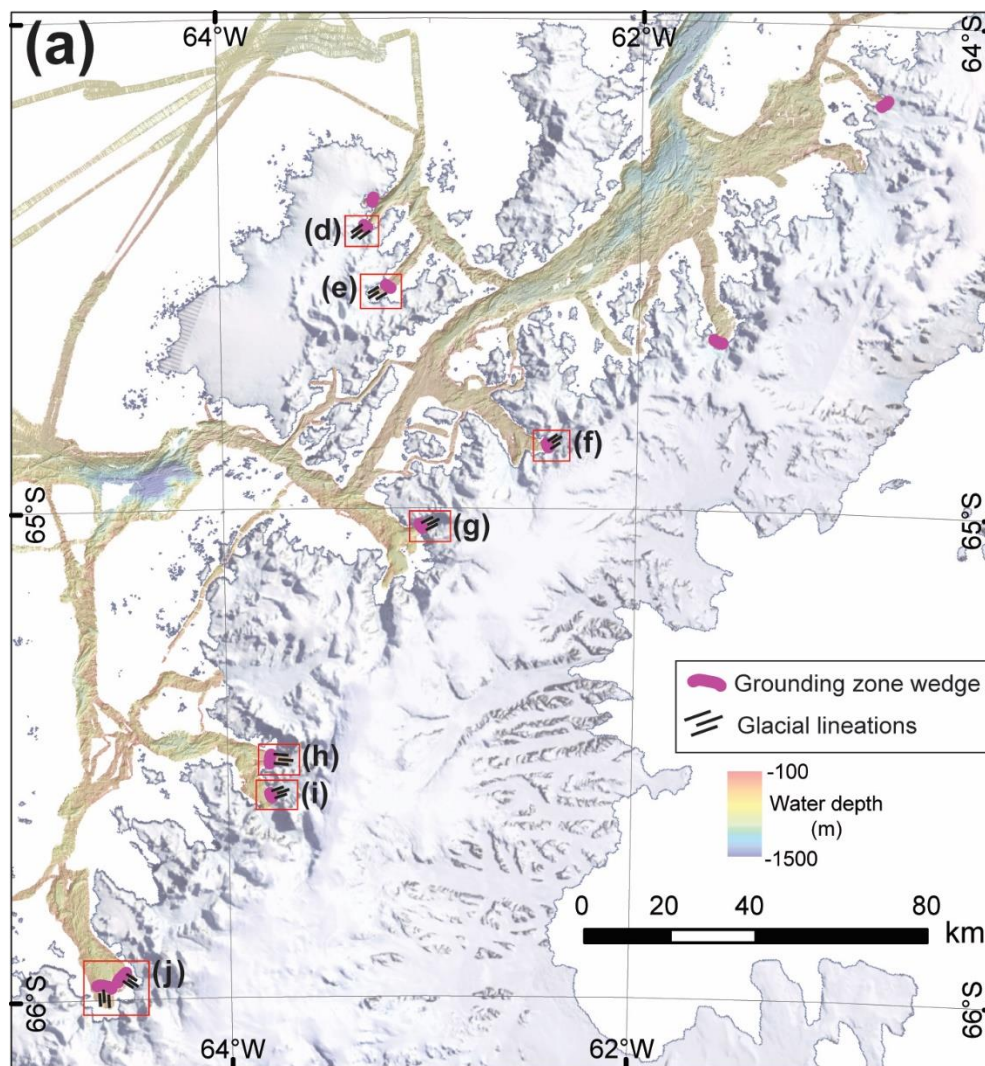
Coastline position

2000	1979	1957
1999	1978	1956
1997	1977	1954
1990	1973	1950
1989	1968	1947
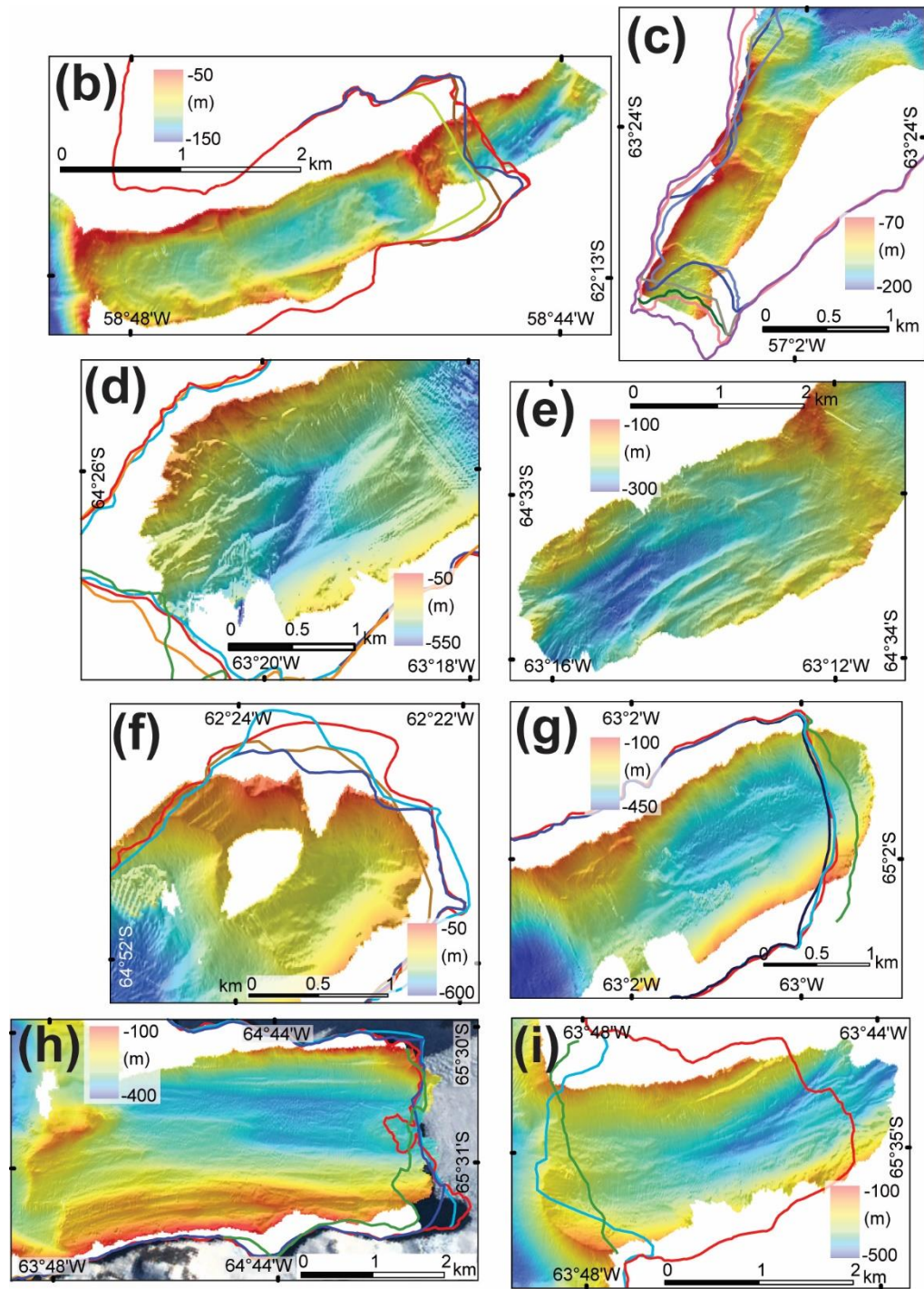
Figure 3.12 (previous page and this page) Map of the northwestern side of the Antarctic Peninsula (a) and features in the inner bays (Figs. b-j). Figures (b) Marian Cove and (c) Hope Bay are not in map (a), for location refer to Fig.1. Barilari Bay (j) from Christ et al. (2014) shows the proximal grounding zone wedge and glacial lineations; the red square shows the location of sediment core collected in 2010 and used for chronology in Christ et al. (2014). Coastline positions from Cook et al. (2014).

85

6. Summary and conclusions

We present multibeam swath bathymetry from bays in the South Shetland Islands and the western Antarctic Peninsula. The subglacial landforms were classified into three categories based on their depositional environment and sedimentary processes forming them: subglacial, ice-marginal, and recent sediment reworking. We propose a schematic model showing geomorphic features present in western AP bays; from glacial lineations and moraines in the inner bay to grounding zone wedges and drumlinoid features in the middle bay, and streamlined features and meltwater channels in the outer bay areas.

We analyzed the local variables of each bay including latitude, bay area, bay length, bay width, glacier catchment area, and the seafloor lithology to understand controls on ice flow behavior. Specific results include the following: 1) bay length and width exert a control on the number of landform features found in the bays, in addition, the geometry of the bays dictates the types of features that will form. Narrower bays tend to form transverse-to-flow features because the lateral drag of the ice flow increases as the valley width narrows which may lead to ice flow stabilization; 2) small size features, e.g. moraines, were only found in narrow bays with smaller drainage areas, and not in larger-sized drainages areas, suggesting that short-lived environmental fluctuations, responsible for the formation of these features, would only be recorded by the smaller glacial systems; and 3) two different types of meltwater channels were identified: straight, wide channels carved in soft sediment are a modern erosional feature, while the complex network of channels carved in bedrock are subglacial, which highlights the presence of

subglacial meltwater production in the northern AP region, possibly through several glacial cycles.

Finally, based on analogous assemblages of landforms reported in other locations, we propose the geomorphic features found in the seafloor of some of the proximal bay areas were formed during the LIA glacial advance. If this is the case, then glacier systems in the AP have a greater sensitivity to minor atmospheric and oceanic fluctuations than previously suggested. Future research should include additional multibeam coverage as well as sedimentological analysis and chronometric constraints in order to confirm LIA in these bays and in other areas of the Antarctic Peninsula.

Chapter 4

MARINE SEDIMENT RECORDS OF HOLOCENE CLIMATIC EVENTS FROM THREE BAYS IN THE WESTERN ANTARCTIC PENINSULA

1. Introduction

Natural climate variability during the Holocene has resulted in environmental changes in the Antarctic Peninsula (AP) that are reflected in the glaciomarine sedimentary records found in basins throughout the AP. Several authors have interpreted these records in order to understand the response of tidewater glaciers to Holocene climatic events (Domack and McClennen, 1996; Anderson, 1999; Domack et al., 2001, 2003; Michalchuk et al., 2009; Milliken et al., 2009; Allen et al., 2010; Simms et al., 2011; Christ et al., 2014; Minzoni et al., 2015). Understanding these past responses throughout the AP would enable us to more accurately predict future trends as climatic conditions fluctuate in this region. A clear example of this variability is that from the 1950s to the late 1990s, atmospheric temperatures in the AP were rising over five times the global average (Vaughan et al., 2003; Turner et al., 2005), contributing to the retreat of 90% of glaciers in the area (Cook et al., 2014). However, since the late 1990s, temperatures have decreased in the AP, especially during the summers (Turner et al., 2016).

During the Last Glacial Maximum, ice was grounded at the shelf edge in most areas around the AP and retreated diachronously to the modern ice front locations during the Holocene (Heroy and Anderson, 2005; Ó Cofaigh et al., 2014). Several mechanisms have been proposed to explain glacial retreat in the AP, including concentrations of greenhouse gases, solar forcing, and changes in oceanographic and atmospheric circulation (Vaughan et al., 2003; Marshall et al., 2006; Bentley et al., 2009). However, recent glacial retreat in the western AP has been attributed to warmer water intrusion into the continental shelf, specifically the warm Circumpolar Deep Water mass (Cook et al., 2016). This water mass has been identified as the main cause of melting occurring in ice sheets and glacier fronts in the western Antarctic continental shelf, south of the AP (Jenkins et al., 2010; Jacobs et al., 2011; 2013; Hillenbrand et al., 2017; Minzoni et al., 2017).

In order to understand past responses to climate variability in the western AP, we examine marine sediment cores from three bays in the western AP: Flandres Bay, Collins Bay, and Beascochea Bay (Fig. 4.1). A detailed sediment record, combined with coupled ^{210}Pb and radiocarbon age model, allows us to interpret depositional environments in these bays throughout the Holocene. We compare our results to similar studies in other areas of the AP to evaluate changes in depositional environments resulting from climatic events during the Holocene, provide a regional context for the observed variations in the sediment record, and identify forcing mechanisms.
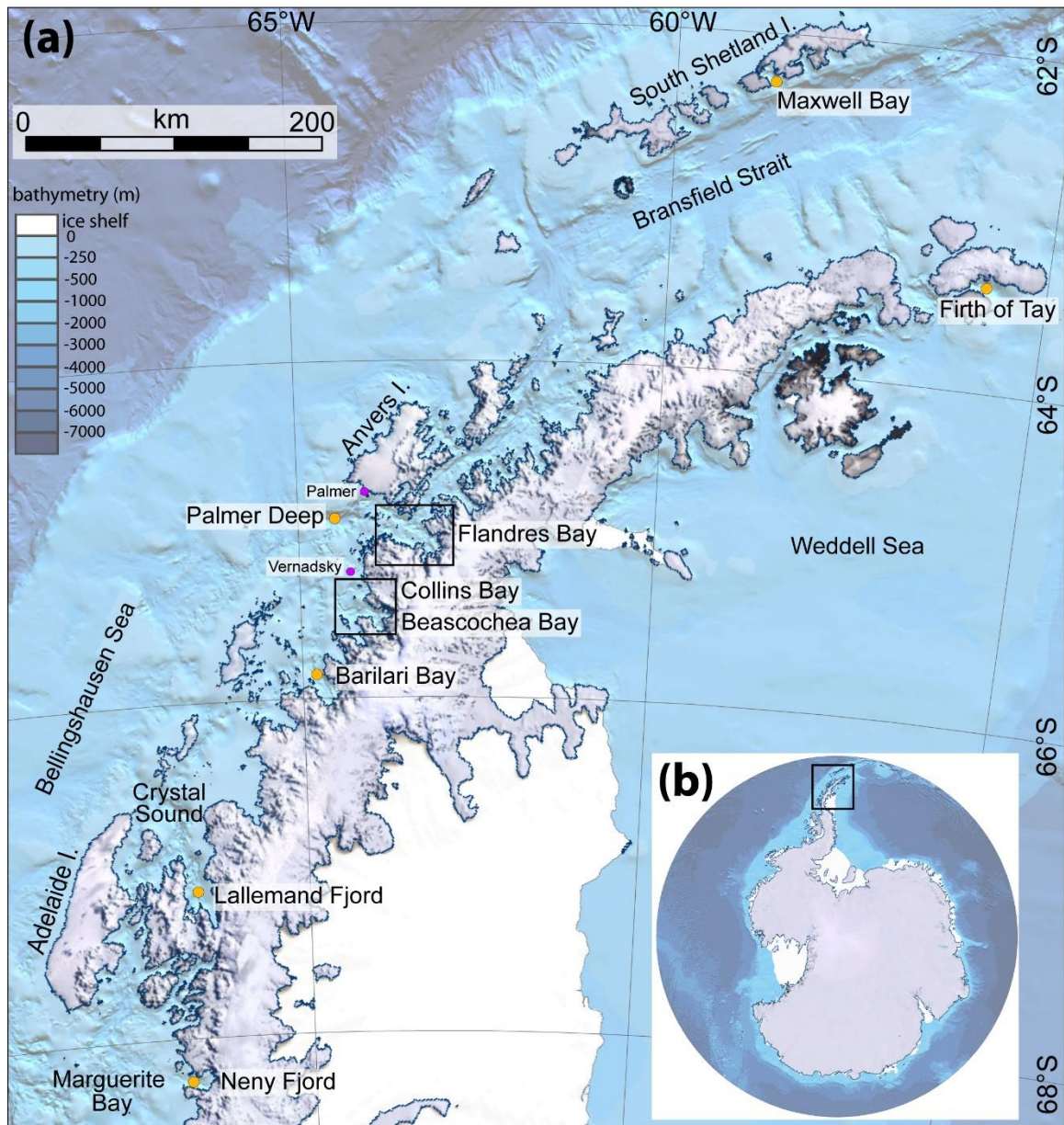
Figure 4.1 (a) Map of the northern Antarctic Peninsula (AP), black boxes show the location of Flandres, Collins, and Beascochea bays; pink circles show the location of Palmer and Vernadsky stations; yellow circles mark the location of other areas mentioned in the text; (b) location of the study area in Antarctica. AP map from the Polar Geospatial Center, bathymetry from IBCSO (Arndt et al., 2013).

2. Study area

2.1. Climate and oceanographic setting

The AP is the northernmost region of Antarctica. Climatic conditions along the western AP bays range from subpolar (in the South Shetland Islands) to polar (in areas south of Adelaide Island); however, all the bays in this study fall within the subpolar range. On average, air temperatures in the western AP vary between 0 °C in the summer to -8 to -11 °C in the winter (King et al., 2003), and precipitation varies from 1100 to 2900 mm/yr in some bays (Thomas et al., 2008; Fernandez et al., 2016). In situ measurements at Vernadsky station, near Beascochea and Collins bays (Fig. 4.1), showed an increase in annual mean air temperature of 2.8 °C between 1951 and 2000, the highest in the AP area, however, recent studies show a cooling trend for the AP region, from 1999 to 2014 (Turner et al., 2005; 2016).

The recent retreat of western AP tidewater glaciers has been linked to increased ocean temperatures, specifically in areas dominated by the Circumpolar Deep Water (CDW) current (Cook et al., 2016). The CDW, which flows northward on the western margin of the AP, floods the continental shelf with relatively warm (>1.5 °C), saline water (34.3-34.8‰) (Ishman and Domack, 1994; Smith and Klinck, 2002; Bentley et al., 2009). Sedimentological and paleontological (diatoms and foraminifera) records suggest episodic incursion of CDW into the western AP shelf during the Holocene (Shevenell and Kennett, 2002; Bentley et al., 2009; Allen et al., 2010).

2.2. Background

Flandres Bay (65°3'S, 63°14'W) is located in the Graham Land Coast of the western AP (Figs. 4.1 and 4.2). It is an elongated, northwest-southeast trending bay, about 30 km long and 20 km wide. Two embayments are located in the bay head, Briand Fjord in the north and Etienne Fjord in the south. Numerous glaciers (with drainage areas varying between <1 and 215 km^2) are located around the perimeter of the bay. These glaciers have been retreating between 55 m (Archer Glacier) and up to 607 m (Talbot Glacier), at least since the late 1940s to the early 2000s (Cook et al., 2005; 2014). Sediment accumulation rates vary within the bay, from 2.8-3 mm/yr in the proximal bay area to 1.2 mm/yr in the distal bay area (Isla et al., 2004; Boldt et al., 2013). Detailed bathymetric maps of the seafloor in Flandres Bay are presented in Munoz and Wellner (2016, 2018). Overall, the proximal bay area is characterized by two large (2000 and 7000 km^2), flat-bottomed, deep basins (>700 m water depth) filled with acoustically layered sediment. Briand Fjord and Etienne Fjord are separated from the main bay by large, transverse ridges, interpreted as grounding zone wedges (Munoz and Wellner, 2018). The seafloor in the distal bay area is rugged with a few elongated, small basins (<1200 km^2) and water depths of up to 730 m. The seafloor in the distal area is characterized by several meltwater channels carved in crystalline bedrock (Munoz and Wellner, 2018). Surface sediments vary throughout the bay; from clay-rich proximal to Etienne Fjord to diatom-rich in the middle bay and sand-rich in the most distal areas (Munoz and Wellner, 2016).

Collins Bay (65°21'S, 64°3'W) is located south of Flandres Bay (Figs. 4.1 and 4.3). Collins is a broad bay, and does not have the typical elongated fjord geometry. Trooz

Glacier, a large glacier with a drainage area of 580 km^2, drains directly into Collins Bay. Cook et al. (2005, 2014) measured a net advance of Trooz Glacier ice front of 1.5 km from 1956 to 1997. Boldt et al. (2013) could not determine sediment accumulation rates for this area, likely due to very rapid sediment deposition from gravity flows or sediment plumes resulting from the fast advance of Trooz Glacier. The seafloor proximal to the glacier is characterized by a flat-bottomed basin (~ 2 km^2) and a few channels flowing from the ice front of Trooz Glacier towards the basin. The area distal to Trooz Glacier is rugged, with a few meltwater channels, and a small basin with an area of 0.3 km^2 (Munoz and Wellner, 2018).

Beascochea Bay (65°31'S, 63°52'W) is located further south of Collins and Flandres bays (Figs. 4.1 and 4.3). It is an elongated, northwest-southeast trending bay with several embayments in the bay head. Beascochea Bay is 30 km long and varies in width (6-14 km) throughout the length of the bay. Several glaciers are found around the perimeter of Beascochea Bay. The glacier drainage areas vary widely in size from <1 km^2 to 307 km^2. Cook et al. (2005, 2014) measured changes in the ice front of nine glaciers in Beascochea Bay, four glaciers show net retreat (between 30 to 380 m, from the 1960s to the late 1990s), including Funk Glacier (120 m of net retreat), and five glaciers show net advance (between 3 to 474 m, from the 1960s to the late 1990s), including Lever Glacier (170 m of net advance) and Cadman Glacier (474 m of net advance). Sediment accumulation rates are much higher compared to Flandres Bay: 7 mm/yr proximal to Cadman Glacier and 6.4 mm/yr proximal to Lever Glacier (Boldt et al., 2013). Detailed maps of the seafloor in Beascochea Bay are presented in Munoz and Wellner (2018). The proximal areas to the glaciers have glacial lineations and are separated from the main bay by

transverse ridges, interpreted as grounding zone wedges. In addition, the inner bay area is

characterized by the presence of elongated features; drumlins, lineations, and crag-and-

tails, trending from Cadman Glacier towards the outer bay. The distal area in Beascochea

Bay is characterized by several anastomosing meltwater channels and streamlined

features carved in crystalline bedrock. Several small basins (<1 km^2) with ponded

sediment and water depths up to 810 m are present in the outer bay area.
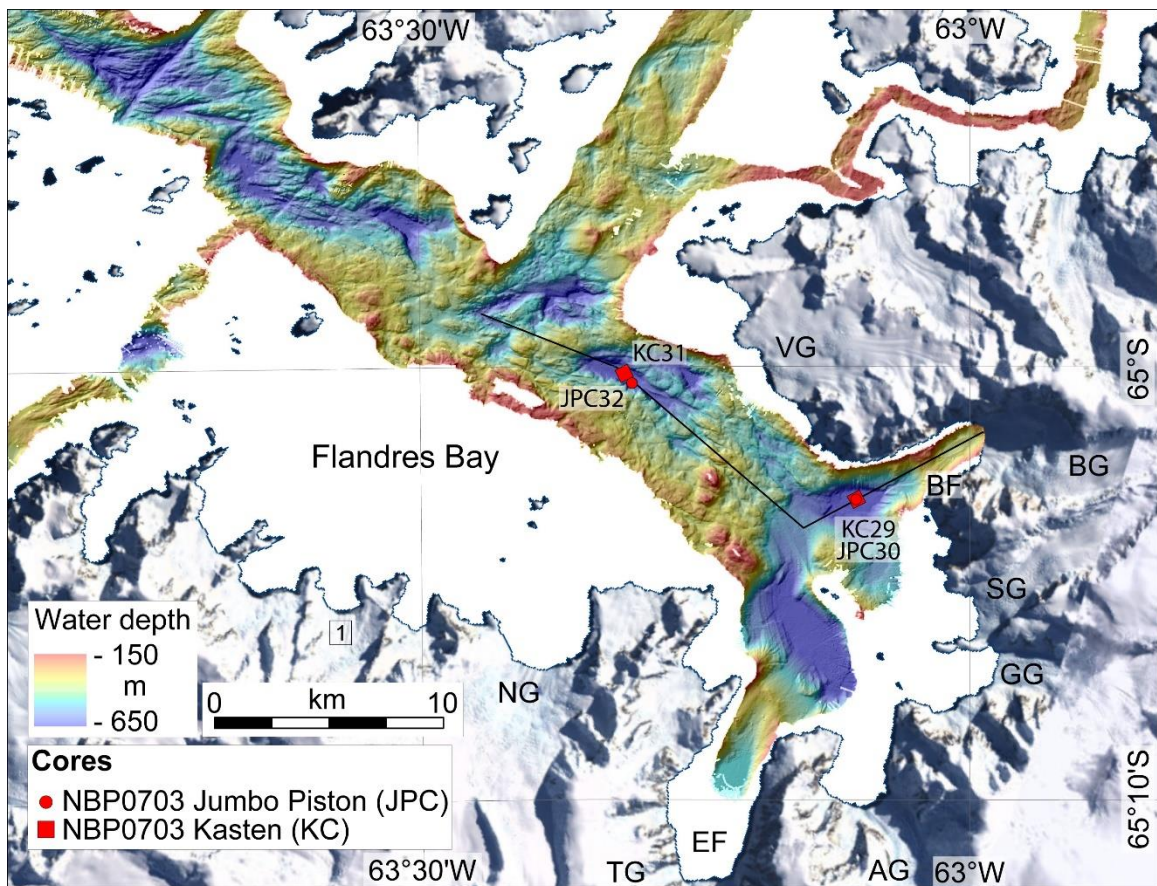
Figure 4.2 Bathymetry and cores from Flandres Bay; BF: Briand Fjord, EF: Etienne Fjord, VG: Vogel Glacier, BG: Bolton Glacier, SG: Sayce Glacier, GG: Goodwin Glacier, AG: Archer Glacier, TG: Talbot Glacier, NG: Niepce Glacier, 1: unnamed glacier. Black line shows the location of the cross section from Bolton Glacier to outer Flandres Bay (Fig. 4.7). AP satellite image from the Polar Geospatial Center.

3. Methods

Sediment cores were collected during the NBP0703 cruise onboard the RV/IB

Nathaniel B. Palmer to the Antarctic Peninsula. The cores were opened, described, and

sampled by the scientific party onboard soon after collection. The archive halves of the

cores were shipped to the Antarctic Research Facility (ARF) at Florida State University.

Additional observations and further core sampling were conducted at ARF.

3.1. Core descriptions

In total, 16 cores are presented in this study; four in Flandres Bay, four in Collins

Bay, and eight in Beascochea Bay (Figs. 4.2 and 4.3, Table 4.1). The core types are short

kasten cores (KC) and long, jumbo piston cores (JPC). Recovery of JPCs tends to be a

high-impact operation and therefore these types of cores over-penetrate the sediment-

water interface. A KC is collected in the same location in order to recover the sediment-

water interface, and magnetic susceptibility is used to correlate both cores and estimate

how much of the JPC has been lost due to over-penetration.

For the purposes of this paper, we only include the description of cores

representative of the sediments found in the bays. Visual descriptions of the sediment

collected included color (using a Munsell color chart), grain size, texture, laminations,

pebble abundance, fossil content, organic matter, and bioturbation. A lithology column

was created for each core; the lithologic name corresponds to the dominant component of

the sediment (>75% of clay, silt, or sand). If the dominant component is <75%, then the

highest secondary component is included in the lithologic name and the adjective sandy,

silty, or clayey is added.

3.2. X-rays and physical properties

Color core photos and X-radiographs were taken at ARF for each core. These images were used to identify sedimentary structures and pebble abundance in the cores. For cores from Beascochea Bay, pebbles >4 mm were quantified on the X-rays every 5 cm throughout each core and every 1 cm in Flandres and Collins Bay. Magnetic susceptibility (MS) and density were measured at ARF in each core using a Geotek Multi-Sensor core logger at approximately 1-cm intervals throughout the core. MS quantifies the degree to which materials can be magnetized, the more magnetic components there are in the sediment, the higher the readings. Low values correspond to a higher percentage of biogenic matter, higher values represent a larger clastic (terrigenous) component. MS can be used as a proxy to measure changes in the composition of the sediment which can be related to depositional processes. Density measures the mass content in the cores, which is related to the lithology and the compaction of the sediment.
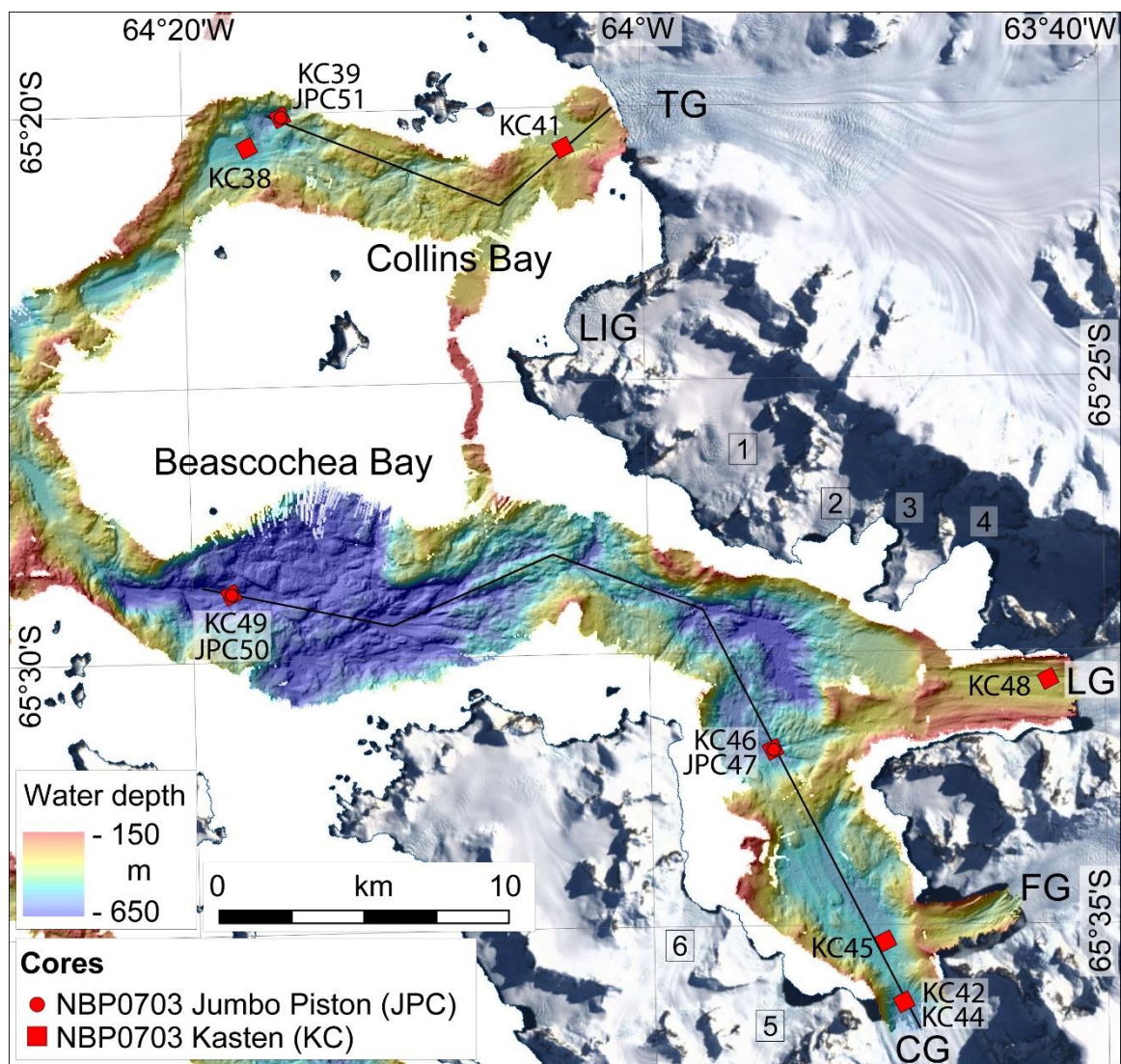
Figure 4.3 Bathymetry and cores from Collins Bay and Beascochea Bay; TG: Trooz Glacier, LIG: Lind Glacier, LG: Lever Glacier, FG: Funk Glacier, CG: Cadman Glacier, 1-6: unnamed glaciers. Black lines show the location of cross sections from the inner bay to the outer bay areas (in Figs. 4.10 and 4.14). AP satellite image from the Polar Geospatial Center.

3.3. Particle size

The cores were sampled at ARF at approximately 20-cm intervals for grain-size

analysis. Sediment samples from Flandres Bay and Beascochea Bay were analyzed at

Rice University using a Malvern Mastersizer 2000 Laser Particle Size Analyzer (LPSA).

Grain size samples from Collins Bay were analyzed at the University of Houston using a CILAS LPSA. Bulk sediment samples were dispersed in water with sodium hexametaphosphate to prevent flocculation of clays and transferred into the LPSA for grain-size analysis. We use the Wentworth grain-size classification: clay (<4 μm), very fine silt (4-8 μm), fine silt (8-16 μm), medium silt (16-32 μm), coarse silt (32-63 μm), and sand (>63 μm) (Wentworth, 1922).

3.4. Chronology

3.4.1. Short-lived isotopes

Sediment samples were analyzed through gamma spectrometry to measure the activity of two isotopes with relatively short half-lives ($t_{1/2}$), ^{137}Cs ($t_{1/2}$=30.1 years) and ^{210}Pb ($t_{1/2}$=22.3 years). ^{137}Cs is attributed to atmospheric radioactive fallout released into the atmosphere by nuclear bomb testing which started in the 1940s and peaked in 1963 (1964 in the southern hemisphere) (Burton, 1975; Harden et al., 1992; Sanders et al., 2010). The highest ^{137}Cs activity identified in the sediment column therefore corresponds to the year 1964. In contrast, ^{210}Pb is a naturally occurring isotope by-product of the ^{238}U decay series. ^{210}Pb escapes into the atmosphere and eventually reaches the water column where it adsorbs to fine particles in suspension. The ^{210}Pb activity in the sediment has two components, a supported component (from decay within the sediment column) and an excess or unsupported component (from the water column) (Appleby and Oldfield, 1978; 1983; Oldfield and Appleby, 1984). After the decay curve reaches the supported level

within the sediment column, a linear sedimentation rate can be calculated. Using the sedimentation rates, ages where assigned to the known depths of the core samples.

Samples were collected at the core depths: 0, 2, 4, 6, 8, 20, and 45 cm in cores NBP0703 KC31, KC39, and KC49. The samples were dried, homogenized, weighed, and placed in plastic petri dishes. The samples were stored for three weeks and then measured for 40 hours using a Canberra high-purity germanium detector with a lead shield at the University of Houston. Data were interpreted using Genie 2000 software. ^{137}Cs activity was measured using the 661 keV gamma peak and ^{210}Pb activity was measured using the 46.5 keV gamma peak.

3.4.2. Radiocarbon

Calcareous foraminifera and shell fragments were used for radiocarbon dating. Sets of samples have been collected from these cores through the past few years and submitted to various facilities for mass spectrometry analysis (NOSAMS- National Ocean Sciences Accelerator Mass Spectrometry facility at the Woods Hole Oceanographic Institution, UCIAMS- Accelerator Mass Spectrometry facility at the University of California-Irvine, and ETHZ- Institute for Particle Physics and Astrophysics at the Swiss Federal Institute of Technology).

Results from ^{210}Pb and ^{14}C were combined to create a statistical age model using BACON, an open source Bayesian age-depth modeling software. BACON divides the core into sections and uses Markov Chain Monte Carlo iterations to estimate accumulation rates within these sections. The starting date is known, in this case 2007

when the sediment was collected, and the age model is built by combining the estimated

accumulation rates of the sections based on the ^{210}Pb and ^{14}C ages (Blaauw and Christen,

2011). Additional inputs can be added to the model, such as hiatus, calibration curves,

and reservoir corrections. ^{210}Pb ages, calculated from the sedimentation rates, and

uncalibrated ^{14}C ages where entered into the software, in addition the MARINE13 curve

(Reimer et al., 2013) and an additional reservoir correction of 700±50 years (Milliken et

al., 2009; Minzoni et al., 2015) were used to calibrate the radiocarbon samples. The age

model curves are the resulting weighted mean age downcore.

Table 4.1 Cores and radiocarbon ages presented in this study

Cruise	Core ID	Core length (cm)	Location	Latitude (°)	Longitude (°)	Water depth (m)	Sample depth interval (cm)	Material sampled	Lab sample ID	14C age (yr BP)	Age error (yr BP)	CALIBRATED 14C AGE (cal yr BP)	2sigma (cal yr BP)
NBP0703	KC29	188	Flandres Bay	-65.05158	-63.10314	684	ns	--	--	--	--	--	--
NBP0703	JPC30	572	Flandres Bay	-65.05154	-63.10381	684	557-559	foraminifera	NOSAMS-124899	3000	±35	1913	1813-2010
NBP0703	KC31	266	Flandres Bay	-65.0028	-63.31439	723	235	shell fragments	UCIAMS-40688	2340	±15	1211	1161-1263
NBP0703	KC32	666	Flandres Bay	-65.00659	-63.30751	713	277	shell fragments	UCIAMS-89912	2255	±25	1116	1037-1205
	JPC32						280-287	foraminifera	ETHZ-65458	2305	±90	1158	957-1319
NBP0703	KC38	250	Collins Bay	-65.34406	-64.28649	501	ns	--	--	--	--	--	--
NBP0703	KC39	250	Collins Bay	-65.33487	-64.26153	555	ns	--	--	--	--	--	--
NBP0703	KC41	272	Collins Bay	-65.34576	-64.05647	356	269-271	foraminifera	ETHZ-65467	1870	±65	723	632-879
NBP0703	JPC51	1364	Collins Bay	-65.33484	-64.26152	554	410	shell fragment	UCIAMS-83303	4560	±20	3825	3720-3901
	JPC51						596-597	foraminifera	NOSAMS-124898	5410	±70	4928	4851-5018
	JPC51						974-975	foraminifera	ETHZ-65460	7020	±70	6784	6618-6962
	JPC51						1217.5-1218.5	shell fragment	ETHZ-65461	9000	±45	8859	8686-8991
	JPC51						1221-1222	shell fragment	ETHZ-65465	9110	±60	9013	8832-9210
	JPC51						1301	scaphopod	UCIAMS-58872	9855	±25	9943*	9800-10099
	JPC51						1360-1361	foraminifera	NOSAMS-124897	8830	±85	8618	8404-8893
NBP0703	KC42	564	Beascochea Bay	-65.60734	-63.81714	539	281	shell fragments	UCIAMS-40849	4840	±30	4205*	4089-4327
	KC42						292-294	foraminifera	UCIAMS-89905	4515	±30	3763*	3662-3863
	KC42						558-560	foraminifera	UCIAMS-89903	2545	±35	1386	1300-1492
	KC42						564	shell fragments	UCIAMS-40845	3825	±25	2900*	2807-2992
NBP0703	KC44	183	Beascochea Bay	-65.607307	-63.817177	536	ns	--	--	--	--	--	--
NBP0703	KC45	106	Beascochea Bay	-65.58871	-63.82999	499	102-104	foraminifera	UCIAMS-89904	2020	±50	860	738-962
NBP0703	KC46	290	Beascochea Bay	-65.52989	-63.9105	567	140-142	foraminifera	UCIAMS-89906	1905	±35	743	665-844
NBP0703	JPC47	1117	Beascochea Bay	-65.52989	-63.91047	568	211-213	foraminifera	UCIAMS-89909	2130	±60	982	848-1142
	JPC47						414-416	foraminifera	UCIAMS-89910	2645	±40	1495	1383-1600
	JPC47						822-824	foraminifera	UCIAMS-89911	5175	±35	4670	4543-4794
NBP0703	KC48	107	Beascochea Bay	-65.50952	-63.70838	318	ns	--	--	--	--	--	--
NBP0703	KC49	289	Beascochea Bay	-65.47988	-64.3048	807	ns	--	--	--	--	--	--
NBP0703	JPC50	1386	Beascochea Bay	-65.47987	-64.30481	806	973-975	foraminifera	UCIAMS-89907	5160	±260	4628	3930-5302
	JPC50						1375-1377	foraminifera	UCIAMS-89908	6060	±60	5728	5597-5871

ns: not sampled

*: reworked date, not used for core chronology

NOSAMS: National Ocean Sciences Accelerator Mass Spectrometry facility, Woods Hole Oceanographic Instituttion

UCIAMS: Accelerator Mass Spectrometry facility, University of California, Irvine

ETHZ: Institute for Particle Physics and Astrophysics, Swiss Federal Institute of Technology

4. Results and interpretation of sediment cores

4.1. Flandres Bay

4.1.1. Core NBP0703 JPC30

JPC30 was collected in a flat-bottomed basin located approximately 6.5 km from the modern ice front of Bolton Glacier, at a water depth of 684 m. The basin is located distally from the grounding zone wedge separating Briand Fjord from Flandres Bay (Fig. 4.2).

We have identified three units in JPC30: unit 1 (0-160 cm), unit 2 (160-210 cm), and unit 3 (210-572 cm) (Fig. 4.4). Unit 1 is olive (5Y, 4/3), clayey silt with black mottling, with a few coarse sand layers. Pebbles are abundant, sand percentage is the largest in the core (between 3-19%), and grain size mode varies between 14-23 μm, with modal size generally increasing upcore. Unit 2 is olive (5Y, 4/3), clayey silt with common laminations throughout and a gravel layer. Pebbles are abundant, but fewer than in unit 1. Sand percentage varies between 2-4%. Grain size mode varies between 14-15 μm. Unit 3 is olive (5Y, 4/3) to dark greenish gray (GLEY 1, 4/1 5GY) bioturbated clayey silt with pebbles throughout. Layers of sand and gravel occur throughout this unit. Sand percentage varies between 2-9%. Grain size mode varies between 12-23 μm.

Due to over-penetration by the JPC30 into the sediment-water interface, we combined the upper 20 cm of KC29 with JPC30. The age model for JPC30 was completed combining ^{210}Pb from KC29 (from results in Boldt et al., 2013) and a radiocarbon age from JPC30 (Table 4.1). The age model includes a hiatus in unit 1. Unit

1 spans from the present to ~640 cal. yr B.P.; unit 2 from ~640 to 820 cal. yr B.P.; and

unit 3 from ~820 to 2120 cal. yr B.P.
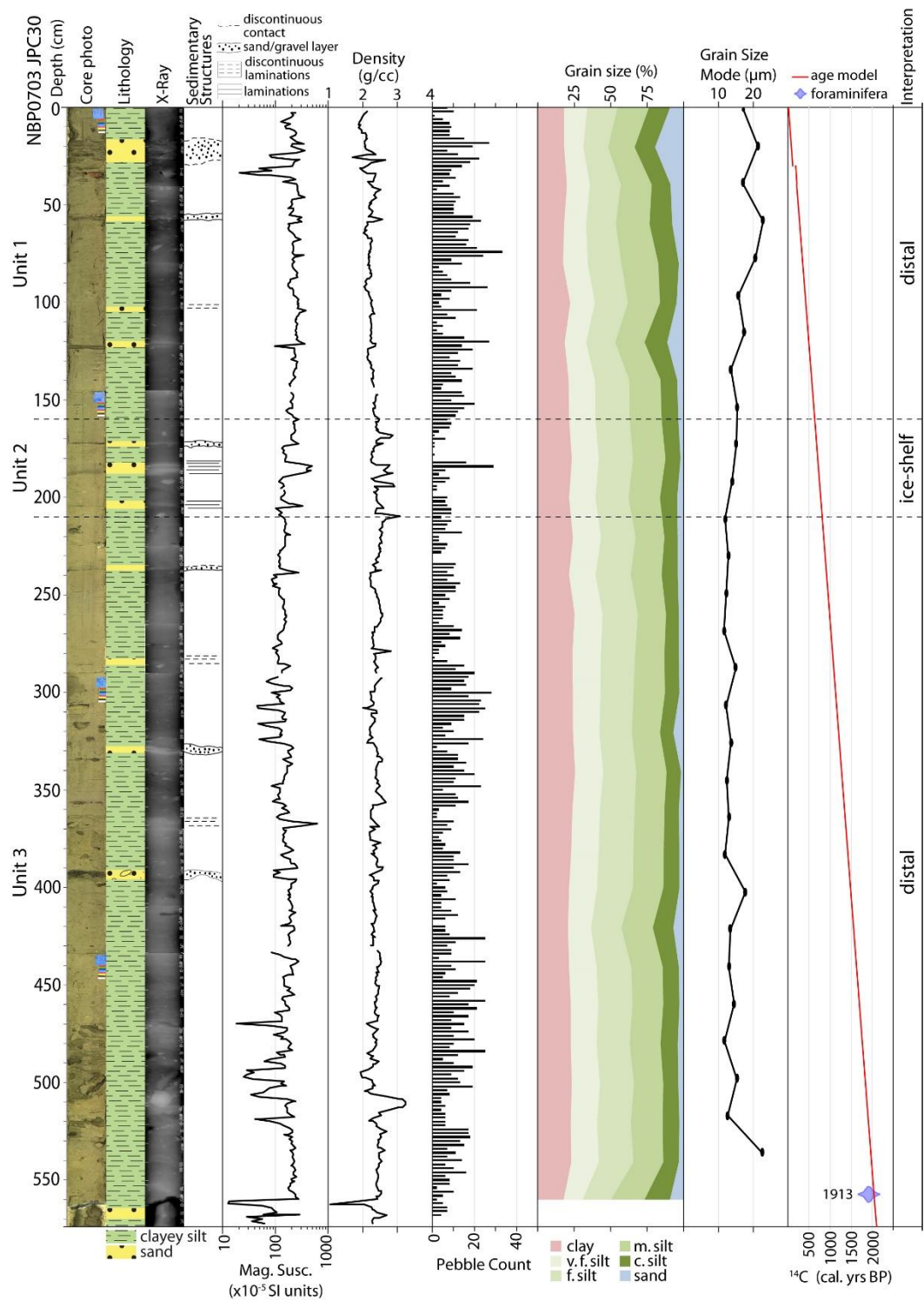
Figure 4.4 Core NBP0703 JPC30, collected in inner Flandres Bay. See Fig. 4.2 for location. Break in age model represents a hiatus; width of symbols in the age model represents uncertainty.

104

4.1.2. Core NBP0703 JPC32

JPC32 was collected in a flat-bottomed basin located distally from Briand Fjord, in the outer area of Flandres Bay (Fig. 4.2). The core was collected approximately 18 km from the modern ice front of Bolton Glacier at a water depth of 713 m. We have divided JPC32 into two units: unit 1 (0-320 cm) and unit 2 (320-666 cm) (Fig. 4.5). Unit 1 is olive (5Y, 4/3) to olive gray (5Y, 4/2) bioturbated clayey silt with abundant pebbles of varying size throughout the core. There are no sand or gravel layers. Sand percentage varies between 3-13%, grain size mode stays relatively constant between 19-24 μm. Unit 2 is olive (5Y, 4/3) to olive brown (2.5Y, 4/3) clayey silt with pebbles throughout. There are no sand or gravel layers. Sand percentage varies between 5-13%. Grain size mode is more variable than unit 1 (8-20 μm).

Due to over-penetration by the JPC32 into the sediment-water interface, we combined the upper 35 cm of KC31 with JPC32. The age model for JPC32 was completed combining ^{210}Pb (Fig. 4.6) calculated ages and a radiocarbon age from KC31, and two radiocarbon ages from JPC32 (Table 1). Unit 1 spans from the present to ~1260 cal. yr B.P. and unit 2 extends to ~2310 cal. yr B.P.

Results from gamma spectrometry show the cores examined had detectable levels of ^{137}Cs activity (Fig. 4.6), however these results were not sufficient to constrain a single peak, which would correspond to 1964. Higher sampling frequency in the cores may be necessary to acquire a complete inventory of ^{137}Cs in the sediment column, especially in the upper 20 cm of the cores.
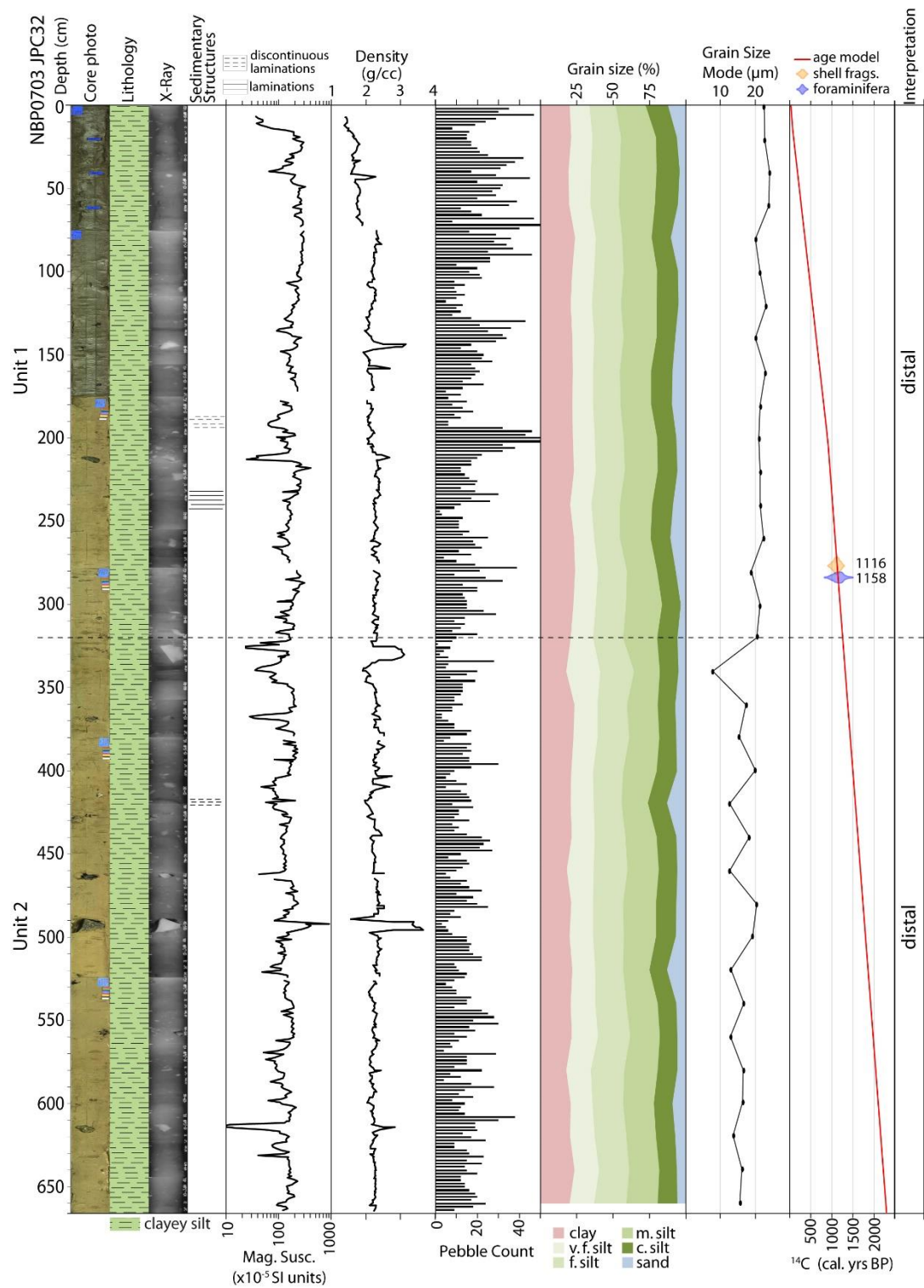
Figure 4.5 Core NBP0703 JPC32, collected in outer Flandres Bay. See Fig. 4.2 for location. Width of symbols in the age model represents uncertainty.
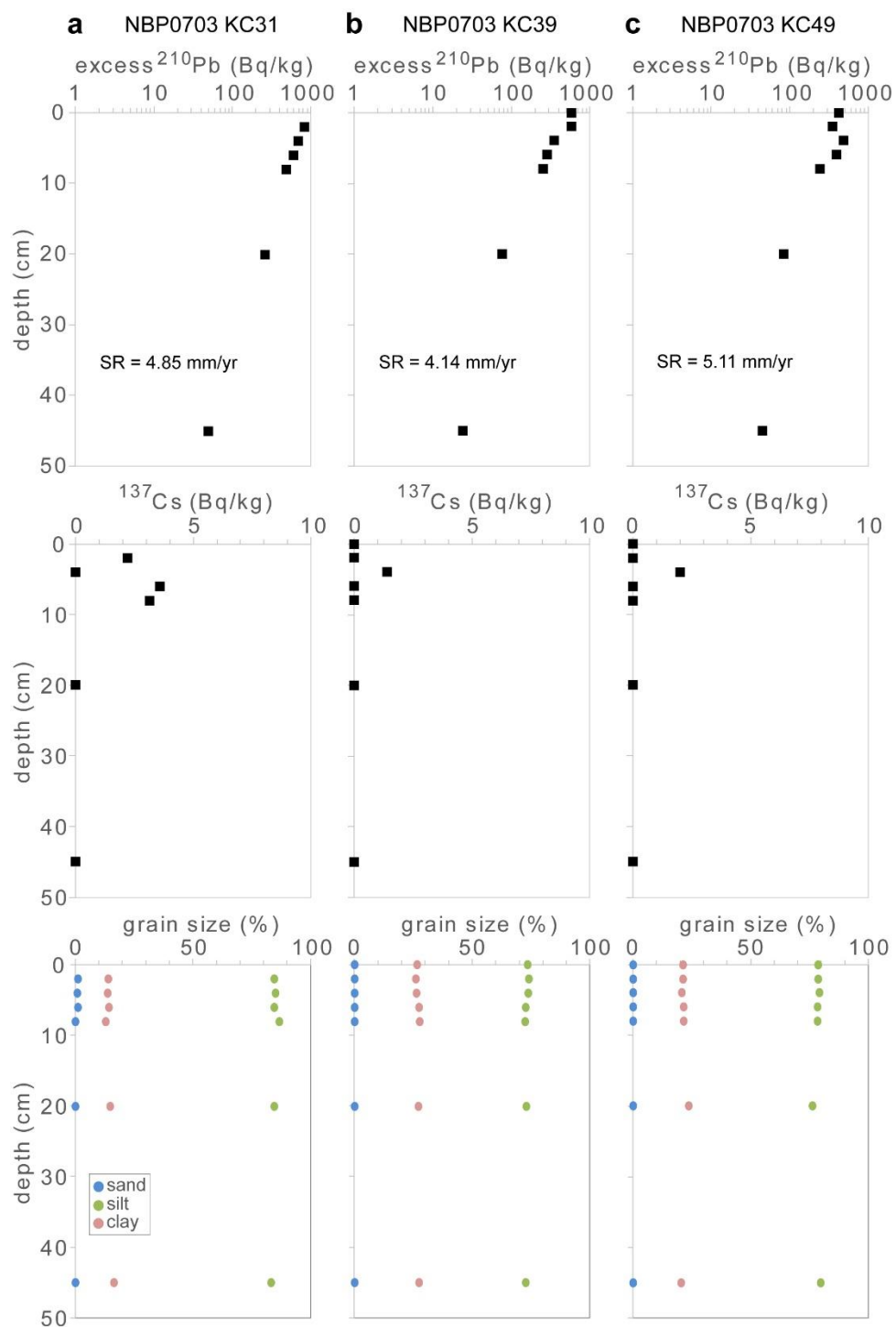
Figure 4.6 Excess ^{210}Pb activity, ^{137}Cs activity, and grain size percent downcore for KC31, KC39, and KC49. SR: sedimentation rate. See Figs. 4.2 and 4.3 for location.

4.1.3. Interpretation of deglaciation history of Flandres Bay

Although there is some variation between the units of JPC30, in general, the sediment in the inner bay area is clayey silt interbedded with thin sand layers, and with abundant pebbles. The exception is unit 2: 50-cm of sediment, presumably deposited in a 180-year period (Fig. 4.4). Laminations and fewer pebbles characterize this unit, likely indicating deposition under a thick ice cover, possibly an ice shelf resulting from a cooling event. Units 1 and 3 likely deposited in an open marine (distal to the glacier front) environment, with occasional gravity flow deposits.

Core JPC32 is fairly homogeneous throughout, composed of clayey silt and lacking any major sedimentary structures. Pebbles are extremely abundant, especially in the upper part of the core. For this reason, we divided the core into two units, however, the environments of deposition are likely open marine, distal to the glacier front, for both units.

Based on these interpretations, we assume distal, open marine, deposits have been accumulating in Flandres Bay at least since 2310 cal. yr B.P. in the location of JPC32, and at least since 2120 cal. yr B.P. in the location of JPC30 (Fig. 4.7). A localized glacial advance and subsequent retreat occurred between 640 and 820 cal. yr B.P. and it is only evident in the areas proximal to Briand Fjord (Fig. 4.2).
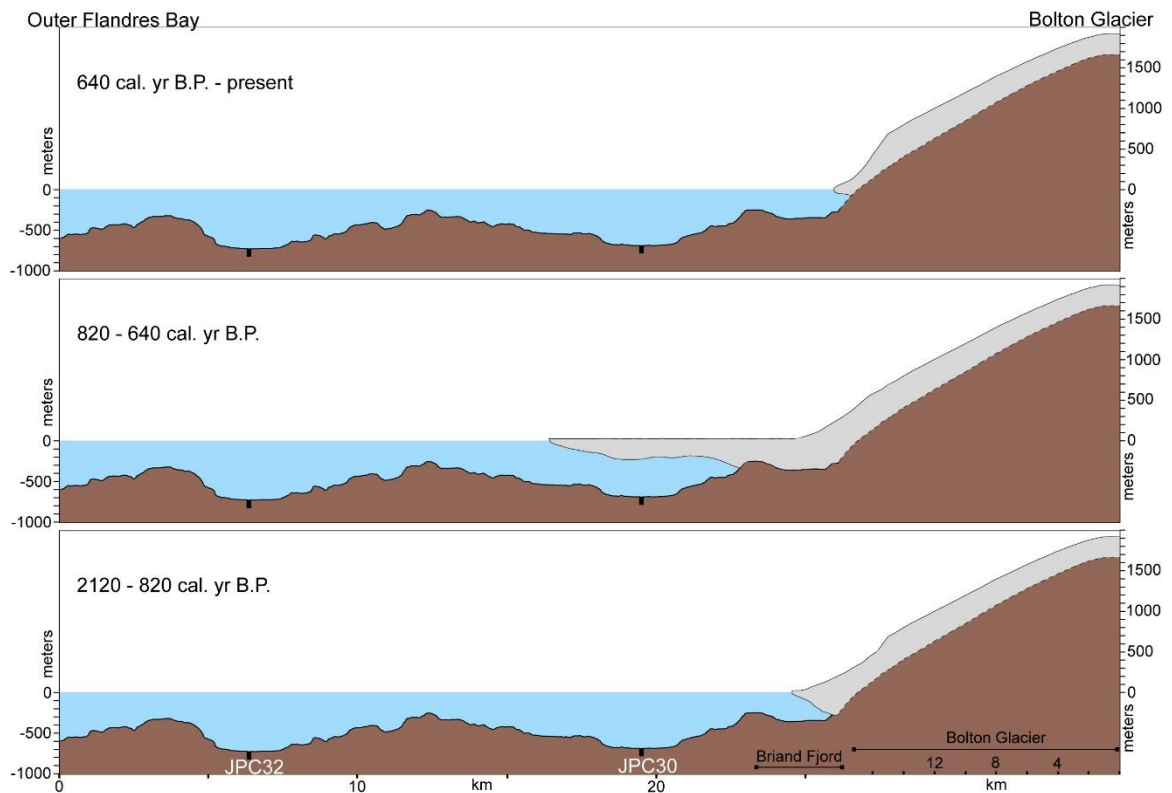
Figure 4.7 Interpretation of glacial retreat in Flandres Bay. See Fig. 4.2 for location of cross section in the bay. Notice horizontal scales are different for the bay and the glacier. Brown: bedrock, grey: ice, blue: water.

4.2. Collins Bay

4.2.1. Core NBP0703 KC41

KC41 was collected in a flat-bottomed basin, 2 km from the modern ice front of Trooz Glacier, at a water depth of 356 m (Fig. 4.3).

We have identified two units in KC41: unit 1 (0-100 cm) and unit 2 (100-272 cm) (Fig. 4.8). Unit 1 is greenish gray (GLEY1, 5/1) sandy silt. Laminations are common throughout the unit. Sand percentages vary between 7-53%, generally increasing upcore. Sand and pebbles are more abundant in the upper 30 cm of the unit. Unit 2 is greenish

gray (GLEY1, 5/1) clayey silt with laminations throughout and very few, small pebbles. Sand percentage varies between 4-91%, but are, on average, lower than unit 1 (14% compared to 27%).

The age model for KC41 was completed using a single radiocarbon age from foraminifera collected from 269-271 cm core depth (Table 4.1). Unit 1 spans from the present to ~190 cal. yr B.P. and unit 2 down to ~610 cal. yr B.P.
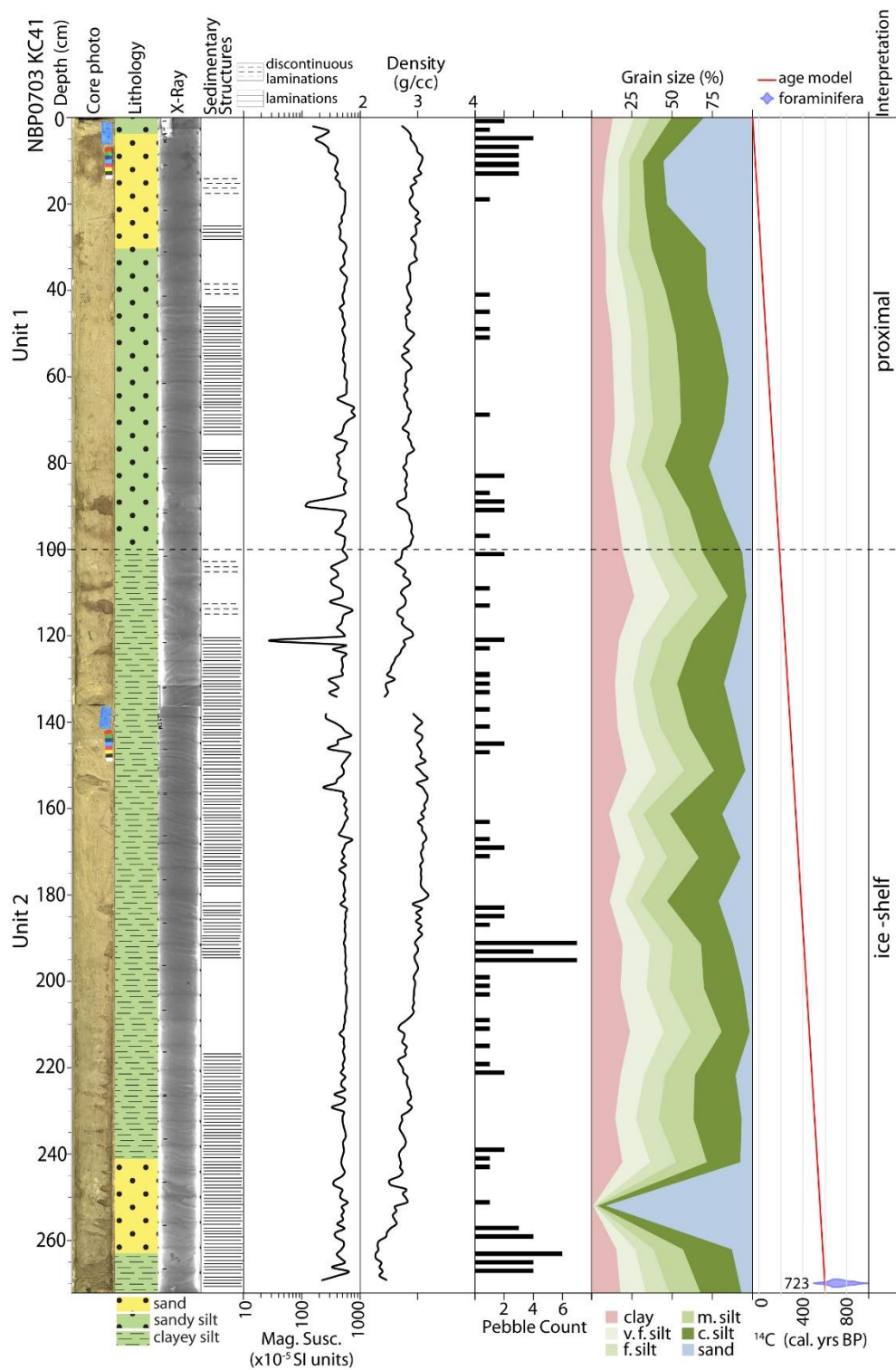
Figure 4.8 Core NBP0703 KC41, collected in inner Collins Bay. See Fig. 4.3 for location. Width of symbols in the age model represents uncertainty.

4.2.2. Core NBP0703 JPC51

JPC51 was collected 12 km away from the modern ice front of Trooz Glacier in a small basin with ponded sediment. Water depth at this location is 554 m (Fig. 4.3).

We have identified five units in JPC51: unit 1 (0-40 cm), unit 2 (40-704 cm), unit 3 (704-810 cm), unit 4 (810-1262 cm), and unit 5 (1262-1364 cm) (Fig. 4.9). Unit 1 is an olive gray (5Y, 5/2) silt deposit with rare, occasional sand grains (<1%), and pebbles scattered throughout. Unit 2 is an olive gray (5Y, 5/2) to dark greenish gray (GLEY1, 4/1) silt deposit with rare sand (<1%) but abundant pebbles throughout and two gravel layers. Unit 3 is a dark greenish gray (GLEY1, 4/1) to very dark gray (GLEY1, 3/1) silt deposit with a coarse-grained sediment layer at the bottom of the unit followed by laminated sediment. The layer is a fining upward sand-gravel with an erosive base, interpreted as a turbidite deposit. Sand percentages are on average <1%, but reach up to 36% in the laminated section. Pebbles are very scarce in this unit, but abundant in the bottom of the unit. Unit 4 is a dark greenish gray (GLEY1, 4/1) to olive gray (5Y, 5/2) silt deposit with abundant pebbles throughout, higher than any other unit in this core. Sand percentages are <1% on average, but the coarser silt component (32-63 μm) increases downcore. Two gravel layers occur near the bottom of this unit. Unit 5 is dark gray (GLEY1, 4/N) silt deposit with scattered pebbles and laminations. Sand percentages increase downcore, from <1% up to 20%.

Due to over-penetration by the JPC51 into the sediment-water interface, we combined the upper 90 cm of KC39 with JPC51. The age model for JPC51 was completed combining ^{210}Pb from KC39 (Fig. 4.6) and six radiocarbon ages from JPC51

(Table 4.1). The age model includes a hiatus at the boundary between units 3 and 4. Unit 1 spans from the present to ~740 cal. yr B.P.; unit 2 from ~740 to 5430 cal. yr B.P.; unit 3 from ~5430 to 6000 cal. yr B.P.; unit 4 from ~6000 to 8880 cal. yr B.P.; and unit 5 extends back to ~9280 cal. yr B.P.

Figure 4.9 Core NBP0703 JPC51, collected in outer Collins Bay. See Fig. 4.3 for location. Width of symbols in the age model represents uncertainty.
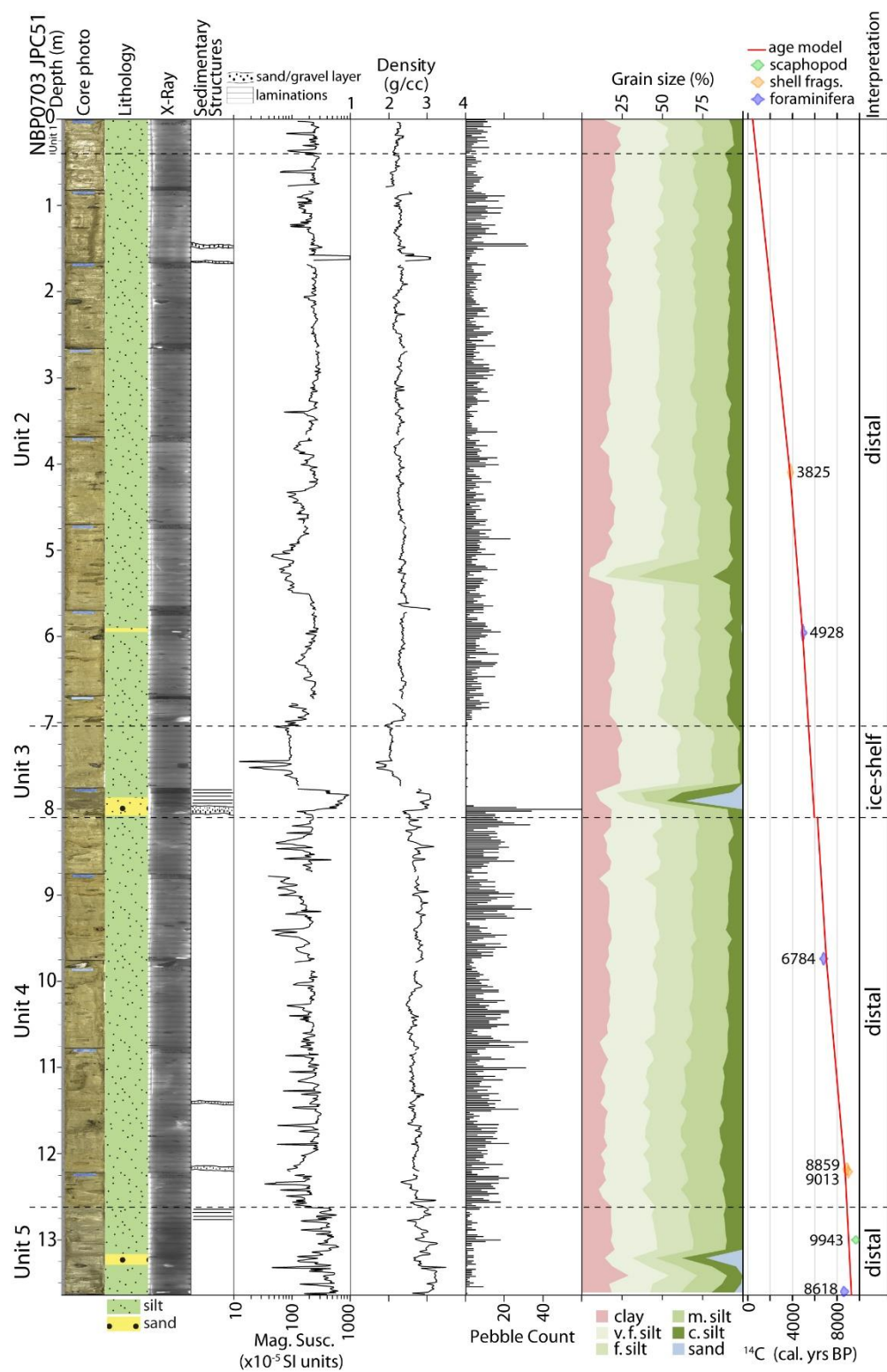
114

4.2.3. Interpretation of deglaciation history of Collins Bay

The complete sediment column of KC41 is interpreted as proximal deposits. Laminations are abundant throughout the core, while pebbles are very rare. The lower unit is clayey silt with an overall finer grain size compared to the upper unit. The lower unit is almost entirely characterized by laminations, which possibly resulted from continuous plume activity below an ice cover but near the grounding line.

JPC51 is much longer than KC41, but the core collected in the distal area has a relatively homogeneous lithology. Silt composes well over 75% of the sediment with very little sand throughout the core. Unit 5 is characterized by some pebbles and a somewhat coarser grain size downcore, indicating a distal environment of deposition. A sudden decrease of MS and relative increase of pebble abundance is observed in unit 4, which indicates a more distal to open marine environment of deposition. A decrease in MS and density values characterize unit 3, in addition to a noticeable lack of pebbles, indicating an environment protected from iceberg activity, likely covered by an ice shelf. The upper two units are interpreted open marine sediments.

The oldest sediments identified in JPC51 are distal, which indicates ice decoupled at this location well before 9280 cal. yr B.P. and likely the floating ice margin retreated landward from this location after 8880 cal. yr B.P. This area remained in an ice distal location until 6000 cal. yr B.P. when an ice shelf formed. The ice shelf persisted until 5430 cal. yr B.P., when present conditions started developing in the outer bay. KC41 only spans through 610 cal. yr B.P. We interpret an ice shelf covered this location at least from ~610 to 190 cal. yr B.P, and the area has remained open since that time (Fig. 4.10).

Figure 4.10 Interpretation of glacial retreat in Collins Bay. See Fig. 4.3 for location of cross section in the bay. Notice horizontal scales are different for the bay and the glacier. Question marks represent uncertainty about the location of the grounding line between 8880 and 5430 cal. yr B.P. Brown: bedrock, grey: ice, blue: water.

116

4.3. Beascochea Bay

4.3.1. Core NBP0703 KC42

KC42 was collected in a basin with 539 m of water depth, <1 km away from the modern ice front of Cadman Glacier in southern Beascochea Bay (Fig. 4.3).

We identified two units in KC42: unit 1 (0-160 cm) and unit 2 (160-564 cm) (Fig. 4.11). Unit 1 is dark gray (5Y, 4/1) silt with a couple of sand layers. Laminations are abundant throughout the unit with no pebbles. Sand percentages vary from <1% to 9%, increasing downcore. Grain size mode is relatively constant (11-12 μm), with the exception of sandy layers with a modal size of 21 μm. Unit 2 is dark gray (5Y, 4/1) silt with very dark gray (5Y, 3/1) sand layers and scattered pebbles. Laminations and coarse-grained sediment layers are abundant throughout the unit. Sand percentages vary from 2% to 18%. Grain size mode varies between 12-34 μm.

The age model for KC42 was derived using the youngest radiocarbon age from foraminifera collected at 558-560 cm core depth. Three anomalously high radiocarbon ages from KC42 are interpreted as being re-worked material and therefore were not used in the age model. In addition, we added ^{210}Pb ages from KC44, calculated from sedimentation rates from Boldt et al. (2013). The age model includes a hiatus at 420 cm. Unit 1 spans from the present to ~240 cal. yr B.P. and unit 2 extends to ~1400 cal. yr B.P.
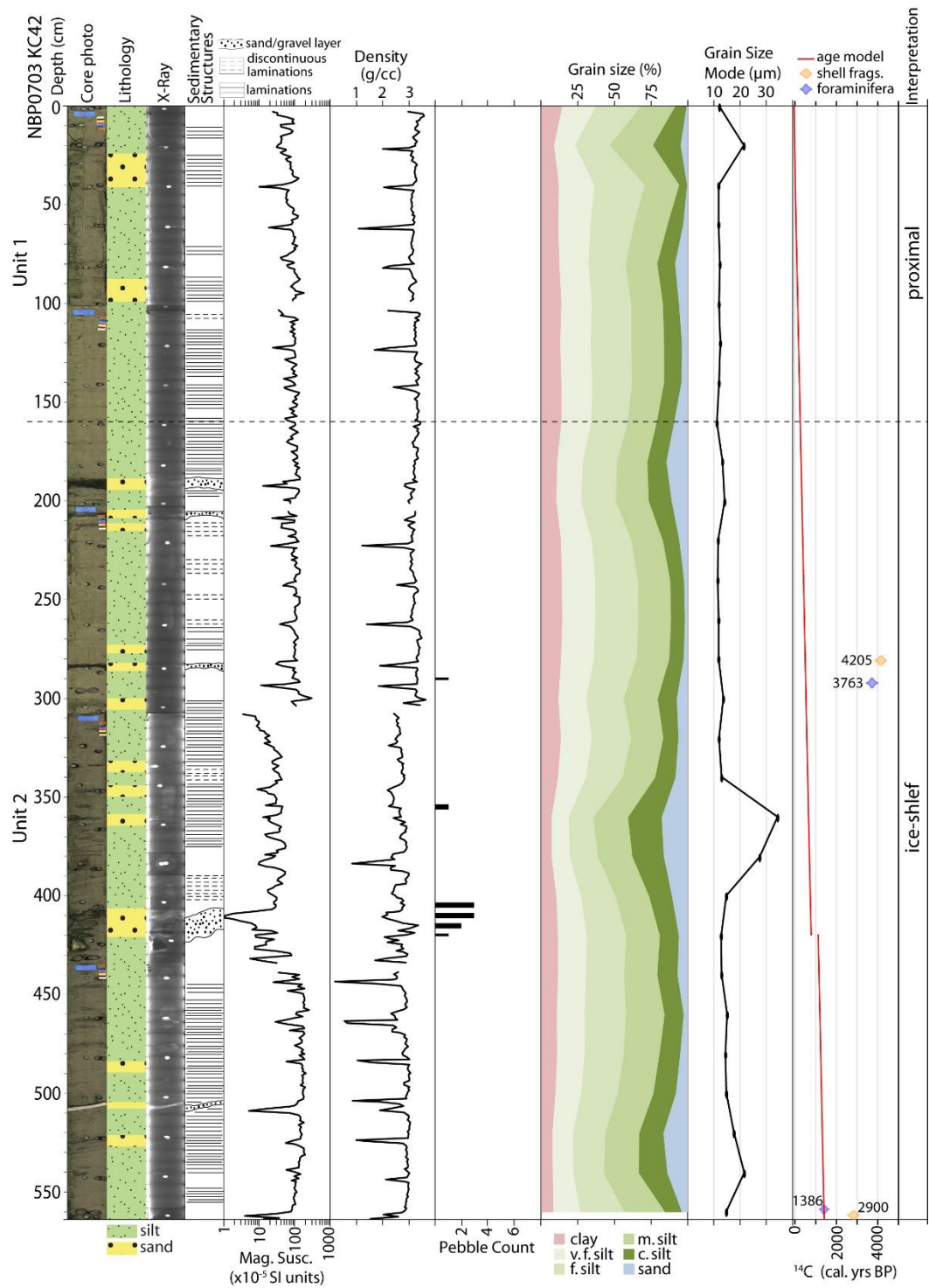
Figure 4.11 Core NBP0703 KC42, collected in inner Beascochea Bay. Open circles in ¹⁴C chronology represent reworked ages. See Fig. 4.3 for location. Break in age model represents a hiatus; width of symbols in the age model represents uncertainty. The three older radiocarbon ages are interpreted as reworked and therefore not used in the age model.

118

4.3.2. Core NBP0703 JPC47

JPC47 was collected about 10 km away from Cadman Glacier, but the location of the core is proximal to a transverse feature identified as a grounding zone wedge (Munoz and Wellner, 2018). Water depths change rapidly and create a high sloping area at this location (Fig. 4.3).

We identified four units in JPC47: unit 1 (0-38 cm), unit 2 (38-170 cm), unit 3 (170-380 cm), and unit 4 (380-1117 cm) (Fig. 4.12). Unit 1 is a dark greenish gray (GLEY1, 4/1) silt deposit with a few scattered pebbles. Sand percentages vary between 3-6%, and grain size mode remains constant (11-12 μm). Unit 2 is dark greenish gray (GLEY1, 4/1) silt with abundant laminations throughout and very few pebbles. Sand percentage varies between <1 and 4%, while grain size mode stays constant throughout the unit (10-11 μm). Unit 3 is dark greenish gray (GLEY1, 4/1) silt with scattered pebbles and no laminations. Sand percentage is larger than the previous units (varies from 3-10%), but grain size mode stays consistently between 10-12 μm throughout this unit. Unit 4 is dark greenish gray (GLEY1, 4/1) to very dark gray (GLEY1, 3/N) sandy silt with abundant pebbles throughout. A sand layer, approximately 30 cm thick, is present in the unit. Sand percentage increases downcore, from 6% to 26%, while grain size mode only increases slightly (from 10-14 μm). Grain size percentage and mode increase in the sand layer (up to 41% and 95 μm, respectively).

Due to over-penetration by JPC47 into the sediment-water interface, we combined the upper 20 cm of KC46 with JPC47. The age model for JPC47 was completed combining one radiocarbon age from KC46 and three radiocarbon ages from JPC47

(Table 4.1). Unit 1 spans from the present to ~280 cal. yr B.P.; unit 2 from ~280 to 880 cal. yr B.P.; unit 3 from ~880 to 1750 cal. yr B.P.; and unit 4 extends to ~6030 cal. yr B.P.
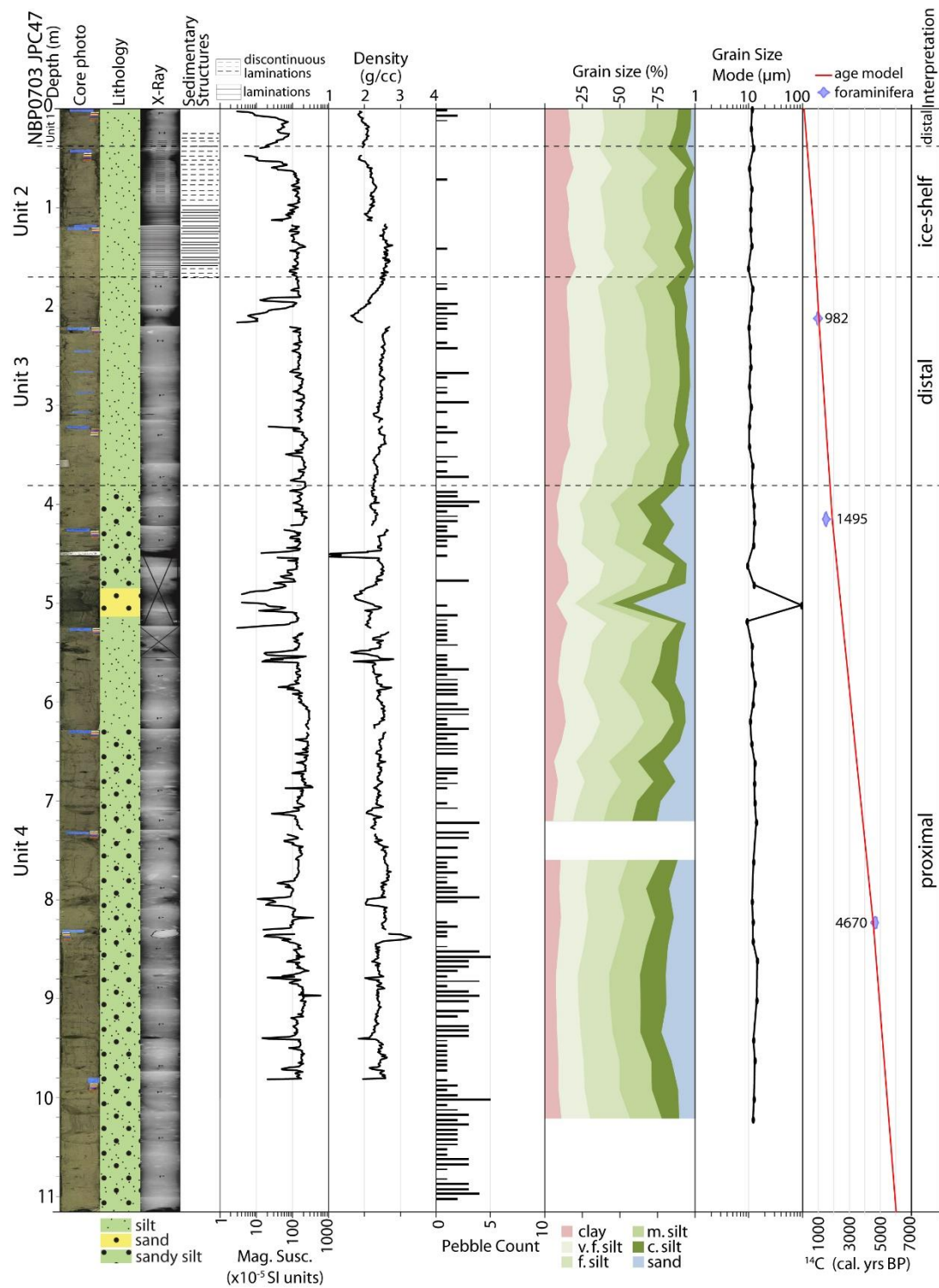
Figure 4.12 Core NBP0703 JPC47, collected in the middle bay area of Beascochea Bay. See Fig. 4.3 for location. Width of symbols in the age model represents uncertainty.

4.3.3. Core NBP0703 JPC50

The location of core JPC50 is the most distal in Beascochea Bay (Fig. 4.3). The core was collected from an 806-meter deep basin with ponded sediments. The core location is approximately 30 km from Cadman Glacier modern ice front and about 20 km from the location of JPC47.

We identified five units in JPC50: unit 1 (0-115 cm), unit 2 (115- 460 cm), unit 3 (460- 1009 cm), unit 4 (1009-1110 cm), and unit 5 (1110-1386 cm) (Fig. 4.13). Unit 1 is a dark greenish gray (GLEY1, 4/1) silt and sand deposit with a few pebbles scattered throughout. The unit is homogeneous throughout with no sedimentary structures. Sand percentage varies between <1 and 9%, and grain size mode varies from 9-12 μm. Unit 2 is a dark greenish gray (GLEY1, 4/1) to dark gray (5Y, 4/1) silt deposit with a 30-cm thick sand layer in the bottom of the unit. A distinct unit characterized by a gravel layer with an erosive bottom surface and overlain by laminated sandy mud occurs in the bottom of this unit. Sand percentage is, on average, <1% but up to 21%. This unit is interpreted as having been formed by repeated hyperpycnal flows emanating from the ice front. Grain size mode varies between 7 and 37 μm. Unit 3 is a dark gray (5Y, 4/1) silt layer with abundant pebbles throughout and some sand layers, usually <10-cm thick. The upper half of the unit is characterized by laminations. Sand percentage is, on average, 3% but up to 42% in the sand layers. Grain size mode is relatively constant (between 8-13 μm), but up to 106 μm. Unit 4 is dark gray (5Y, 4/1) silt with two sand layers (forming laminations in the sediment) and very few pebbles. Sand percentage varies between <1 to 10%. Grain size mode is relatively constant (between 9-13 μm), but up to 37 μm. Unit 5

is dark greenish gray (GLEY1, 4/1) silt with abundant pebbles and a few, thin sand layers. Sedimentary structures include sand-gravel layers, overlain by sand and silt laminations, interpreted as hyperpycnal flows. Sand percentage varies between 2% and 7%. Grain size mode varies between 10-13 μm.

Due to over-penetration by JPC50 into the sediment-water interface, we combined the upper 20 cm of KC49 with JPC50. The age model for JPC50 was completed combining ^{210}Pb dates from KC49 (Fig. 4.6) and two radiocarbon dates from JPC50 (Table 4.1). The age model includes a hiatus at the boundary between units 2 and 3. Unit 1 spans from the present to ~420 cal. yr B.P.; unit 2 from ~420 to 1910 cal. yr B.P.; unit 3 from ~1910 to 4380 cal. yr B.P.; unit 4 from ~4380 to 4780 cal. yr B.P.; and unit 5 extends to ~5910 cal. yr B.P.

Figure 4.13 Core NBP0703 JPC50, collected in outer Beascochea Bay. See Fig. 4.3 for location. Width of symbols in the age model represents uncertainty.

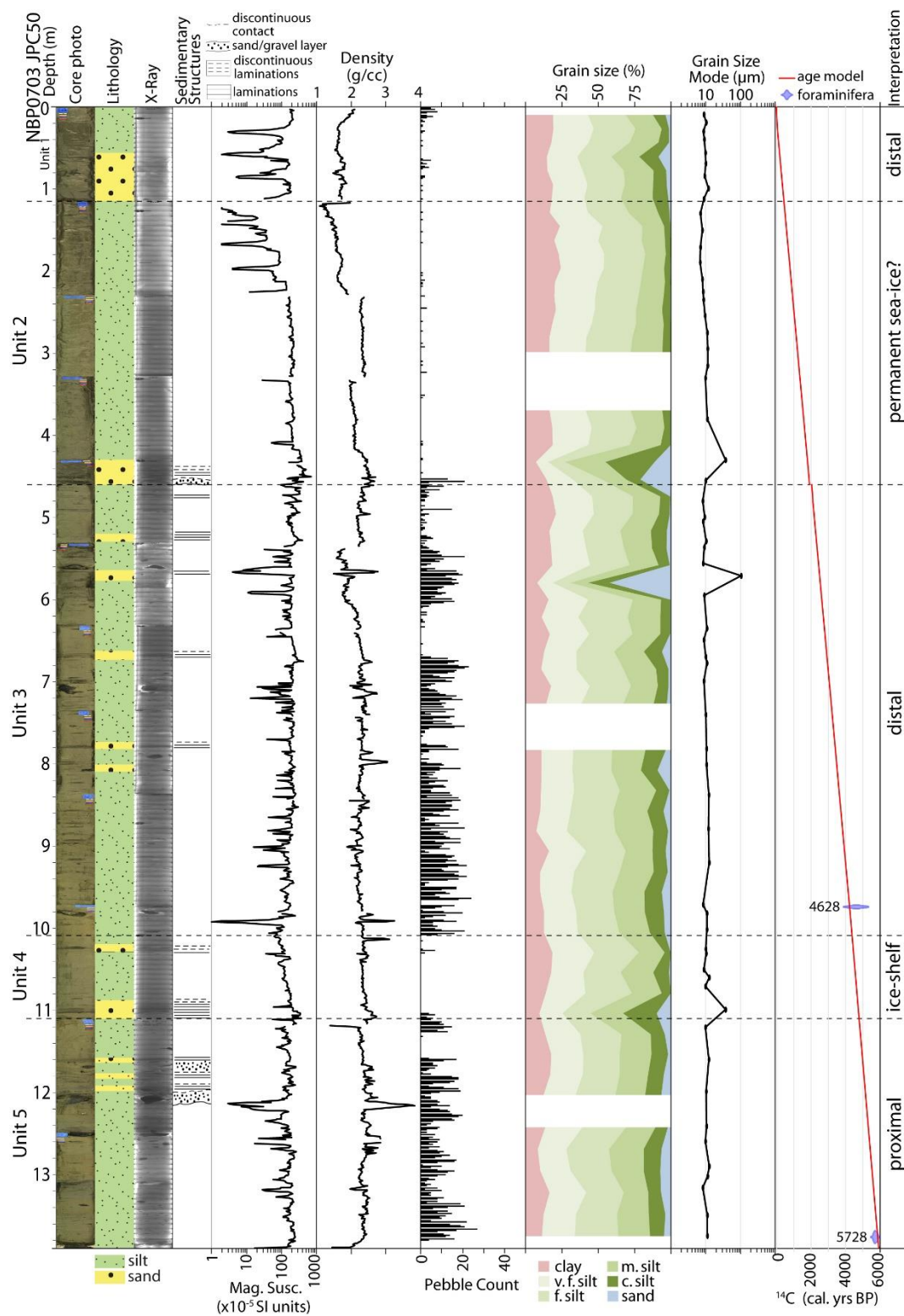### 4.3.4. Interpretation of deglaciation history of Beascochea Bay

Over 75% of the sediments in KC42 are silt size. Several sandy layers are also identified throughout the sediment column, as well as laminations and gravel layers. We interpret the core as proximal deposits, however we make a distinction between the upper and lower unit, since an ice cover was likely present during the accumulation of unit 2. Laminations and gravel layers are found throughout the core indicating that the environment of deposition has not changed extensively, except for a likely recent ice front migration away from this location, as mapped by Cook et al. (2005).

JPC47 was divided into four units. The thicker, lowermost unit is characterized by the highest abundance of pebbles and largest overall grain size. We interpret this unit as proximal deposits. A clear decrease in sand size is observed in unit 3, as well as a decrease in pebble abundance. We interpret the silty, homogeneous unit 3 as distal deposits. A lack of pebbles along with the presence of laminations throughout unit 2 indicate an ice shelf was covering this area at the time of deposition. The upper 38 cm of the core is likely the result of a distal, open marine environment.

JPC50 is also mostly composed of silt-size sediments. The lowest unit (unit 5) has abundant pebbles and relatively thick sediment gravity flow deposits. We interpret this unit as proximal sediments. A sudden decrease in pebble abundance, almost down to zero, immediately follows the proximal unit. Unit 4 is also characterized by sandy laminations, likely sourced from turbid deposits below an ice shelf. Unit 3 is the thickest unit in JPC50. Silt deposits interbedded with sand layers, and abundant pebbles characterize unit 3, which we interpret as being deposited distally from the glacier front.

Sediment homogeneity, lower density and MS values, as well as lower pebble abundance are observed in units 2 and 1. The lack of pebbles indicates an ice cover in unit 2, possibly an ice shelve or thick sea ice. Unit 1 has a higher grain size and pebble abundance, possibly ice-rafted debris, which indicates a distal, open marine environment.

Ice retreated from the outer bay prior to 5910 cal. yr B.P., when proximal deposits accumulated at the location of JPC50. The ice front retreated to a location near JPC47 around 4780 cal. yr B.P., possibly forming grounding zone wedges in the middle bay area (Munoz and Wellner, 2018). Between 4780 and 4380 cal. yr B.P., an ice-shelf likely covered the outer bay. Between 4380 and 1750 cal. yr B.P, ice retreated further inland, likely close to the modern location of ice front margins. During this time sediments were deposited and reworked, which explains sediments of 4000 cal. yr B.P. age in the proximal area to Cadman Glacier (Table 4.1). An ice-shelf (or thick sea ice) covered the entire bay between 1750 and 420 cal. yr B.P. The ice cover lasted at least until 240 cal. yr B.P. in the proximal area to the glacier fronts (Fig. 4.14). There is no evidence of ice grounding over the location of KC42 since at least 4000 cal. yr B.P, but seafloor geomorphology proximal to Lever and Funk glaciers suggest glacial re-advance (Munoz and Wellner, 2018), likely during the time the most recent ice shelves formed over KC42 and JPC47. Unfortunately, no radiocarbon dates are available for cores proximal to Lever and Funk glaciers.
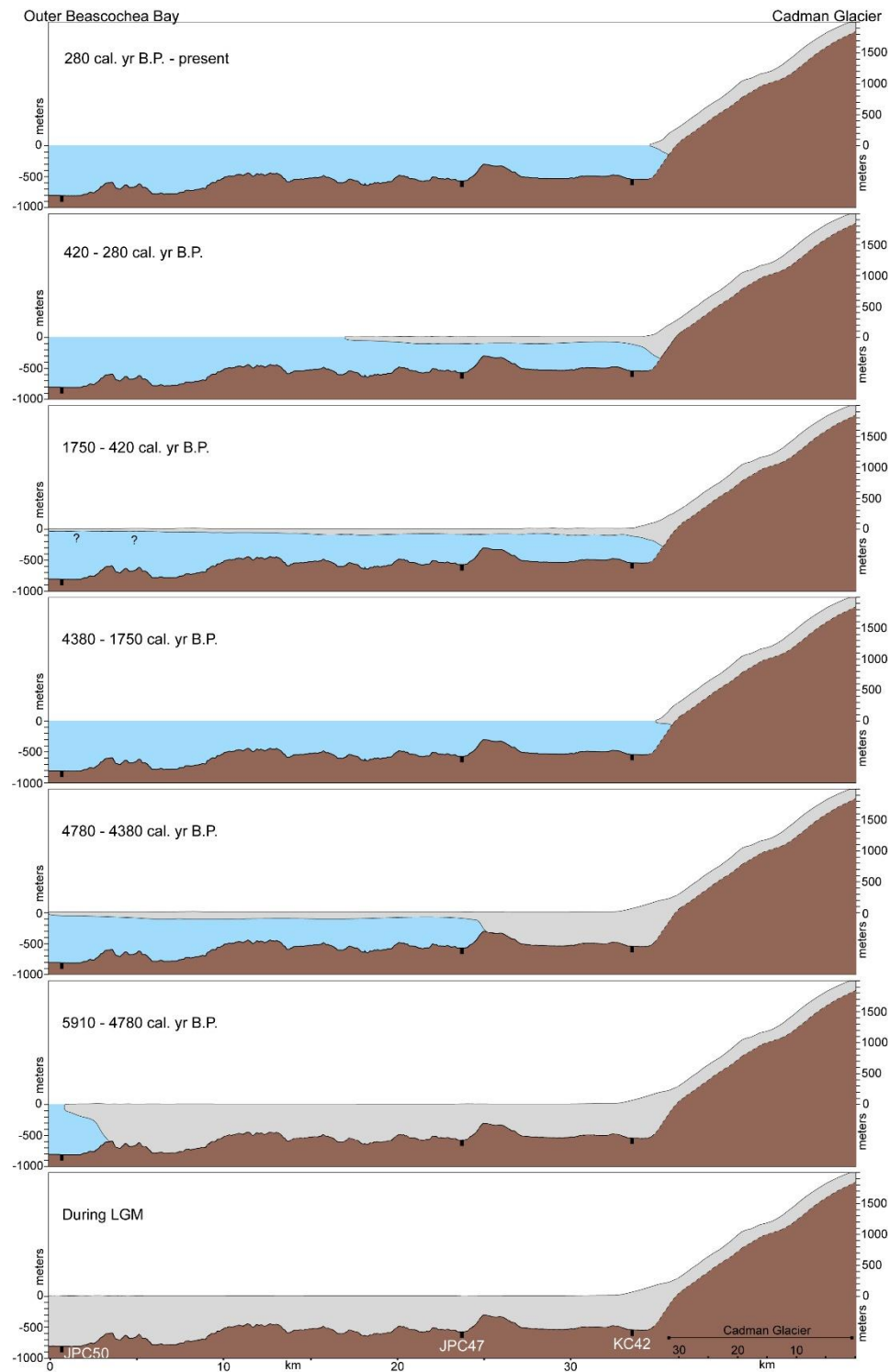
Figure 4.14 Interpretation of glacial retreat in Beascochea Bay. See Fig. 4.3 for location of cross section in the bay. Notice horizontal scales are different for the bay and the glacier. Question marks represent uncertainty over the presence of fast sea ice or an ice shelf between 1750 and 420 cal. yr B.P. Brown: bedrock, grey: ice, blue: water.

127

5. Sediment units as related to Holocene climatic events

Studies of the Antarctic Peninsula continental shelf have provided compelling evidence for a much expanded Antarctic Peninsula ice cap that extended across the continental shelf on both sides of the AP and included a number of discrete ice streams (e.g. Heroy and Anderson, 2005; Livingstone et al., 2013; ÓCofaigh et al., 2014). Radiocarbon ages from sediment cores reveal that the ice sheet retreated from the outer to inner shelf ~14 to ~11 ka. This was followed by a more variable and diachronous retreat as the grounding line of the collapsing ice sheet shifted onto the rugged bedrock relief of the inner continental shelf and drainage from the peninsula became separated into multiple outlet and valley glaciers (Heroy and Anderson, 2005). Ever since, the behavior of these individual glaciers has been influenced by multiple factors, including drainage basin area and hypsometry, the physiography of the bays and fjords into which they drain, oceanographic influence and climate.

Multibeam data from the study areas reveal glacially sculpted bedrock that is typically exposed or covered by relatively thin sediment (Griffith and Anderson, 1989; Munoz and Wellner, 2018). Sedimentation is largely confined to basins in the bays and ice proximal locations. While glacial advance and retreat can be caused by both climate change and oceanographic influences, previous studies have led to the conclusion that climate variability has been the principle driver in regulating glacier behavior during the Holocene as glaciers retreated further inland and became more isolated from oceanographic influence (Shevenell et al., 1996; Domack et al., 2001; Sjunneskog and Taylor, 2002; Domack et al., 2003; Milliken et al., 2009; Michalchuk et al., 2009; Allen

et al., 2010; Barnard et al., 2014; Christ et al., 2014; Minzoni et al., 2015). While individual facies changes are highly variable from one bay to another, general trends in each location do occur and environmental changes indicated by sedimentary facies is aided by results from these previous investigations (Fig. 15).

5.1. Climatic Reversal

The oldest sedimentary unit (unit 5) was sampled in JPC51 (1262 to 1364 cm core depth) in outer Collins Bay (Fig. 4.16). This event spans from 9280 to 8880 cal. yr B.P. The sediment is silt with scattered pebbles and a sand content increasing downcore. Evidence suggest these sediments were deposited distal to the glacier front, therefore this area was ice free by 9280 cal. yr B.P. At least one older date is found in this unit (Table 4.1, Fig. 4.9), which indicates reworking at this location. Unit 5 records the final stage of ice retreat from the continental shelf and the onset of marine conditions within Collins Bay.
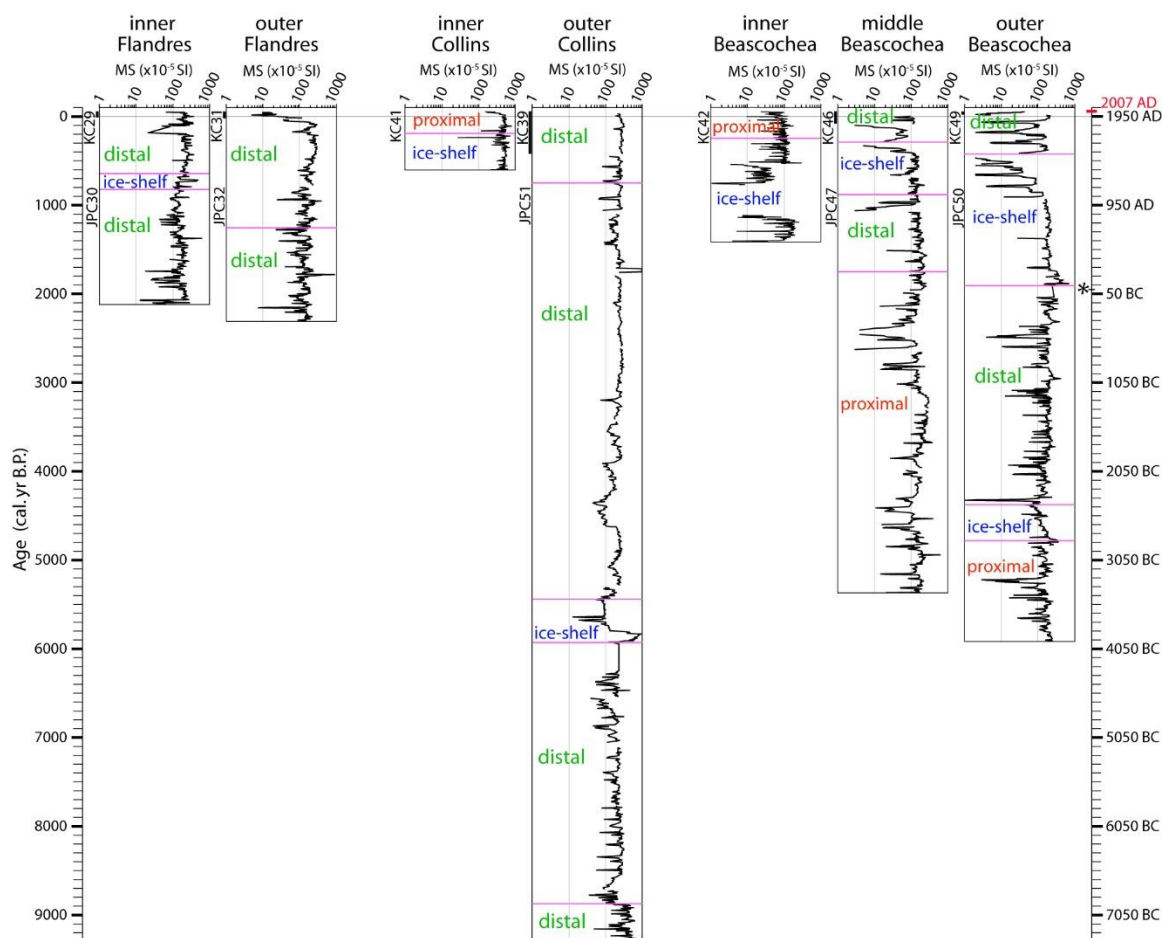
Figure 4.15 Magnetic Susceptibility (MS) plotted in calibrated years B.P. for cores in Flandres, Collins, and Beascochea bays showing interpreted facies (from Figs. 4.4, 4.5, 4.8, 4.9, 4.11, 4.12, and 4.13). 0 cal. yr B.P. is 1950 A.D. Asterisk shows 0 A.D. Black bar to the right of the core name identifies the length of the KC core top that was added to the longer JPC to compensate for over-penetration into the sediment-water interphase at the time of coring.

5.2. Mid-Holocene Climatic Optimum (MHCO)

Multiple proxies, including sedimentary and paleontological (diatoms and foraminifera) indicate warming during the middle Holocene in Maxwell Bay (Milliken et al., 2009), Firth of Tay (Michalchuk et al., 2009), Palmer Deep (Domack et al., 2001), Barilari Bay (Christ et al., 2014), Lallemand Fjord (Shevenell et al., 1996), and Neny Fjord (Allen et al., 2010), consistent with our interpretations. In Collins Bay, unit 4 of

JPC51 show a sudden increase in pebble abundance and a slight decrease in grain size starting around 8880 cal. yr B.P. (Fig. 4.9), suggesting glacial retreat in the area that was likely triggered by relatively warmer conditions.

In outer Beascochea Bay, unit 5 of JPC50, is characterized by abundant pebbles and hyperpycnal flows, interpreted as proximal sediments (Fig. 4.13), deposited ~5910 cal. yr B.P. While it is not possible to constrain the onset of the MHCO at this location, unit 5 does place an upper limit on the MHCO prior to this time.

5.3. Neoglacial

A cooling event identified as the Neoglacial is observed in several locations in the AP including: Maxwell Bay beginning at ~2600 cal. yr B.P. (Milliken et al., 2009), Palmer Deep beginning at 3360 cal. yr B.P. (Domack et al., 2001), Firth of Tay beginning at ~3500 cal. yr B.P. (Michalchuk et al., 2009), Barilari Bay beginning at 2815 cal. yr B.P. (Christ et al., 2014), Lallemand Fjord beginning at 2880 cal. yr B.P. (Taylor et al., 2001), and Neny Fjord beginning at 2850 cal. yr B.P. (Allen et al., 2010).

An abrupt decrease in pebble abundance observed in unit 3 of JPC51 (Fig. 4.9) indicates decreased ice rafting, likely due to establishment of a thick ice canopy that restricted iceberg from drifting into outer Collins Bay. Unit 3 spans from 6000 to 5430 cal. yr B.P. Similar sediment characteristics are observed in unit 4 of JPC50, outer Beascochea Bay, starting at around 4780 cal. yr B.P (Fig. 4.13). A cooling event is the simplest explanation for the growth of an ice shelf in the outer bay areas. We interpret these events as the onset of the Neoglacial period. We also interpret a cooling trend in

outer Flandres Bay, however, its timing is not as well constrained as in the other bays

(Fig. 4.16). These observations are consistent with the Neoglacial starting around 6000

cal. yr B.P. in Collins Bay and lasting until around 700 cal. yr B.P. in Flandres Bay. The

earlier onset of Neoglacial conditions in Collins and Beascochea bays compared to

Flandres Bay may be due to their more southern location.

5.4. Medieval Warm Period (MWP)

The Medieval Warm Period marked by summer-dominated conditions and enhanced

productivity is recognized in a couple locations in the western AP; Maxwell Bay (Hass et

al., 2010; Monien et al., 2011), Lallemand Fjord, and Crystal Sound (Domack et al.,

2003). We do not observe strong evidence for the Medieval Warm Period (MWP) in

JPC51 and JPC47 (Fig. 4.16). JPC51 in outer Collins Bay shows a slight increase in

pebble abundance, which may correspond to a warming event starting at around 1700 cal.

yr B.P. While around the same time period, JPC47 (middle Beascochea Bay) shows a

relative decrease in pebble abundance and a decrease in grain size, characteristic of a

cooler environment. Although these sediment characteristics in Beascochea Bay may be

related to the distal location of the core, and not to the MWP. In Lallemand Fjord and

Crystal Sound, the MWP was identified from 1150-700 cal yr B.P. and is marked by

increased biogenic productivity (Domack et al., 2003), therefore including biogenic

proxies would help elucidate the presence of the MWP in Flandres, Collins, and

Beascochea bays.

5.5. Little Ice Age (LIA)

Similarly to the MWP, the Little Ice Age is identified only in a few marine sediment records in the AP: Maxwell Bay (Hass et al., 2010; Monien et al., 2011), Palmer Deep (Domack et al. 2001), Barilari Bay (Christ et al., 2014), and Lallemand Fjord (Domack et al., 1995; 2003). This event is marked by low total organic carbon and lower primary productivity.

Unit 2 in cores JPC30 (Flandres Bay), KC41 (Collins Bay), and KC42 (Beascochea Bay) have laminations and scattered pebbles, suggesting the presence of a recent ice shelve in the inner bay area, most likely triggered by a cooling event (Figs. 4.4, 4.8, 4.11). Unit 2 in cores JPC47 and JPC50 in the middle and outer Beascochea Bay, respectively, also show the same characteristics (Figs. 4.12, 4.13). Although the onset of this event is variable in these locations, as early as 1910 cal. yr B.P. in outer Beascochea, and as late as 820 cal. yr B.P. in inner Flandres Bay, the cooling event may be related to the Little Ice Age.

5.6. Recent warming

Results from ^{210}Pb show very high sedimentation rates for the past 100 years in the AP bays (Fig. 4.6). These may be related to the recent regional warming identified in the AP from the 1950-1960s to the late 1990s (Vaughan et al., 2003; Turner et al., 2005). The sediment proxies show a high variability in the core tops. Decreased MS in some of the core tops may be related to a higher attenuation of the terrigenous input due to a higher biogenic input (Allen et al., 2010). In addition, the inner bay cores show indications of

high meltwater activity; JPC30 and KC41 show an increase in the sand percentage, while KC42 is heavily laminated, also interpreted as indicative of increased meltwater sedimentation. Sediment in the outer bay areas is mainly homogeneous clayey silt to silt, with pebbles. Flandres Bay shows a slight increase in the sand percentage, possibly explained by high ocean current activity in that area (Munoz and Wellner, 2016).
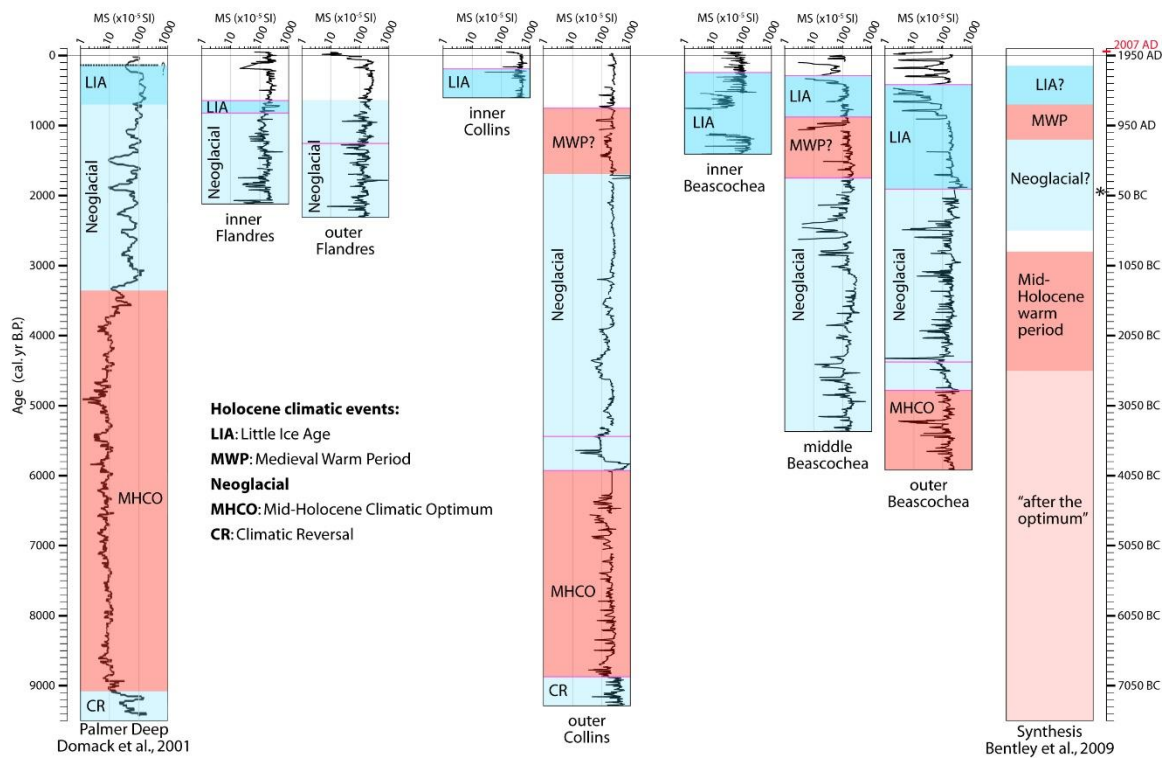
Figure 4.16 Magnetic Susceptibility (MS) plotted in calibrated years B.P. for cores in Flandres, Collins, and Beascochea compared to MS from Palmer Deep (Domack et al., 2001) and the synthesis of climatic events in the Antarctic Peninsula (Bentley et al., 2009). Shades of blue represent cooler climatic events, shades of red represent warmer climatic events.

6. Regional correlation of climatic events in the AP

Bentley et al. (2009) presented a synthesis of climate events in the AP based on various paleoenvironmental records including ice cores, lakes sediments, marine sediments, and terrestrial and marine geomorphology. They identified the following events throughout the AP: early Holocene climate optimum (~11000-9500 cal. yr B.P.), after the optimum (~9500-4500 cal. yr B.P.), Mid-Holocene warm period (~4500-2800 cal. yr B.P.), a possible Neoglacial interval (~2500-1200 cal. yr B.P.), Medieval warm period (~1200-600 cal. yr B.P.), a possible Little Ice Age, and the recent warming throughout the AP. We compare our interpreted climate events to the synthesis from Bentley et al. (2009) in Fig. 4.16 and observe that there is some variation in the timing of onset and termination of these events, we explain some of the discrepancies below.

In addition, in Fig. 4.16 we compare our climate event interpretations to a marine drill core results from Palmer Deep, located about 40 km west of Flandres Bay and 60 km northwest of Collins and Beascochea bays (Fig. 4.1). Domack et al. (2001) used MS, mass accumulation rates, and ice-rafted debris, as well as a radiocarbon age model, to identify the following paleoenvironmental intervals: Last Glacial Maximum (older than 13180 cal. B.P), deglacial episode (13180-11460 cal. B.P.), climatic cooling/reversal (11460-9070 cal. B.P.), mid-Holocene climatic optimum (9070-3360 cal. B.P.), and Neoglacial interval (3360-100 cal. B.P) which includes the Little Ice Age (700-100 cal. B.P.). Similar to the AP synthesis, there are some differences between our interpretations and the results from Palmer Deep.

We interpret the MHCO in Collins Bay from 8880-6000 cal. yr B.P. (Fig. 4.16). In Palmer Deep, Domack et al. (2001) identified a very long lasting MHCO (9070-3360 cal. yr BP). Milliken et al. (2009) interpreted this same climatic event from 8200-5900 cal. yr B.P. in Maxwell Bay, in closer agreement to our interpretation. Additionally, Allen et al. (2010) interpreted the end of the climatic optimum around 7000 cal. yr B.P. in Neny Fjord, similar timing to our interpretation. However, they interpreted less sea ice cover between ~7000-2800 cal yr B.P., while we see the formation of ice shelves in Collins and Beascochea during that time interval.

Sjunneskog and Taylor (2002) identified a cooling event between 6000-5000 cal. yr B.P. in Palmer Deep which coincides with our interpretation of a cooling event forming an ice shelf in outer Collins Bay (between 6000-5430 cal. yr B.P. in Fig. 4.9). Sjunneskog and Taylor (2002) however, still place this cooling event within the Holocene optimum, and not as part of the Neoglacial period.

We interpret the onset of the Neoglacial period much earlier than other authors. In JPC51, we identify a cooling trend, which we interpret as the Neoglacial starting around 6000 cal. yr B.P. (Fig. 4.16). In other areas like Maxwell Bay, Palmer Deep, Barilari Bay, Lallemand Fjord, and Neny Fjord, the onset of this period is identified at 2600, 3360, 2815, 2880, and 2800 cal. yr B.P., respectively (Domack et al., 2001; Taylor et al., 2001; Milliken et al., 2009; Allen et al., 2010; Christ et al., 2014). In outer Beascochea Bay, the cooling trend occurs later, between 4780 and 4380 cal. yr B.P. (Fig. 4.13). This timing is roughly consistent with a glacial readvance in Firth of Tay, between 6000-4500 cal. yr B.P. (Michalchuk et al., 2009), but nevertheless considered an early onset compared to the locations mentioned above.

The MWP is recognized only in a few locations in the western AP: Maxwell Bay, Lallemand Fjord, and Crystal Sound (Domack et al., 2003; Hass et al., 2010; Monien et al., 2011). Similarly, the LIA is identified in marine sediments only in a few locations: Maxwell Bay, Palmer Deep, Barilari Bay, and Lallemand Fjord (Domack et al., 1995; Shevenell et al., 1996; Domack et al., 2001; Hass et al., 2010; Monien et al., 2011; Christ et al., 2014). While our evidence of MWP is not compelling, the growth of an ice sheet in Flandres, Collins, and Beascochea bays is more evident and roughly occurs during the LIA period. The MWP and LIA may be the result of small climate fluctuations and therefore only distinguishable in proximal cores. In the distal cores, a more detailed sedimentological study may be necessary to identify signals of MWP and LIA.

Regarding the recent warming, there is some sedimentological evidence, such as increased primary productivity (Christ et al., 2014) and increased mass accumulation rates (Monien et al., 2011) but the sediment records do not vary widely from older warm climate events. Although we measured high accumulation rates in Flandres, Collins, and Beascochea bays (Fig. 4.6), a more holistic approach should be taken to analyze sediment accumulation in the past 100 years to distinguish the recent rapid warming from other past warm periods in order to assess its magnitude.

7. Forcing mechanisms

Recent glacial retreat in the western AP has been attributed to warm Circumpolar Deep Water intrusion into the continental shelf (Cook et al., 2016), flowing northward flanking the western AP. The oceanic forcing is creating a synchronous behavior of

glacial retreat, especially in glaciers in the south AP which are in direct contact with the water mass. The effect of the CDW has been well documented in areas south of the AP, where incursions of the CDW onto the West Antarctic continental shelf melt the ice shelves and glacier fronts accelerating retreat (Jenkins et al., 2010; Jacobs et al., 2011; 2013; Hillenbrand et al., 2017; Minzoni et al., 2017).

The warmer environment of the mid-Holocene climatic optimum has also been attributed to an influx of Circumpolar Deep Water (CDW) into the southern AP continental shelf, driving the glacial retreat (Allen et al., 2010). Logically, the absence of the warm water mass, would contribute to the development of an ice shelf in the bays, as may have occurred during the LIA (Shevenell and Kenneth, 2002; Christ et al., 2014).

The asynchronous onset and length of the MHCO we observe in the cores (Fig. 4.16) may be the result of a combination of forcing mechanisms. Additionally, due to the close location of Palmer Deep to Flandres, Collins, and Beascochea bays, the influence of atmospheric and oceanic circulation should be very similar, and the sediment deposits would therefore be similar, but this is not the case. An obvious difference is the relative location of the core site to the glacier front and the number of glaciers feeding into any particular bay. For example, Beascochea Bay deglaciated much later than Palmer Deep and Collins Bay, possibly due to a high influx from the large glaciers feeding into the bay. If this is the case, an important driver for the mid-Holocene was also atmospheric warming. Shevenell and Kenneth (2002) also proposed an atmospheric forcing for the Palmer Deep area; weaker westerly winds allowed for an increase in CDW intrusion into the Palmer Deep area for ~9000-3600 cal. yr B.P, correlating to the MHCO.

In summary, a combination of oceanographic and atmospheric forcing drove fluctuations for the largest part of the Holocene. However, changes in the late-Holocene may be attributed mainly to oceanic forcing, making the marine-terminating glaciers extremely susceptible to increased warm water intrusion into the bays.

8. Summary and conclusions

Sediment cores from Collins and Beascochea bays yielded a complete sediment record of Holocene deglaciation in the bays. Cores in Flandres Bay are shorter and only span to the late Holocene. In Flandres Bay, a cooling event, roughly corresponding to the LIA time period, covered the inner bay area, proximal to Briand Fjord (Fig. 4.7).

Deglaciation in Collins Bay started before 9280 cal. yr B.P., ice retreated landward between 8880 and 6000 cal. yr B.P., when an ice shelf formed over the outer bay area. The ice cover lasted until 5430 cal. yr B.P. when present conditions started developing in the outer bay area. The inner bay area was covered by an ice shelf from 610 to 190 cal. yr B.P., and has remained open since that time (Fig. 4.10).

Deglaciation in Beascochea Bay occurred later, possibly around 5910 cal. yr B.P. in the outer bay, and around 4780 cal. yr B.P. in the middle bay area. An ice shelf covered the bay from 4780 to 4380 cal. yr B.P. Ice continued to retreat inland, and possibly up to the modern glacial ice fronts between 4380 and 1750 cal. yr B.P., reworking some of the sediment. There is no evidence of glacial re-advance over the bay, but there is at least one event of ice shelf growth in the bay between 1750 and 280 cal. yr B.P. Modern conditions likely started around 280 cal. yr B.P. (Fig. 4.14).

139

The mid-Holocene climatic optimum and the Neoglacial periods are widely recognized in several locations around the AP, including Collins and Beascochea bays. Although, the timing of onset and termination of these periods varies from location to location. These variations may be due to a combination of forcing mechanisms, including oceanographic and atmospheric. The more recent climatic events, MWP and LIA, present in Collins and Beascochea are, however, not observed throughout the AP. The identification of these recent climatic events may require a more detailed sedimentological analysis, including accounting for organic material, diatoms, and foraminifera. Overall, glacial behavior may have been more diachronous in the past and became more synchronous in recent time, as glaciers throughout the AP have been experiencing retreat since the past 50 years. In addition, local factors in the bays may be obscuring regional signals, which may explain variation in timing of onset and termination of climatic events when comparing Palmer Deep (in the continental shelf, away from glaciers), Collins Bay (an open bay system with a large glacier), and Beascochea Bay (a fjord-type bay with several glaciers).

Sediment deposits from the last 100 years should be analyzed more in depth since we observe high variability in the core tops. Short-lived isotopes are useful to establish sediment chronology but should be sampled at a high frequency in the core tops. While ocean forcing is the primary cause of retreat of glaciers (Cook et al., 2016), some bays experience localized variations, for example some glaciers are retreating and some are advancing within Beascochea Bay. Therefore, a holistic approach is needed to understand forcing mechanisms and sediment processes within the bays.

Chapter 5

CONCLUSIONS

The goal of my dissertation research was to understand the local variations in the AP, the environments of deposition, and analyze the products as well as the responses to climate variability through the Holocene. I studied modern surface sediment distribution in a bay with subpolar climate; mapped geomorphic seafloor features in bays throughout the AP; and analyzed cores of Holocene sediment from bays in the central AP.

In Flandres Bay, grain size coarsens from the inner to the outer bay. Sediments sampled in the head of the bay have the highest clay component whereas samples collected in the mouth of the bay have the highest sand component. Our findings suggest that discrete areas of the bay are affected differently by varying factors to distribute sediment; these factors include persistent fast sea ice, differential rates of primary productivity, and winnowing of fine grained sediments away from the bay.

The geomorphology found in the seafloor of western AP bays indicate that bay length and width exert a control on the number of landform features found in the bays. In addition, narrower bays tend to form transverse-to-flow features because the lateral drag of the ice flow increases as the valley width narrows which may lead to ice flow stabilization. Small size features, e.g. moraines, were only found in narrow bays with smaller drainage areas, and not in larger-sized drainages areas, suggesting that short-lived environmental fluctuations, responsible for the formation of these features, would only be

recorded by the smaller glacial systems. We identified networks of channels carved in bedrock, likely produced by subglacial meltwater channels, which highlights the presence of subglacial meltwater production in the northern AP region, possibly through several glacial cycles. Finally, based on analogous assemblages of landforms reported in other locations, we propose the geomorphic features found in the seafloor of some of the proximal bay areas were formed during the LIA glacial advance.

We also analyzed climatic events throughout the Holocene by studying the sediment accumulated in basins of Flandres, Collins, and Beascochea bays. Deglaciation, following the LGM, in Collins Bay started before 9280 cal. yr B.P., while in Beascochea Bay deglaciation started much later, possibly around 5910 cal. yr B.P. in the outer bay, and around 4780 cal. yr B.P. in the middle bay area. A recent glacial advance was interpreted in the inner bay areas of Collins Bay (610-190 cal. yr B.P.), Beascochea Bay (1750-280 cal. yr B.P.), and Flandres Bay (820-640 cal. yr B.P.), roughly corresponding to the LIA time period. The mid-Holocene climatic optimum (MHCO) and the Neoglacial periods are widely recognized in several locations around the AP, including Collins and Beascochea bays, although the timing of onset and termination of these periods varies from location to location. These variations may be due to a combination of forcing mechanisms, including oceanographic and atmospheric. The more recent climatic events, MWP and LIA, present in Collins and Beascochea are, however, not observed throughout the AP, possibly due to their smaller scale in comparison to MHCO and Neoglacial. The modern glacial retreat is observed in most bays studied in the AP indicating a common forcing mechanism, the intrusion of warmer water melting the glacier fronts.

REFERENCES

Adie, R.J. 1969. Geologic map of Antarctica, northern Antarctic Peninsula. Sheet 1, plate 1, folio 12. Geology. Antarctic Map Folio Series. New York: American Geographical Society.

Allen, C.S., Oakes-Fretwell, L., Anderson, J.B. & Hodgson, D.A. 2010. A record of Holocene glacial and oceanographic variability in Neny Fjord, Antarctic Peninsula. The Holocene 20, 551-564.

Alley, R.B., Anandakrishnan, S., Dupont, T.K., Parizek, B.R. & Pollard, D. 2007. Effect of sedimentation on ice-sheet grounding-line stability. Science 315, 1838-1841.

Alley, R.B., Blankenship, D.D., Rooney, S.T. & Bentley, C.R. 1989. Sedimentation beneath ice shelves- The view from ice stream B. Marine Geology 85, 101-120.

Anderson, J.B. 1999. Antarctic Marine Geology. Cambridge, UK: Cambridge University Press.

Anderson, J.B., Brake, C., Domack, E.W., Myers, N. & Wright, R. 1983. Development of a polar glacial–marine sedimentation model from Antarctic Quaternary deposits and glaciological information. In B.F. Molnia (ed.): Glacial marine sedimentation. Pp. 233-264. New York: Plenum Press.

Anderson, J.B. & Fretwell, L.O. 2008. Geomorphology of the onset area of a paleo-ice stream, Marguerite Bay, Antarctic Peninsula. Earth Surface Processes and Landforms 33, 503-512.

Anderson, J.B., Kurtz, D.D., Domack, E.W. & Balshaw, K.M. 1980. Glacial and glacial marine sediments of the Antarctic Continental Shelf. The Journal of Geology 88, 399-414.

Anderson, J.B., Shipp, S.S., Lowe, A.L., Wellner, J.S. & Mosola, A.B. 2002. The Antarctic Ice Sheet during the Last Glacial Maximum and its subsequent retreat history: a review. Quaternary Science Reviews 21, 49-70.

Anderson, J.B., Warny, S., Askin, R.A., Wellner, J.S., Bohaty, S.M., Kirshner, A.E., Livsey, D.N., Simms, A., Smith, A.R., Smith, T.R., Ehrmann, W., Lawver, L.A., Barbeau, D., Wise, S.W., Kulhanek, D.K., Weaver, F.M. & Majewski, W. 2011. Progressive Cenozoic cooling and the demise of Antarctica's last refugium. Proceedings of the National Academy of Sciences of the United States of America 108, 11356-11360.

Anderson, J.B., Wellner, J.S., Lowe, A.L., Mosola, A.B. & Shipp, S.S. 2001. Footprint of the expanded West Antarctic Ice Sheet: ice stream history and behaviour. Geological Society of America Today 11, 4–9.

Appleby, P.G. & Oldfield, F. R. 1978. The calculation of lead-210 dates assuming a constant rate of supply of unsupported 210Pb to the sediment. Catena 5, 1-8.

Appleby, P.G. & Oldfield, F.R. 1983. The assessment of 210Pb data from sites with varying sediment accumulation rates. Hydrobiologia 103, 29-35.

Arndt, J. E., Schenke, H.W., Jakobsson, M., Nitsche, F.O., Buys, G., Goleby, B., Rebesco, M., Bohoyo, F., Hong, J., Black, J., Greku, R., Udintsev, G., Barrios, F., Reynoso-Peralta, W., Taisei, M. & Wigley, R. 2013. The International Bathymetric Chart of the Southern Ocean (IBCSO) Version 1.0 - A new bathymetric compilation covering circumAntarctic waters. Geophysical Research Letters 40, 3111-3117.

Ashcroft, W.A. 1972. Crustal structure of the South Shetland Islands and Bransfield Strait. British Antarctic Survey Scientific Reports, no. 66. Natural Environment Research Council, London.

Ashley, G.M. & Smith, N.D. 2000. Marine sedimentation at a calving glacier margin. Geological Society of America Bulletin 112, 657-667.

Barker, P.F., Dalziel, I.W.D. & Storey, B.C. 1991. Tectonic evolution of the Scotia Arc Region. In: Antarctic Geology, R.J. Tingey (ed.), Oxford University Press, Oxford, 215-248.

Barnard, A., Wellner, J.S. & Anderson, J.B. 2014. Late Holocene climate change recorded in proxy records from a Bransfield Basin sediment core, Antarctic Peninsula. Polar Research 33, 17236. (doi.org/10.3402/polar.v33.17236)

Batchelor, C.L. & Dowdeswell, J.A. 2015. Ice-sheet grounding zone wedges (GZWs) on high-latitude continental margins. Marine Geology 363, 65-92.

Bennet, M. & Glasser, N. 2009. Glacial Geology: ice sheets and landforms. UK: Wiley-Blackwell.

Bentley, M.J., Hodgson, D.A., Smith, J.A., Ó Cofaigh, C.O., Domack, E.W., Larter, R.D., Roberts, S.J., Brachfeld, S., Leventer, A., Hjort, C., Hillenbrand, C.D. & Evans, J. 2009. Mechanisms of Holocene palaeoenvironmental change in the Antarctic Peninsula region. The Holocene 19, 51-69.

Bi, D., Budd, W.F., Hirst, A.C. & Wu, X. 2002. Response of the Antarctic circumpolar current transport to global warming in a coupled model. Geophysical Research Letters 29, article no. 2173. (doi: 10.1029/2002GL015919)

Blaauw, M. & Christen, J.A. 2011. Flexible paleoclimate age-depth models using an autoregressive gamma process. Bayesian Analysis 6, 457-474.

Boldt, K.V., Nittrouer, C.A., Hallet, B., Koppes, M.N., Forrest, B.K., Wellner, J.S. & Anderson, J.B. 2013. Modern rates of glacial sediment accumulation along a 15° S–N transect in fjords from the Antarctic Peninsula to southern Chile. Journal of Geophysical Research—Earth Surface 118, 2072–2088.

Bradwell, T., Stoker, M. & Krabbendam, M. 2008. Megagrooves and streamlined bedrock in NW Scotland: the role of ice streams in landscape evolution. Geomorphology 97, 135-156.

Bryan, J.R. (ed.) 1992a. Descriptions of sediments recovered by the USCGC Glacier USARP. Operation Deep Freeze 1985. South Orkney Plateau, South Shetland Shelf, Bransfield Strait, Marguerite Bay, Pine Island Bay. Sedimentology Research Laboratory Contribution 54. Tallahassee, FL: Antarctic Marine Geology Research Facility.

Bryan, J.R. (ed.) 1992b. Descriptions of sediments recovered by the USCGC Glacier. USARP Operation Deep Freeze 1986. Bransfield Strait, Gerlache Strait, Marguerite Bay. Sedimentology Research Laboratory Contribution 55. Tallahassee, FL: Antarctic Marine Geology Research Facility.

Burton, J.D. 1975. Radioactive nuclides in the marine environment. In: Riley, J.P., Skirrow, G.S. (eds.). Chemical Oceanography. Academic Press, London. 91-191.

Campo, J.M., Wellner, J.S., Domack, E., Lavoie, C. & Yoo, K.C. 2017. Glacial geomorphology of the northwestern Weddell Sea, eastern Antarctic Peninsula continental shelf: Shifting ice flow patterns during deglaciation. Geomorphology 280, 89-107.

Canals, M., Urgeles, R. & Calafat, A.M. 2000. Deep sea-floor evidence of past ice streams off the Antarctic Peninsula. Geology 28, 31-34.

Canals, M., Casamor, J.L., Urgeles, R., Calafat, A.M., Domack, E.W., Baraza, J., Farran, M. & DeBatist, M. 2002. Seafloor evidence of a subglacial sedimentary system off the northern Antarctic Peninsula. Geology 30, 603-604.

Cassidy, D.S. (ed.) 1984. USCGC Glacier: Operations Deep Freeze 1982 and 1983 Sediment Descriptions. Sedimentology Research Laboratory Contribution 52. Tallahassee, FL: Antarctic Marine Geology Research Facility.

Cowan, E.A., Christoffersen, P., Powell, R.D. & Talarico, F.M. 2014. Dynamics of the late Plio-Pleistocene West Antarctic Ice Sheet documented in subglacial diamictites, AND-1B core. Global and Planetary Change 119, 56-70.

Christ, A.J., Talaia-Murray, M., Elking, N., Domack, E.W., Leventer, A., Lavoie, C., Brachfeld, S., Yoo, K., Gilbert, R., Jeong, S., Petrushak, S., Wellner, J. & the LARISSA group: Late Holocene glacial advance and ice shelf growth in Barilari Bay, Graham Land, west Antarctic Peninsula. Geological Society of America Bulletin 127.1-2, 297-315.

Cook, A.J., Fox, A.J., Vaughan, D.G. & Ferrigno, J.G. 2005. Retreating glacier fronts on the Antarctic Peninsula over the past half-century. Science 308, 541-544.

Cook, A.J., Holland, P.R., Meredith, M.P., Murray, T., Luckman, A. & Vaughan, D.G. 2016. Ocean forcing of glacier retreat in the western Antarctic Peninsula. Science 353, 283-286.

Cook, A.J. & Vaughan, D.G. 2010. Overview of areal changes of the ice shelves on the Antarctic Peninsula over the past 50 -years. The Cryosphere 4, 77-98.

Cook, A.J., Vaughan, D.G., Luckman, A.J. & Murray T. 2014. A new Antarctic Peninsula glacier basin inventory and observed area changes since the 1940s. Antarctic Science 26, 614-624.

Domack, E.W. 1990. Laminated terrigenous sediments from the Antarctic Peninsula: the role of subglacial and marine processes. In Dowdeswell, J.A. and Scourse, J.D. (eds.) Glaciomarine environments: processes and sediments, Geological Society Special Publication 53, 91-103.

Domack, E., Amblas, D., Gilbert, R., Brachfeld, S., Camerlenghi, A., Rebesco, M., Canals, M., & Urgeles, R. 2006. Subglacial morphology and glacial evolution of the Palmer deep outlet system, Antarctic Peninsula. Geomorphology 75, 125–142.

Domack, E.W., Burnett, A. & Leventer, A. 2003. Environmental setting of the Antarctic Peninsula. In E. Domack (ed.): Antarctic Peninsula climate variability. Pp. 1-13. Washington, DC: American Geophysical Union.

Domack, E., Duran, D., Leventer, A., Ishman, S., Doane, S., McCallum, S., Amblas, D., Ring, J., Gilbert, R. & Prentice, M. 2005. Stability of the Larsen B ice shelf on the Antartic Peninsula during the Holocene epoch. Nature 436, 681-685.

Domack, E.W., Foss, D.J.P., Syvitski, J.P.M. & McClennen, C.E. 1994. Transport of suspended particulate matter in an Antarctic fjord. Marine Geology 121, 161-170.

Domack, E.W. & Ishman, S. 1993. Oceanographic and physiographic controls on modern sedimentation within Antarctic fjords. Geological Society of America Bulletin 105, 1175-1189.

Domack, E.W., Ishman, S.E., Stein, A.B., McClennen, C.E. & Jull, A.J.T. 1995. Late Holocene advance of the Muller Ice Shelf, Antarctic Peninsula: sedimentological, geochemical, and palaeontological evidence. Antarctic Science 7, 159-170.

Domack, E.W., Jacobson, E.A., Shipp, S. & Anderson, J.B. 1999. Late Pleistocene–Holocene retreat of the West Antarctic Ice-Sheet system in the Ross Sea: part 2—sedimentologic and stratigraphic signature. Geological Society of America Bulletin 111, 1517-1536.

Domack, E.W., Leventer, A., Dunbar, R., Taylor, F., Brachfeld, S., Sjunneskog, C. & ODP Leg 178 Scientific Party. 2001. Chronology of the Palmer Deep site, Antarctic Peninsula: a Holocene palaeoenvironmental reference for the circum-Antarctic. The Holocene 11, 1-9.

Domack, E.W., Leventer, A., Root, S., Ring, J., Williams, E., Carlson, D., Hirshorn, E., Wright, W., Gilbert, R. & Burr, G. 2003. Marine sedimentary record of natural environmental variability and recent warming in the Antarctic Peninsula. In: Domack E. (ed.) Antarctic Peninsula Climate Variability, Antarctic Research Series 79, 205-224.

Domack, E.W. & McClennen, C.E. 1996. Accumulation of glacial marine sediments in fjords of the Antarctic Peninsula and their use as late Holocene paleoenvironmental indicators. In: R.M. Ross et al. (eds.): Foundations for ecological research west of the Antarctic Peninsula. Pp. 135-154. Washington, DC: American Geophysical Union.

Dowdeswell, J.A. & Vasquez, M. 2013. Submarine landforms in the fjords of southern Chile: implications for glacimarine processes and sedimentation in a mild glacier-influenced environment. Quaternary Science Reviews 64, 1-19.

Dowdeswell, J.A., Ó Cofaigh, C. & Pudsey, C.J. 2004. Continental slope morphology and sedimentary processes at the mouth of an Antarctic palaeo-ice stream. Marine Geology 204, 203-214.

Dowdeswell, J.A., Otessen, D., Evans, J., Ó Cofaigh, C. & Anderson, J.B. 2008. Submarine glacial landforms and rates of ice-stream collapse. Geology 36, 819-822.

Dowdeswell, J.A., Hogan, K.A., Evans, J., Noormets, R., Ó Cofaigh, C., & Otessen, D. 2010. Past-ice sheet flow east of Svalbard inferred from streamlined subglacial landforms. Geology 38, 163-166.

Dowdeswell, J.A., Hogan, K.A. & Ó Cofaigh, C. 2016. Submarine glacial-landform distribution across the West Greenland margin: a fjord-shelf-slope transect through the Uummannaq system (70° to 71° N). In: Atlas of Submarine Glacial Landforms: Modern, Quaternary and Ancient, edited by Dowdeswell J.A., Canals, M., Jakobsson, M, Todd, B.J., Dowdeswell, E.K., and Hogan, K.A. Geological Society of London Memoirs 46, 1-4.

Elverhoi, A. 1984. Glacigenic and associated marine sediments in the Weddell Sea, fjords of Spitsbergen, and the Barents Sea: a review. Marine Geology 57, 53-88.

Elverhoi, A., Lonne, O. & Seland, R. 1983. Glaciomarine sedimentation in a modern fjord environment, Spitsbergen. Polar Research 1, 127-149.

Evans, J., Dowdeswell, J.A., & Ó Cofaigh, C. 2004. Late Quaternary submarine bedforms and ice-sheet flow in Gerlache Strait and on the adjacent continental shelf, Antarctic Peninsula. Journal of Quaternary Science 19, 397-407.

Fernandez, R., Anderson J., Bertrand S. & Wellner J. 2011a. Gualas Glacier sedimentary record of climate and environmental change, Golfo Elefantes, western Patagonia (46.5°S). The Holocene 22, 451-463.

Fernandez, R.A., Anderson, J.B., Wellner, J.S. & Hallet, B. 2011b. Timescale dependence of glacial erosion rates: a case study of Marinelli Glacier, Cordillera Darwin, southern Patagonia. Journal of Geophysical Research-Earth Surface 116, F01020. (doi:10.1029/2012JF001685)

Fernandez, R.A., Anderson J.B., Wellner J.S., Minzoni R.L., Halet B. & Smith R.T. 2016. Latitudinal variation in glacial erosion rates from Patagonia and the Antarctic Peninsula (46°S-65°S). Geological Society of America Bulletin 128, 1000-1023.

Folk, R.L. & Ward, W.C. 1957. Brazos River bar: a study in the significance of grain-size parameters. Journal of Sedimentary Petrology 27, 3-26.

Fox, A.J. & Cooper, A.P.R. 1998. Climate-change indicators from archival aerial photography of the Antarctic Peninsula. Annals of Glaciology 27, 636-642.

Fretwell, P., Pritchard, H.D., Vaughan, D.G., Bamber, J.L., Barrand, N.E., Bell, R., Bianchi, C., Bingham, R.G., Blankenship, D.D., Casassa, G., Catania, G., Callens, D., Conway, H., Cook, A.J., Corr, H.F.J., Damaske, D., Damm, V., Ferraccioli, F., Forsberg, R., Fujita, S., Gim, Y., Gogineni, P., Griggs, J.A., Hindmarsh, R.C.A., Holmlund, P., Holt, J.W., Jacobel, R.W., Jenkins, A., Jokat, W., Jordan, T., King, E. C., Kohler, J., Krabill, W., Riger-Kusk, M., Langley, K. A., Leitchenkov, G., Leuschen, C., Luyendyk, B.P., Matsuoka, K., Mouginot, J., Nitsche, F.O., Nogi, Y., Nost, O.A., Popov, S.V., Rignot, E., Rippin, D.M., Rivera, A., Roberts, J., Ross, N., Siegert, M.J., Smith, A.M., Steinhage, D., Studinger, M., Sun, B., Tinto, B.K., Welch,

B.C., Wilson, D., Young, D.A., Xiangbin, C., & Zirizzotti, A. 2013. Bedmap2: improved ice bed, surface and thickness datasets for Antarctica. The Cryosphere 7, 375–393. (doi.org/10.5194/tc-7-375-2013)

Gales, J.A., Larter, R.D., Mitchell, N.C. & Dowdeswell J.A. 2013. Geomorphic signature of Antarctic submarine gullies: implications for continental slope processes. Marine Geology 337, 112-124.

Garcia, M., Dowdeswell, J.A., Noormets, R., Hogan, K.A., Evans, J., Ó Cofaigh, C. & Larter, R.D. 2016. Geomorphology and shallow-acoustic investigation of an Antarctic Peninsula fjord system using high resolution ROV and shipboard geophysical observations: ice dynamics and behaviour since the Last Glacial Maximum. Quaternary Science Reviews 153, 122-138.

Gilbert, R. 1983. Sedimentary processes of Canadian Arctic fjords. Sedimentary Geology 36, 147-175.

Gilbert, R., Nielsen, N., Moller, H., Desloges, J.R. & Rasch, M. 2002. Glaciomarine sedimentation in Kangerdluk (Disko Fjord), West Greenland, in response to a surging glacier. Marine Geology 191, 1-18.

Gille, S.T. 2002. Warming of the Southern Ocean since the 1950s. Science 295, 1275-1277.

González-Ferran, O. 1985. Volcanic and tectonic evolution of the northern Antarctic Peninsula-Late Cenozoic to recent. Tectonophysics 114, 389-409.

Grad, M., Guterch, A., Janik, T. & Sroda, P. Seismic characteristic of the crust in the transition zone from the Pacific Ocean to the northern Antarctic Peninsula, West Antarctica. Royal Society of New Zealand Bulletin 35, 493-498.

Graham, A. G. C. & Smith, J. A. 2012. Palaeoglaciology of the Alexander Island ice cap, western Antarctic Peninsula, reconstructed from marine geophysical and core data, Quaternary Sci. Rev., 35, 63–81.

Graham, A.G.C., Larter, R.D., Gohl, K., Hillenbrand, C.D., Smith, J.A. & Kuhn, G. 2009. Bedform signature of a West Antarctic palaeo-ice stream revels a multi-temporal record of flow and substrate control. Quaternary Science Reviews 28, 2774-2793.

Graham, A.G.C., Kuhn, G., Meisel, O., Hillenbrand, C.D., Hodgson, D.A., Ehrmann, W., Wacker, P., Wintersteller, P., Ferreira, C.D.S., Romer, M., White, D., and Bohrmann, G. 2017. Major advance of South Georgia glaciers during the Antarctic Cold Reversal following extensive sub-Antarctic glaciation. Nature Communications 8, 14798. (doi.org/10.1038/ncomms14798)

Graham, D.J. & Midgley, N.G. 2000. Graphical representation of particle shape using triangular diagrams: an Excel spreadsheet method. Earth Surface Processes and Landforms 25, 1473-1477.

Griffith, T.W. & Anderson, J.B. 1989. Climatic control of sedimentation in bays and fjords of the northern Antarctic Peninsula. Marine Geology 85, 181-204.

Halberstadt, A.R., Simkins, L.M., Greenwood, S.L. & Anderson, J.B. 2016. Past ice-sheet behaviour: retreat scenarios and changing controls on the Ross Sea, Antarctica. The Cryosphere 10, 1003-1020.

Hall, B.L. 2007. Late-Holocene advance of the Collins Ice Cap, King George Island, South Shetland Islands. The Holocene 17, 1253-1258.

Hall, A. & Visbeck, M. 2002. Synchronous variability in the southern hemisphere atmosphere, sea ice, and ocean resulting from the annular mode. Journal of Climate 15, 3043-3057.

Harden, S.L., DeMaster, D.J. & Nittrouer, C.A. 1992. Developing sediment geochronologies for high-latitude continental shelf deposits: a radiochemical approach. Marine Geology 103, 69-97.

Hass, H.C., Kuhn, G., Monien, P., Brumsack, H.J. & Forwick, M. 2010. Climate fluctuations during the past two millennia as recorded in sediments from Maxwell Bay, South Shetland Islands, West Antarctica. In: (eds.) Howe J.A., Austin W.E.N., Forwick M. & Paetsel M. Fjord systems and archives, Geological Society of London 344, 243-260.

Hawkes, D.D. 1981. Tectonic segmentation of the northern Antarctic Peninsula. Geology 9, 220-224.

Hellmer, H.H., Kauker, F., Timmermann, R., Determann, J. & Rae, J. 2012. Twenty-first-century warming of a large Antarctic ice-shelf cavity by a redirected coastal current. Nature 485, 225-228.

Henriet, J.P., Meissner, R., Miler, H. & the GRAPE Team. 1992. Active margin processes along the Antarctic Peninsula. Tectonophysics 201, 229-253.

Heroy, D.C. & Anderson, J.B. 2005. Ice-sheet extent of the Antarctic Peninsula region during the Last Glacial Maximum (LGM) – Insights from glacial geomorphology. Geological Society of America Bulletin 117, 1497-1512.

Heroy, D.C., Sjunneskog, C. & Anderson, J.B. 2008. Holocene climate change in the Bransfield Basin, Antarctic Peninsula: evidence from sediment and diatom analysis. Antarctic Science 20, 69-87.

Hillenbrand, C.D. & Ehrmann, W. 2005. Late Neogene to Quaternary environmental changes in the Antarctic Peninsula region: evidence from drift sediments. Global and Planetary Change 45, 165-191.

Hillenbrand, C.D., Smith, J.A., Hodell, D.A., Greaves, M., Poole, C.R., Kender, S., Williams, M., Andersen, T.J., Jernas, P.E., Elderfield, H., Klages, J.P., Roberts, S.J., Gohl, K., Larter. R.D. & Kuhn, G. 2017. West Antarctic ice sheet retreat driven by Holocene warm water incursions. Nature 547, 43-48.

Hodgson, D.A., Graham, A.G.C., Griffiths, H.J., Roberts, S.J., Ó Cofaigh, C., Bentley, M.J. & Evans, D.J.A. 2014. Glacial history of sub-Antarctic South Georgia based on the submarine geomorphology of its fjords. Quaternary Science Reviews 89, 129-147.

Hovan, S.A. & Janecek, T.R. (eds.) 1994a. Descriptions of sediment recovered by the R/V Polar Duke. Cruise III United States Antarctic Program 1988. Sedimentology Research Laboratory Contribution 59. Tallahassee, FL: Antarctic Marine Geology Research Facility.

Hovan, S.A. & Janecek, T.R. (eds.) 1994b. Descriptions of sediment recovered by the R/V Polar Duke. Cruises II and VII United States Antarctic Program 1990. Sedimentology Research Laboratory Contribution 51. Tallahassee, FL: Antarctic Marine Geology Research Facility.

Howat, I.M. & Domack, E.W. 2003. Reconstructions of western Ross Sea palaeo-ice-stream grounding zones from high-resolution acoustic stratigraphy. Boreas 32, 56–75.

Ishman, S.E. & Domack, E.W. 1994. Oceanographic controls on benthic foraminifers from the Bellingshausen margin of the Antarctic Peninsula. Marine Micropaleontology 24, 119-155.

Isla, E., Masque, P., Palanques, A., Guillen, J., Puig, P. & Sanchez-Cabeza, J.A. 2004. Sedimentation of biogenic constituents during the last century in western Bransfield and Gerlache Straits, Antarctica: a relation to currents, primary production, and sea floor relief. Marine Geology 209, 265-277.

Isla, E., Masque, P., Palanques, A., Sanchez-Cabeza, J.A., Bruach, J.M., Guillen, J. & Puig, P. 2002. Sediment accumulation rates and carbon burial in the bottom sediment in a high-productivity area: Gerlache Strait (Antarctica). Deep-Sea Research Part II 49, 3275-3287.

Jacobs, S.S., Giulivi, C., Dutrieux, P., Rignot, E., Nitsche, F. & Mouginot, J. 2013. Getz Ice Shelf melting response to changes in ocean forcing. Journal of Geophysical Research: Oceans 118, 4152-4168.

Jacobs, S.S., Jenkins, A., Giulivi, C.F. & Dutrieux, P. 2011. Stronger ocean circulation and increased melting under Pine Island Glacier ice shelf. Nature Geoscience 4, 519-523.

Jamieson, S.S.R., Vieli, A., Livingstone, S.J., Ó Cofaigh, C., Stokes, C., Hillenbrand, C.D. & Dowdeswell, J.A. 2012. Ice-stream stability on a reverse bed slope. Nature Geoscience 5, 799-802.

Jenkins, A., Dutrieux, P., Jacobs, S.S., McPhail, S.D., Perret, J.R., Webb, A.T. & White, D. 2010. Observations beneath Pine Island Glacier in West Antarctica and implications for its retreat. Nature Geoscience 3, 468-472.

Jennings, A.E. & Weiner, N.J. 1996. Environmental change in eastern Greenland during the last 1300 years: evidence from foraminifera and lithofacies in Nansen Fjord, 68°N. The Holocene 6, 179-191.

Joughin, I., Howat, I.M., Fahnestock, M., Smith, B., Krabill, W., Alley, R.B., Stern, H. & Truffer, M. 2008. Continued evolution of Jakobshavn Isbrae following its rapid speedup. Journal of Geophysical Research 113, F04006. (doi:10.1029/2008JF001023)

Kennedy, D.S. & Anderson, J.B. 1989. Glacial-marine sedimentation and Quaternary glacial history of Marguerite Bay, Antarctic Peninsula. Quaternary Research 31, 255-276.

King, J.C., Turner, J., Marshall, G.T., Connelley, W.M. & Lachlan-Cope, T.A. 2003. Antarctic Peninsula climate variability and its causes as revealed by analysis of instrumental records. In: (ed.) Domack E., Antarctic Peninsula climate variability. Washington, DC: American Geophysical Union.

Klages, J.P., Kuhn, G., Hillenbrand, C.D., Graham, A.G.C., Smith, J.A., Larter, R.D. & Gohl, K. 2013. First geomorphological record and glacial history of an inter-ice stream ridge on the West Antarctic continental shelf. Quaternary Science Reviews 61, 47-61.

KOPRI. 2014. Annual report of environmental monitoring on human impacts around the King Sejong Station, Antarctica. Korea Polar Research Institute, Incheon, South Korea, Report, No. BSE 413040-1-11.

Kuhn, G., Hillenbrand, C.D., Kasten, S. Smith, J.A., Nitsche, F.O., Frederichs, T., Wiers, S., Ehrmann, W., Klages, J.P., & Mogollon, J.M. 2017. Evidence for a palaeo-

subglacial lake on the Antarctic continental shelf. Nature Communications 8, 15591. (doi.org/10.1038/ncomms15591)

Larter, R.D., Graham, A.G.C., Gohl, K., Kuhn, G., Hillenbrand, C.D., Smith, J.A., Deen, T.J., Livermore, R.A., & Schenke, H.W. 2009. Subglacial bedforms reveal complex basal regime in a zone of paleo-ice stream convergence, Amundsen Sea Embayment, West Antarctica. Geology 37, 411–414.

Lavoie, C., Domack, E.W., Pettit, E.C., Scambos, T.A., Larter, R.D., Schenke, H.W., Yoo, K.C., Gutt, J., Wellner, J., Canals, M., Anderson, J.B. & Amblas, D. 2015. Configuration of the Northern Antarctic Peninsula Ice Sheet at LGM based on a new synthesis of seabed imagery. The Cryosphere 9, 613-629.

Lee, J., Jin, Y.K., Hong, J.K., Yoo, H.J. & Shon, H. 2008. Simulation of a tidewater glacier evolution in Marian Cove, King George Island, Antarctica. Geosciences Journal 12, 33-39.

Leventer, A., Domack, E.W., Ishman, S.E., Brachfeld, S., McClennen, C.E. & Manley, P. 1996. Productivity cycles of 200-300 years in the Antarctic Peninsula region: understanding linkages among the sun, atmosphere, oceans, sea ice, and biota. Geological Society of America Bulletin 108, 1626-1644.

Livingstone, S.J., Ó Cofaigh, C., Stokes, C.R., Hillenbrand, C.D., Vieli, A. & Jamieson, S.S.R. 2013. Glacial geomorphology of Marguerite Bay palaeo-ice stream, western Antarctic Peninsula. Journal of Maps 9, 558-572.

Lowe, A.L. & Anderson, J.B. 2002. Reconstruction of the West Antarctic ice sheet in Pine Island Bay during the Last Glacial Maximum and its subsequent retreat history. Quaternary Science Reviews 21, 1879-1897.

Lubin, D., Wittenmyer, R.A., Bromwich, D.H. & Marshall, G.J. 2008. Antarctic Peninsula mesoscale cyclone variability and climatic impacts influences by the SAM. Geophysical Research Letters 35, L02808. (doi: 10.1029/2007GL032170)

Majewski, W., Wellner, J.S., Szczucinski, W. & Anderson, J.B. 2012 Holocene oceanographic and glacial changes recorded in Maxwell Bay, West Antarctica. Marine Geology 326-328, 67-79.

Marshall, G.J., Orr, A., van Lipzig, N.P.M. & King, J.C. 2006. The impact of a changing southern hemisphere annular mode on Antarctic Peninsula summer temperatures. Journal of Climate 19, 5388-5404.

Martinson, D.G., Stammerjohn, S.E., Iannuzzi, R.A., Smith, R.C. & Vernet, M. 2008. Western Antarctic Peninsula physical oceanography and spatio-temporal variability. Deep-Sea Research Part II 55, 1964-1987.

Meredith, M.P. & King, J.C. 2005. Rapid climate change in the ocean west of the Antarctic Peninsula during the second half of the 20th century. Geophysical Research Letters 32, L19604. (doi: 10.1029/2005GL024042)

Michalchuk, B.R., Anderson, J.B., Wellner, J.S., Manley, P. L., Majewski, W. & Bohaty, S. 2009. Holocene climate and glacial history of the northern Antarctic Peninsula: the marine sedimentary record from a long SHALDRIL core. Quaternary Science Reviews 28, 3049-3065.

Milliken, K.T., Anderson, J.B, Wellner, J.S., Bohaty, S.M. & Manley, P.L. 2009. High resolution Holocene climate record from Maxwell Bay, South Shetland Islands, Antarctica. Geological Society of America Bulletin 121, 1711-1725.

Minzoni, R.T., Anderson, J.B., Fernandez, R. & Wellner, J.S. 2015. Marine record of Holocene climate, ocean, and cryosphere interactions: Herbert Sound, James Ross Island, Antarctica. Quaternary Science Reviews 129, 239-259.

Minzoni, R.T., Majewski, W., Anderson, J.B., Yokoyama, Y., Fernandez, R. & Jakobsson, M. 2017. Oceanographic influences on the stability of the Crosgrove Ice Shelf, Antarctica. The Holocene 27, 1645-1658.

Molnia, B.F. 1983. Subarctic glaciomarine sedimentation: a model. In B.F. Molnia (ed.): Glacial–marine sedimentation. Pp. 95-144. New York: Plenum Press.

Monien, P., Schnetger, B., Brumsack, H.J., Hass, H.C. & Kuhn, G. 2011. A geochemical record of late Holocene palaeoenvironmental changes at King George Island (maritime Antarctica). Antarctic Science 23, 255-267.

Moon, H.W., Wan Hussin, W. M. R., Kim, H.C. & Ahn, I.Y. 2015. The impacts of climate change on Antarctic nearshore mega-epifaunal benthic assemblages in a glacial fjord on King George Island: Responses and implications. Ecological Indicators 57, 280-292.

Morris, E.M. & Vaughan, D.G. 2003. Spatial and temporal variation of surface temperature on the Antarctic Peninsula and the limit of variability of ice shelves. Antarctic Research Series 79, 61-68.

Munoz, Y.P. & Wellner, J.S. 2016. Local controls on sediment accumulation and distribution in a fjord in the West Antarctic Peninsula: implications for palaeoenvironmental interpretations. Polar Research 35, 25284.

Munoz, Y.P. & Wellner, J.S. 2018. Seafloor geomorphology of western Antarctic Peninsula bays: a signature of ice flow behaviour. The Cryosphere, 12, 205-225. (doi.org/10.5194/tc-12-205-2018)

Naish, T., Powell, R., Levy, R., Wilson, G., Scherer, R., Talarico, F., Krissek, L., Niessen, F., Pompilio, M., Wilson, T., Carter, L., DeConto, R., Huybers, P., McKay, R., Pollard, D., Ross, J., Winter, D., Barrett, P., Browne, G., Cody, R., Cowan, E., Crampton, J., Dunbar, G., Dunbar, N., Florindo, F., Gebhardt, C., Graham, I., Hannah, M., Hansaraj, D., Harwood, D., Helling, D., Henrys, S., Hinnov, L., Kuhn, G., Kyle, P., Läufer, A., Maffioli, P., Magens, D., Mandernack, K., McIntosh, W., Millan, C., Morin, R., Ohneiser, C., Paulsen, T., Persico, D., Raine, I., Reed, J., Riesselman, C., Sagnotti, L., Schmitt, D., Sjunneskog, C., Strong, P., Taviani, M., Vogel, S., Wilch, T. & Williams, T. 2013. Obliquity-paced Pliocene West Antarctic ice sheet oscillations. Nature 458, 322-328.

Nitsche, F.O., Gohl, K., Larter, R.D., Hillenbrand, C.D., Kuhn, G., Smith, J.A., Jacobs, S., Anderson, J.B. & Jakobsson, M. 2013. Paleo ice flow and subglacial meltwater dynamics in Pine Island Bay, West Antarctica. The Cryosphere 7, 249-262.

Ó Cofaigh, C. & Dowdeswell, J.A. 2001. Laminated sediments in glacimarine environment: diagnostic criteria for their interpretations. Quaternary Science Reviews 20, 1411-1436.

Ó Cofaigh, C., Pudsey, C.J., Dowdeswell, J.A. & Morris, P. 2002. Evolution of subglacial bedforms along a paleo-ice stream, Antarctic Peninsula continental shelf. Geophysical Research Letters 29, 1199.

Ó Cofaigh, C., Larter, R.D., Dowdeswell, J.D., Hillenbrand, C.D., Pudsey, C.J., Evans, J. & Morris, P. 2005. Flow of the West Antarctic Ice Sheet on the continental margin of the Bellingshausen Sea at the Last Glacial Maximum. Journal of Geophysical Research 110, B11103.

Ó Cofaigh, C., Davies, B.J., Livingstone, S.T., Smith, J.A., Johnson, J.S., Hocking, E.P., Hodgson, D.A., Anderson, J.B., Bentley, M.J., Canals, M., Domack, E., Dowdeswell, J.D., Evans, J., Glasser, N.F., Hillenbrand, C.D., Larter, R.D., Roberts, S.J., & Simms, A. 2014. Reconstruction of ice-sheet changes in the Antarctic Peninsula since the Last Glacial Maximum. Quaternary Science Reviews 100, 87–110.

Oldfield, F. & Appleby, P.G. 1984. A combined radiometric and mineral magnetic approach to recent geochronology in lakes affected by catchment disturbance and sediment redistribution. Chemical Geology 44, 67-83.

O'Neel, S., Pfeffer, W.T., Krimmel, R. & Meier, M. 2005. Evolving force balance a Columbia Glacier, Alaska, during its rapid retreat. Journal of Geophysical Research 110, F03012.

Otessen, D. & Dowdeswell, J.A. 2006. Assemblages of submarine landforms produced by tidewater glaciers in Svalbard. Journal of Geophysical Research 111, F01016.

Otessen, D. & Dowdeswell, J.A. 2009. An inter-ice-stream glaciated margin: Submarine landforms and a geomorphic model based on marine geophysical data from Svalbard. Geological Society of America Bulletin 121, 1647-1665.

Otessen, D., Dowdeswell, J.A. & Rise, L. 2005. Submarine landforms and the reconstruction of fast-flowing ice streams within a large Quaternary ice sheet: The 2500-km-long Norwegian-Svalbard margin (57°-80°N). Geological Society of America Bulletin 117, 1033-1050.

Pereira, T.T.C., Schaefer, C.E.G.R., Ker, J.C., Almeida, C.C., Almeida, I.C.C. & Pereira, A.B. 2013. Genesis, mineralogy and ecological significance of ornithogenic soils from a semi-desert polar landscape at Hope Bay, Antarctic Peninsula. Geoderma 209-210, 98-109.

Powell, R. D. 1981. A model for sedimentation by tidewater glaciers. Annals of Glaciology 2, 129–134.

Powell, R.D. 1984. Glacimarine processes and inductive lithofacies modeling of ice shelf and tidewater glacier sediments based on Quaternaty examples. Marine Geology 57, 1-52.

Powell, R.D. & Domack, E.W. 1995. Modern glaciomarine environments. In J. Menzies (ed.) Modern glacial environments: processes, dynamics, and sediments. Boston, MA: Butterworth-Heinmann.

Powell, R.D. & Molnia, B.F. 1989. Glaciomarine sedimentary processes, facies, and morphology of the southeast Alaska Shelf and fjords. Marine Geology 85, 359-390.

Pritchard, H.D., Ligtenberg, S.R.M., Fricker, H.A., Vaugham, D.G., van den Broeke, M.R. & Padman, L. 2012. Antarctic ice-sheet loss driven by basal melting of ice shelves. Nature 484, 502-505.

Pudsey, C.J., Barker, P.F. & Larter, R.D. 1994. Ice sheet retreat from the Antarctic Peninsula shelf. Continental Shelf Research 14, 1647-1675.

Reimer, P.J., Bard, E. & Bayliss, A. 2013. IntCal13 and MARINE13 radiocarbon age calibration curves 0-50000 years cal BP. Radiocarbon 55, 1869-1887.

Rignot, E., Bamber, J.L., van den Broeke, M.R., Davis, C., Li, Y., van de Berg, W. J. & van Meijgaard, E. 2008. Recent Antarctic ice mass loss from radar interferometry and regional climate modeling. Nature Geoscience 1, 106-110.

Robel, A.A. 2017. Thinning sea ice weakens buttressing force of iceberg melange and promotes calving. Nature Communications 8, 14596.

Ruckamp, M., Braun, M., Suckro, S. & Blindow, N. 2011. Observed glacial changes on the King George Island ice cap, Antarctica, in the last decade. Global and Planetary Change 79, 99-109.

Sanders, C.J., Santos, I.R., Patchineelam, S.R., Schaefer, C. & Silva-Filho, E.V. 2010. Recent 137-Cs deposition in sediments of Admiralty Bay, Antarctica. Journal of Environmental Radioactivity 101, 421-424.

Schaefer, C.E.G.R., Pereira, T.T.C., Almeida, I.C.C., Michel, R.F.M., Correa, G.R., Figueiredo, L.P.S. & Ker, J.C. 2016. Penguin activity modify the thermal regime of active layer in Antarctica: A case study from Hope Bay. Catena 2016.07.021.

Shevenell, A.E., Domack, E.W. & Kernan, M. 1996. Record of Holocene palaeoclimate change along the Antarctic Peninsula: evidence from glacial marine sediments, Lallemand Fjord. In: (eds.) Banks M.R. & Brown M.J. Climatic succession and glacial history of the southern hemisphere over the last five million years. Papers and Proceedings of the Royal Society of Tasmania 130, 55-64.

Shevenell, A.E. & Kennett, J.P. 2002. Antarctic Holocene climate change: A benthic foraminifeal stable isotope record from Palmer Deep. Paleoceanography 17, 1019. (10.1029/2000PA000596)

Skei, J. 1983. Why sedimentologists are interested in fjords. Sedimentary Geology 36, 75-80.

Simms, A.R., Milliken, K.T., Anderson, J.B. & Wellner, J.S. 2011. The marine record of deglaciation of the South Shetland Islands, Antarctica since the Last Glacial Maximum. Quaternary Science Reviews 30, 1583-1601.

Simms, A.R., Ivins, E.R., DeWitt, R., Kouremenos, P. & Simkins, L.M. 2012. Timing of the most recent Neoglacial advance and retreat in the South Shetland Islands, Antarctic Peninsula, insights from raised beaches and Holocene uplift rates. Quaternary Science Reviews 47, 41-55.

Sjunneskog, C. & Taylor, F. 2002. Postglacial marine diatom record of the Palmer Deep, Antarctic Peninsula (ODP Leg 178, Site 1098) 1. Total diatom abundance. Paleoceanography 17. (10.1029/2000PA000563)

Smith, D.A., Hofmann, E.E., Klinck, J.M. & Lascara, C.M. 1999. Hydrography and circulation of the west Antarctic Peninsula continental shelf. Deep-Sea Research Part I 46, 925-949.

Smith, D.A. & Klinck, J.M. 2002. Water properties on the west Antarctic Peninsula continental shelf: a model study of effects of surface fluxes and sea ice. Deep-Sea Research Part II 49, 4863-4886.

Smith, J. N. & Schafer, C.T. 1987. A 20th-century record of climatologically modulated sediment accumulation rates in a Canadian fjord. Quaternary Research 27, 232-247.

Stammerjohn, S.E., Martinson, D.G., Smith, R.C. & Iannuzzi, R.A. 2008. Sea ice in the western Antarctic Peninsula region: spatio-temporal variability from ecological and climate change perspectives. Deep-Sea Research Part II 55, 2041-2058.

Stammerjohn, S., Massom, R., Rind, D. & Martinson, D. 2012. Regions of rapid sea ice change: An inter-hemispheric seasonal comparison. Geophysical Research Letters 39, L06501. (doi:10.1029/2012GL050874)

Stokes, C.R., Tarasov, L., Blomdin, R., Cronin, T.M., Fisher, T.G., Gyllencreutz, R., Hattestrand, C., Heyman, J., Hindmarsh, R.C.A., Hughes, A.L.C., Jakobsson, M., Kirchner, N., Livingstone, S.J., Margold, M., Murton, J.B., Noormets, R., Peltier, W.R., Peteet, D.M., Piper, D.J.W., Preusser, F., Renssen, H., Roberts, D.H., Roche, D.M., Saint-Ange, F., Stroeven, A.P. & Teller, J.T. 2015. On the reconstruction of palaeo-ice sheets: Recent advances and future challenges. Quaternary Science Reviews 125, 15-49.

Syvitski, J.P.M. 1989. On the deposition of sediment within glacier-influenced fjords: oceanographic controls. Marine Geology 85, 301-329.

Syvitski, J.P.M. 1991. Towards an understanding of sediment deposition on glaciated continental shelves. Continental Shelf Research 11, 897-937.

Syvitski, J.P.M., Burrell, D.C. & Skei, J.M. 1987. Fjords: processes and products. Berlin: Springer.

Syvitski, J.P.M. & Murray, J.W. 1981. Particle interaction in fjord suspended sediment. Marine Geology 39, 215-242.

Thomas, E. R., Marshall, G. J., & McConnell, J. R. 2008. A doubling in snow accumulation in the western Antarctic Peninsula since 1850. Geophysical Research Letters 35, L01706. (doi.org/10.1029/2007GL032529)

Thomson, M.R.A., Pankhurst, R.J. & Clarkson, P.D. 1983. The Antarctic Peninsula-A late Mesozoic-Cenozoic Arc (review). In Antarctic Earth Science, R.L. Oliver, P.R. James, and J.B., Jago (eds.) Cambridge University Press, Cambridge, 289-294.

Turner, J., Barrand, N.E., Bracegirdle, T.J., Convey, P., Hodgson, D.A., Jarvis, M., Jenkins, A., Marshall, G., Meredith, M.P., Roscoe, H., Shanklin, J., French, J.,

Goosse, H., Guglielmin, M., Gutt, J., Jacobs, S., Kennicutt, M.C. II, Masson-Delmotte, V., Mayewski, P., Navarro, F., Robinson, S., Scambos, T., Sparrow, M., Summerhayes, C., Speer, K. & Klepikov, A. 2013. Antarctic climate change and the environment: an update. Polar Record 50, 237-259.

Turner, J., Colwell, S.R., Marshall, G.J., Lachlan-Cope, T.A., Carleton, A.M., Jones, P.D., Lagun, V., Reid, P.A. & Iagovkina, S. 2005. Antarctic climate change during the last 50 years. International Journal of Climatology 25, 279-294.

Turner, J., Lachlan-Cope, T., Colwell, S. & Marshall, G.J. 2005. A positive trend in western Antarctic Peninsula precipitation over the last 50 years reflecting regional and Antarctic-wide atmospheric circulation changes. Annals of Glaciology 41, 85-91.

Turner, J., Lu, H., White, I., King, J.C., Phillips, T., Hosking, J.S., Bracegirdle, T.J., Marshall, G.J., Mulvaney, R. & Deb, P. 2016. Absence of 21st century warming on Antarctic Peninsula consistent with natural variability. Nature Letter 535, 411-415.

Vaughan, D.G., Marshall, G.J., Connolley, W.M., Parkinson, C., Mulvaney, R., Hodgson, D.A., King, J.C., Pudsey, C.J. & Turner, J. 2003. Recent rapid regional climate warming on the Antarctic Peninsula. Climatic Change 60, 243-274.

Warner, N.R. & Domack, E.W. 2002. Millennial- to decadal-scale paleoenvironmental change during the Holocene in the Palmer Deep, Antarctica, as recorded by particle size analysis. Paleoceanography 17, article no. 8004, doi: 10.1029/2000PA000602.
Wentworth, C.K. 1922. A scale of grade and class terms for clastic sediments. The Journal of Geology, v. 30, p. 377–392. (doi: 10.1086/622910)

Wellner, J.S., Lowe, A.L., Shipp, S.S. & Anderson, J.B. 2001. Distribution of glacial geomorphic features on the Antarctic continental shelf and correlation with substrate: implications for ice behaviour. Journal of Glaciology 47, 397-411.

Wellner, J.S., Heroy, B.C. & Anderson, J.B. 2006. The death mask of the Antarctic ice sheet: comparison of glacial geomorphic features across the continental shelf. Geomorphology 75, 157–171.

Whillans, I.M. & van deer Veen, C.J. 1997. The role of lateral drag in the dynamics of Ice Stream B Antarctica. Journal of Glaciology 43, 231-237.

Wölfl, A. C., Lim, C.H., Hass, H. C., Lindhorst, S., Tosonotto, G., Lettmann, K. A., Kuhn, G., Wolff, J. O., & Abele, D. 2014. Distribution and characteristics of marine habitats in a subpolar bay based on hydroacoustics and bed shear stress estimates – Potter Cove, King George Island, Antarctica. Geo-Mar. Letters 34, 435– 446. (doi.org/10.1007/s00367-014-0375-1)

Wölfl, A.C., Wittenberg, N., Feldens, P., Hass, H.C., Betzler, C., & Kuhn, G. 2016. Submarine landforms related to glacier retreat in a shallow Antarctic fjord. Antarctic Science 28, 475–486. (doi.org/10.1017/S0954102016000262)

Yoon H.I., Yoo K.C., Park B.K., Kim Y., Khim B.K. & Kang C.Y. 2004. The origin of massive diamicton in Marian and Potter coves, King George Island, West Antarctica. Geosciences Journal 8, 1-10.

APPENDIX A - Supplementary Material for Chapter 2

Surface sediments in Flandres Bay
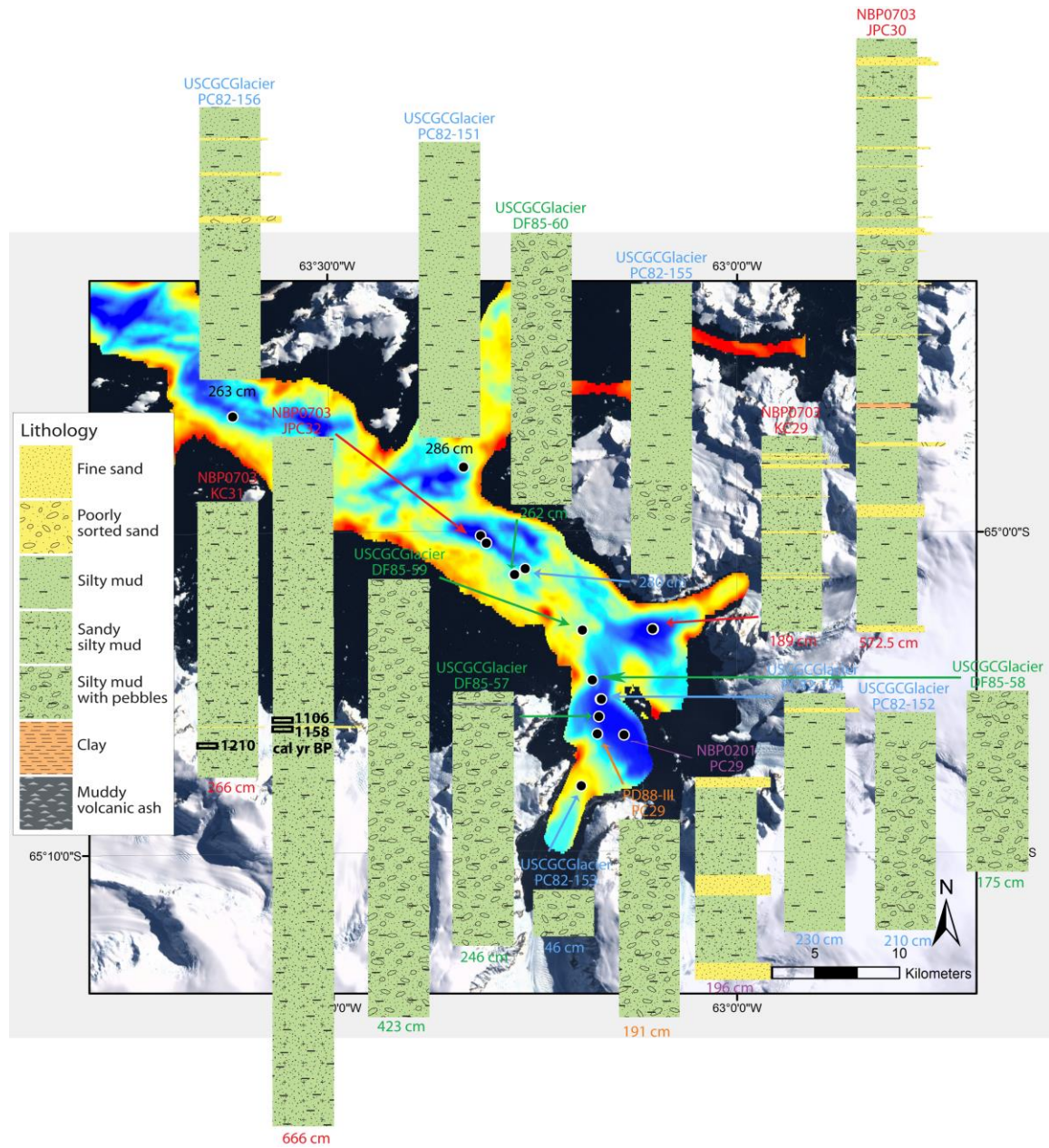
Figure A.1 Cores collected in Flandres Bay, also showing bathymetry (blue- deep, red- shallow), cores NBP0703 KC31, NBP0703 JPC32 have radiocarbon dates (cal. yr B.P.).
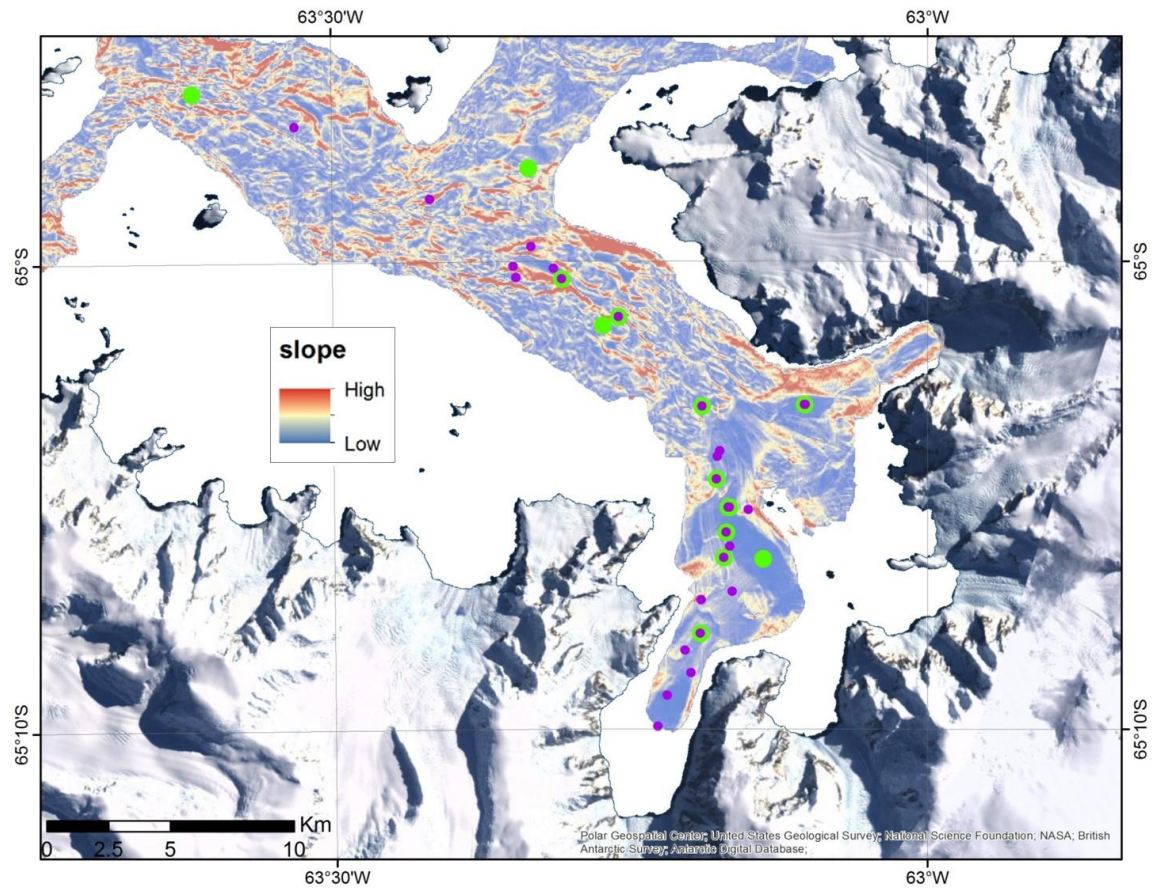
Figure A.2 Slope map Flandres Bay. Purple circles represent grab samples, box cores, kasten cores, or trigger cores. Green circles represent piston cores or jumbo piston cores.
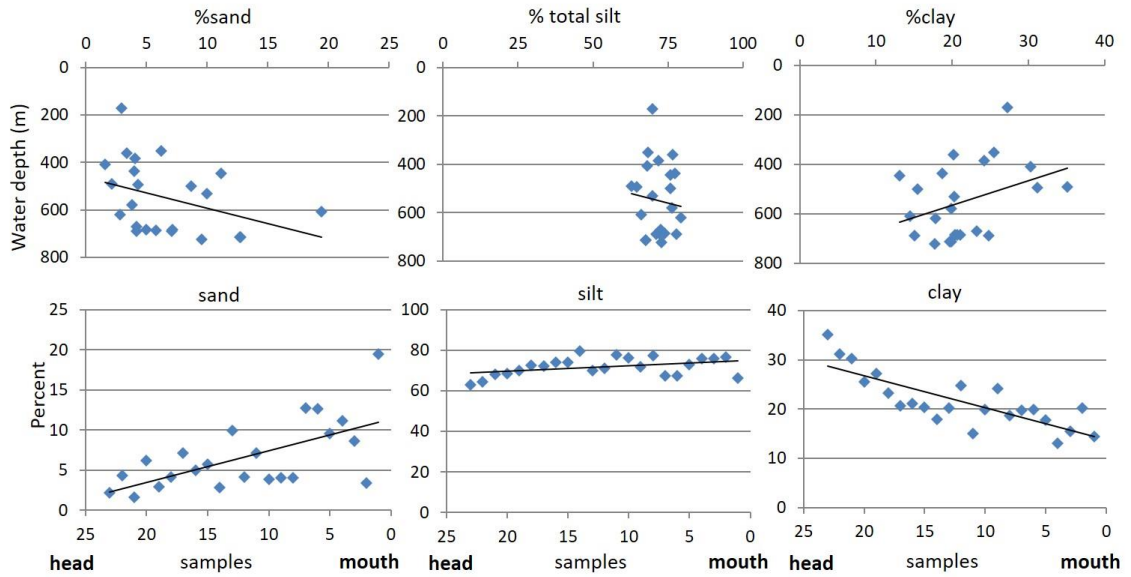
Figure A.3 Grain size as it varies with water depth and distance from head (Etienne Fjord) to mouth (Bismarck Strait). Black line represents trend of data, head: closest to modern glacier front, mouth: furthest from modern glacier front.
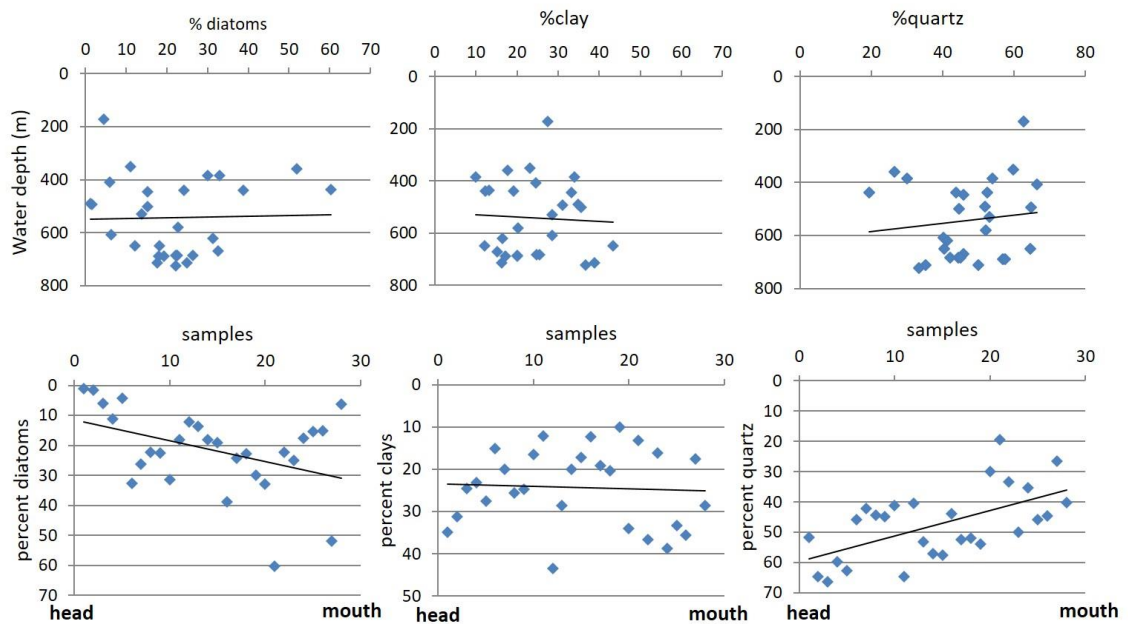
Figure A.4 Lithology as it varies with water depth and distance from head (Etienne Fjord) to mouth (Bismarck Strait). Black line represents trend of data, head: head of the bay, mouth: mouth of the bay.

163
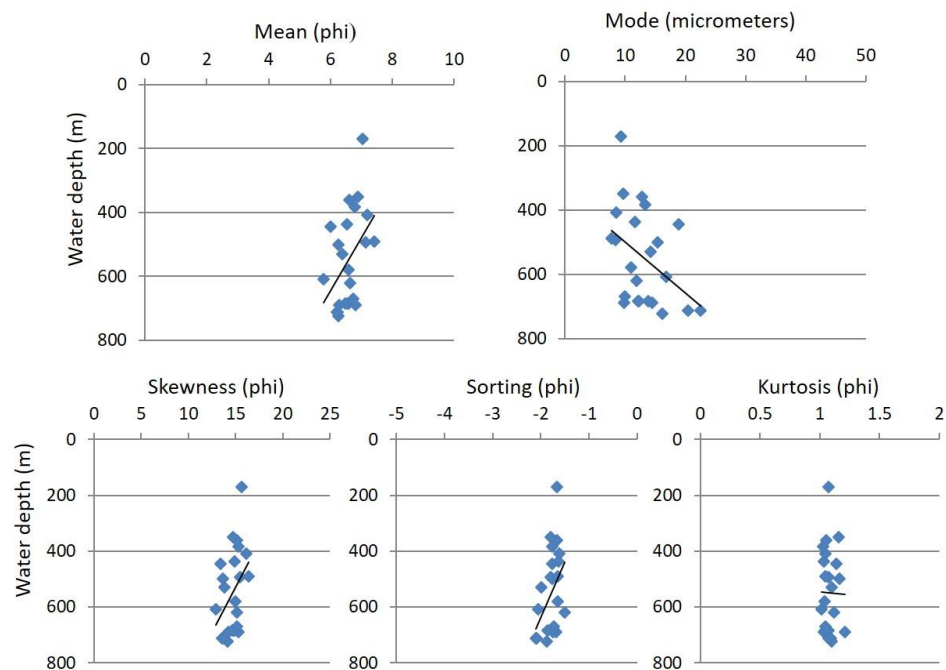
Figure A.5 Grain size calculations compared to water depth. Black line represents trend of data.
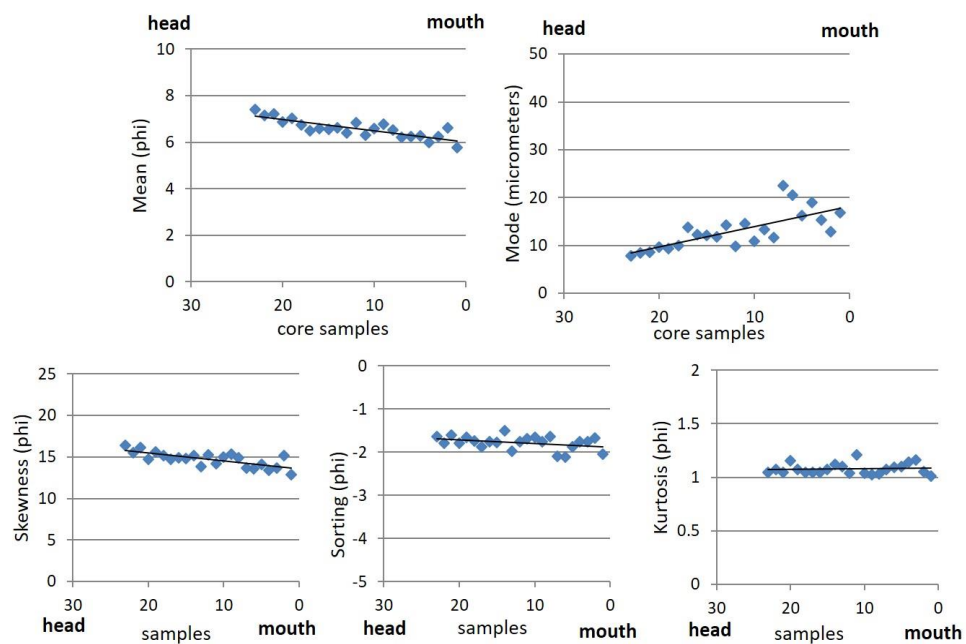
Figure A.6 Grain size calculations compared to distance from head (Etienne Fjord) to mouth (Bismarck Strait). Black line represents trend of data.

APPENDIX B - Supplementary Material for Chapter 3

Geomorphology of western Antarctic Peninsula bays

**Table B.1** Measurements of western Antarctic Peninsula bays. Light grey shows narrow bays, dark grey shows broad and open bays.

Bay Name	Longitude	Latitude	Bay Length (km)	Bay Width (km)	Ratio length/width	Bay Geometry	Number of Glaciers in Total	Total Glacier Catchment Area (km²)	Bay Area (km²)
Maxwell-Marian Cove	-58.769	-62.213	3.8	1.2	3.2	narrow	1	14.99	4.868
Maxwell Bay	-58.848	-62.229	15	10.4	1.4	broad	4	92.14	140.666
Maxwell-Potter Cove	-58.687	-62.232	4.3	1.6	2.7	narrow	1	20.26	7.093
Hope Bay	-57.046	-63.407	5.8	2	2.9	narrow	4	27.36	11.448
Hughes-Cierva Cove	-60.87	-64.155	5	3	1.7	broad	2	256.36	14.056
Hughes-Brialmont Cove	-60.987	-64.281	11	7.5	1.5	broad	5	842.53	85.500
Lapeyrere's unnamed	-63.286	-64.37	4.6	1.8	2.6	narrow	2	60.05	7.959
Lapeyrere Bay	-63.284	-64.421	11	2.6	4.2	narrow	7	271.06	32.496
Fournier Bay	-63.178	-64.546	16	5.3	3.0	narrow	12	169.27	89.906
Charlotte Bay	-61.611	-64.614	15	7.5	2.0	narrow	13	238.14	103.153
Advord Bay	-62.566	-64.857	15	6	2.5	narrow	8	78.83	79.785
Andvord-Moser Gl. cove	-62.425	-64.872	9	3.5	2.6	narrow	6	161.14	26.027
Andvord-Lester Gl. cove	-62.58	-64.901	5	3.8	1.3	broad	2	276.33	16.997
Flandres-Briand Fjord	-63.021	-65.035	4.2	2	2.1	narrow	4	81.26	8.931
Flandres Bay	-63.148	-65.072	30	16	1.9	broad	23	774.64	453.073
Flandres-Etienne Fjord	-63.234	-65.171	8	3.2	2.5	narrow	7	244.5	24.587
Collins Bay	-64.054	-65.346	5.6	9.5	0.6	open	4	614.11	52.430
Beascochea-Lever Gl. cove	-63.723	-65.512	5.3	2.5	2.1	narrow	4	190.72	16.000
Beascochea Bay	-63.87	-65.515	24	10	2.4	narrow	17	155.02	235.377
Beascochea-Funk Gl. cove	-63.756	-65.58	4	2	2.0	narrow	2	157.77	7.874
Beascochea-Cadman Gl. cove	-63.812	-65.612	3	3	1.0	broad	1	307.04	8.915

Table B.2 Seafloor features mapped in western Antarctic Peninsula bays. Light grey shows narrow bays, dark grey shows broad and open bays.

| Bay name	crevasse squeeze ridges	moraines	GZW	lineations	drumlins	crag-and-tails	streamlined features	meltwater channels	gullies	basins	total features per bay
Maxwell-Marian cove	0	6	0	8	0	0	0	2	0	3	19
Maxwell Bay	0	0	0	0	0	0	15	6	30	2	53
Maxwell-Potter cove	14	8	0	0	0	0	0	1	0	1	24
Hope Bay	18	12	1	0	0	0	0	4	0	3	38
Hughes-Cierva cove	0	0	2	12	0	0	0	6	0	1	21
Hughes-Brialmont cove	0	0	0	3	0	9	0	20	0	4	36
Lapeyrere's unnamed	0	0	1	0	0	0	0	3	10	1	15
Lapeyrere Bay	0	0	1	8	0	0	3	20	60	2	94
Fournier Bay	0	0	1	30	0	0	0	14	0	1	46
Charlotte Bay	0	0	2	0	0	0	12	22	0	2	38
Andvord Bay	0	0	0	8	4	12	0	25	0	1	50
Andvord-Moser Gl. cove	0	0	3	4	0	0	0	5	0	1	13
Andvord-Lester Gl. cove	0	0	0	0	0	5	0	4	0	1	10
Flandres-Briand fjord	0	0	2	3	0	0	0	1	10	1	17
Flandres Bay	0	0	0	14	0	17	12	42	20	6	111
Flandres-Etienne fjord	0	0	1	0	0	0	0	4	10	1	16
Collins Bay	0	0	0	0	0	6	0	16	0	3	25
Beascochea-Lever Gl. cove	0	0	2	28	0	0	0	0	0	1	31
Beascochea Bay	0	0	1	4	6	13	26	44	30	8	132
Beascochea-Funk Gl. cove	0	0	1	17	0	0	0	30	0	1	49
Beascochea-Cadman Gl. cove	0	0	1	0	0	0	0	0	20	1	22
total features per type:	32	26	19	139	10	62	68	269	190	45	860
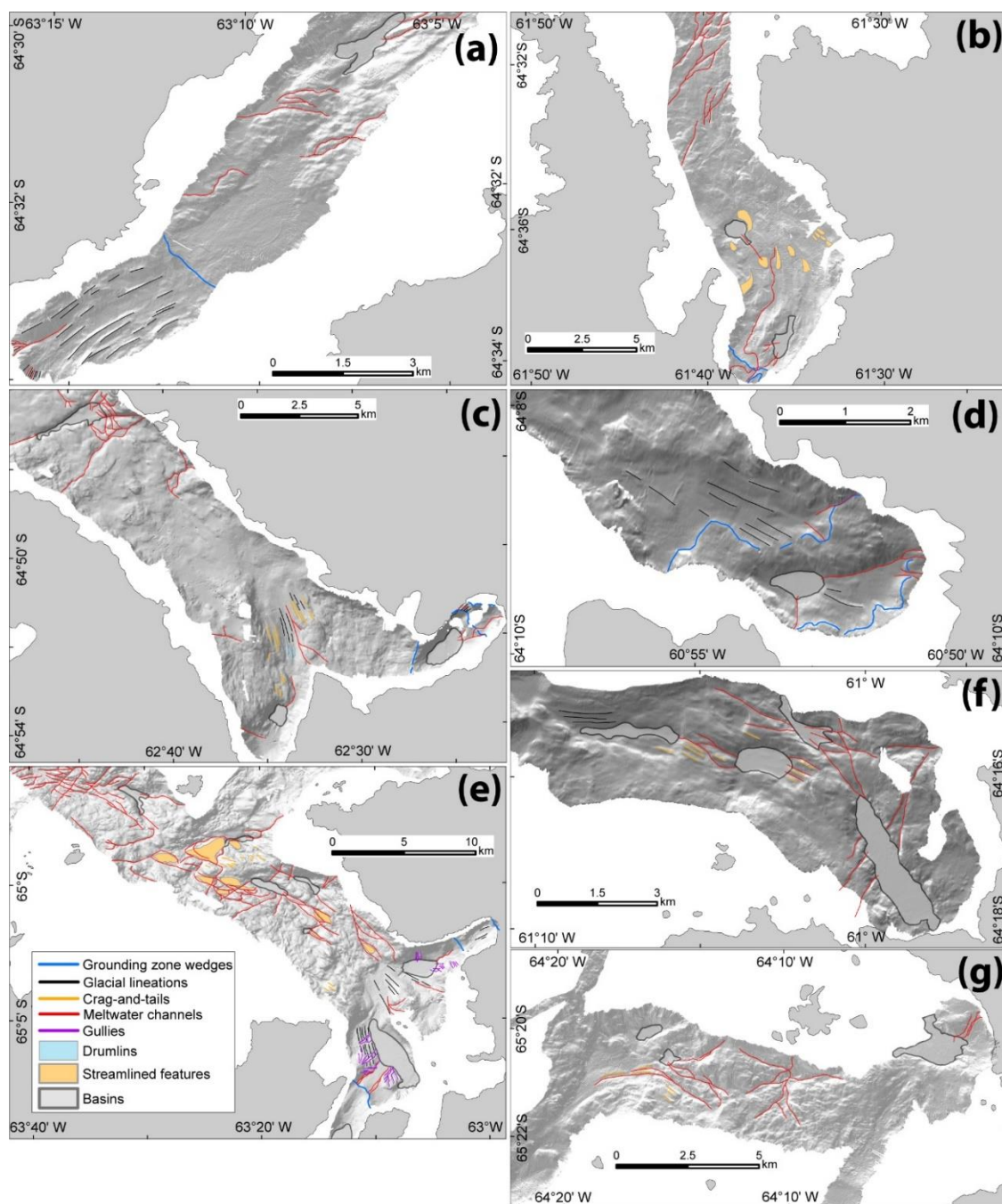
Figure B.1 Interpretation of geomorphic features with hillshade as background in western Antarctic Peninsula bays: (a) Fournier Bay, (b) Charlotte Bay, (c) Andvord Bay, (d) Cierva Cove, (e) Flandres Bay, (f) Brialmont Cove, and (g) Collins Bay. Multibeam data shown in Figures B.2-B.7.
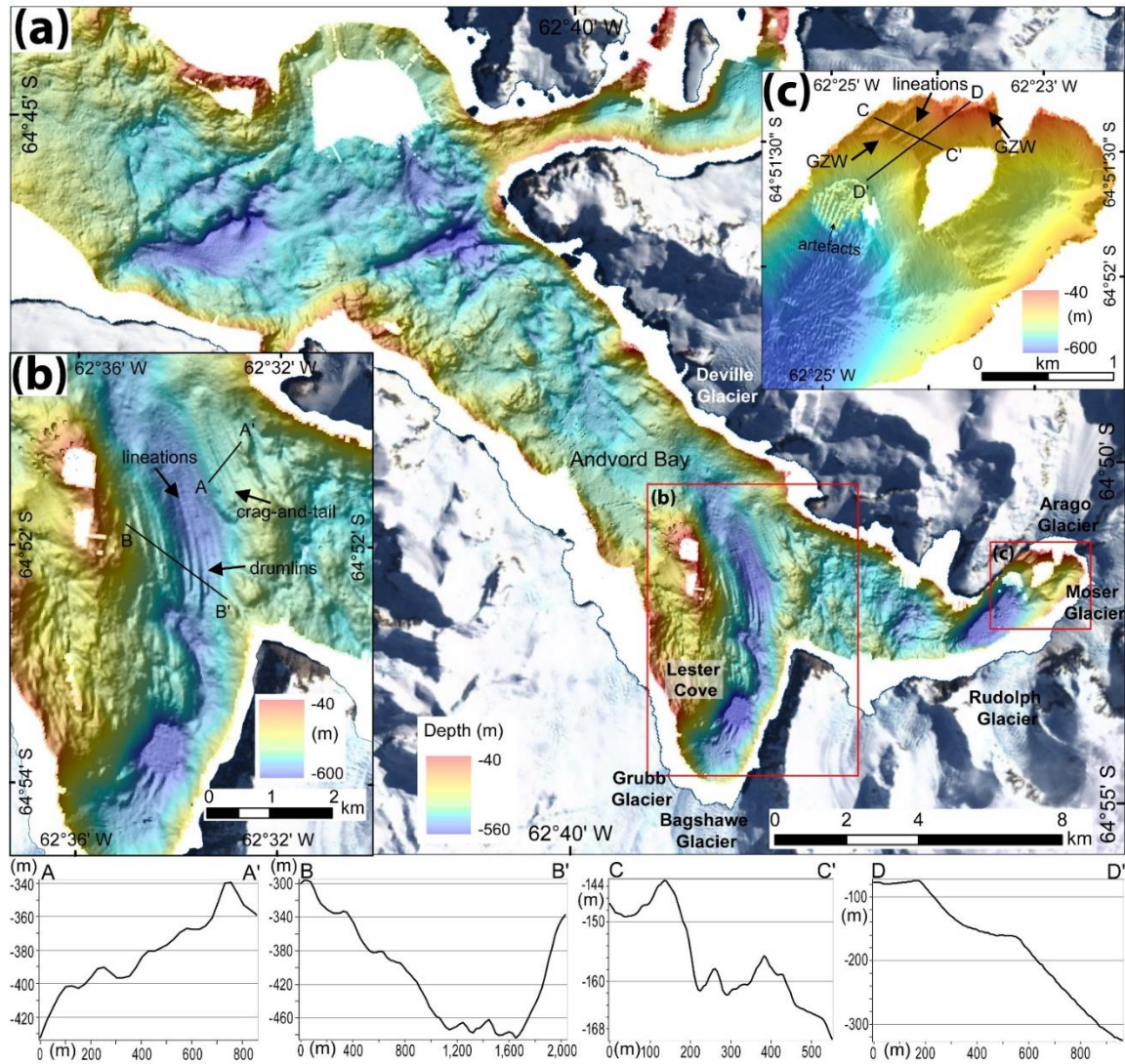
166
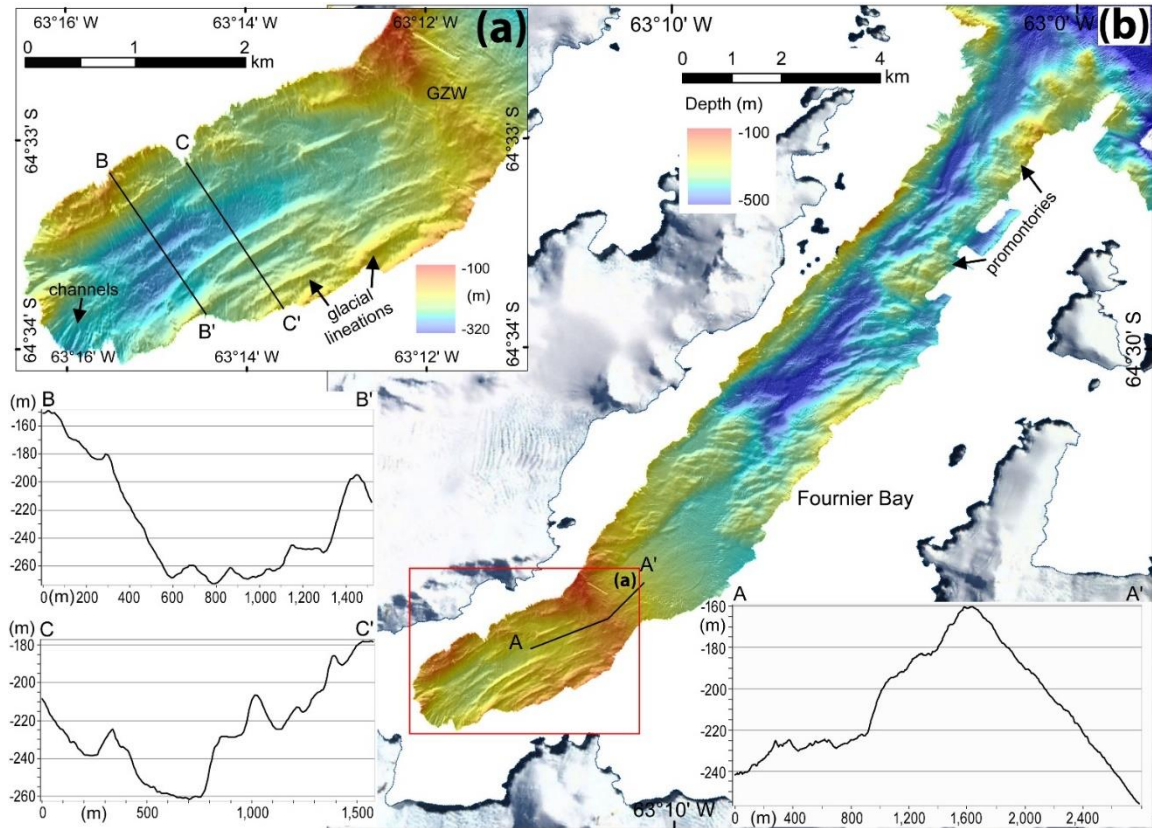
Figure B.2 Multibeam bathymetry map of Fournier Bay. Vertical exaggeration is 5x in (a) and 3x in (b). Interpretation of seafloor features in Figure B.1.
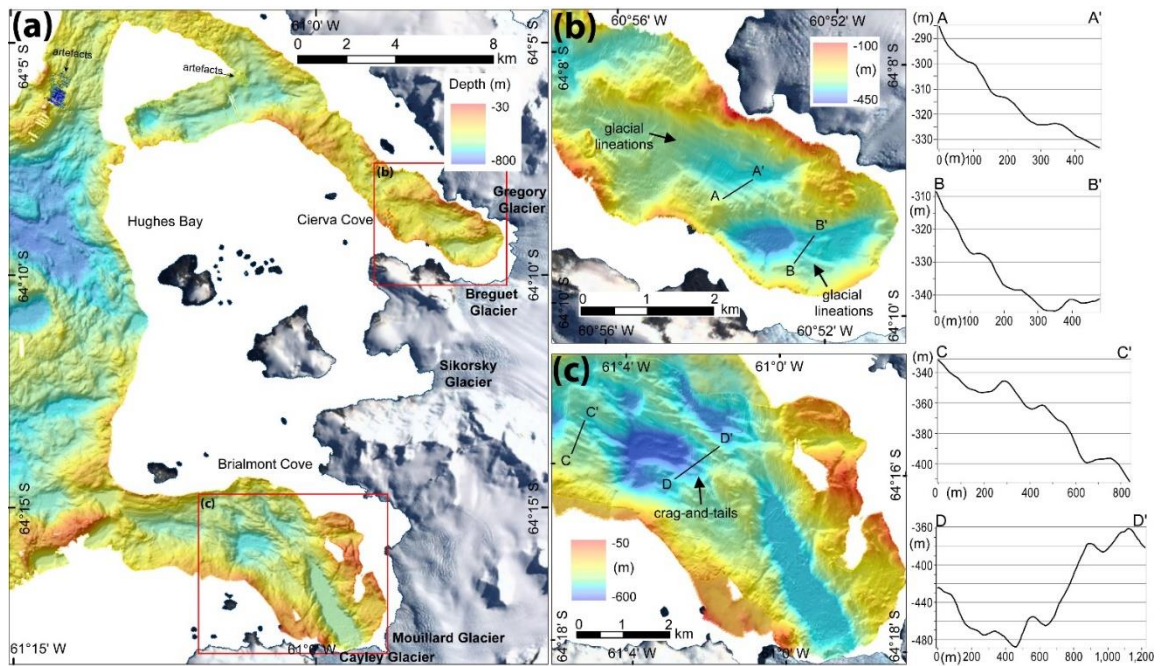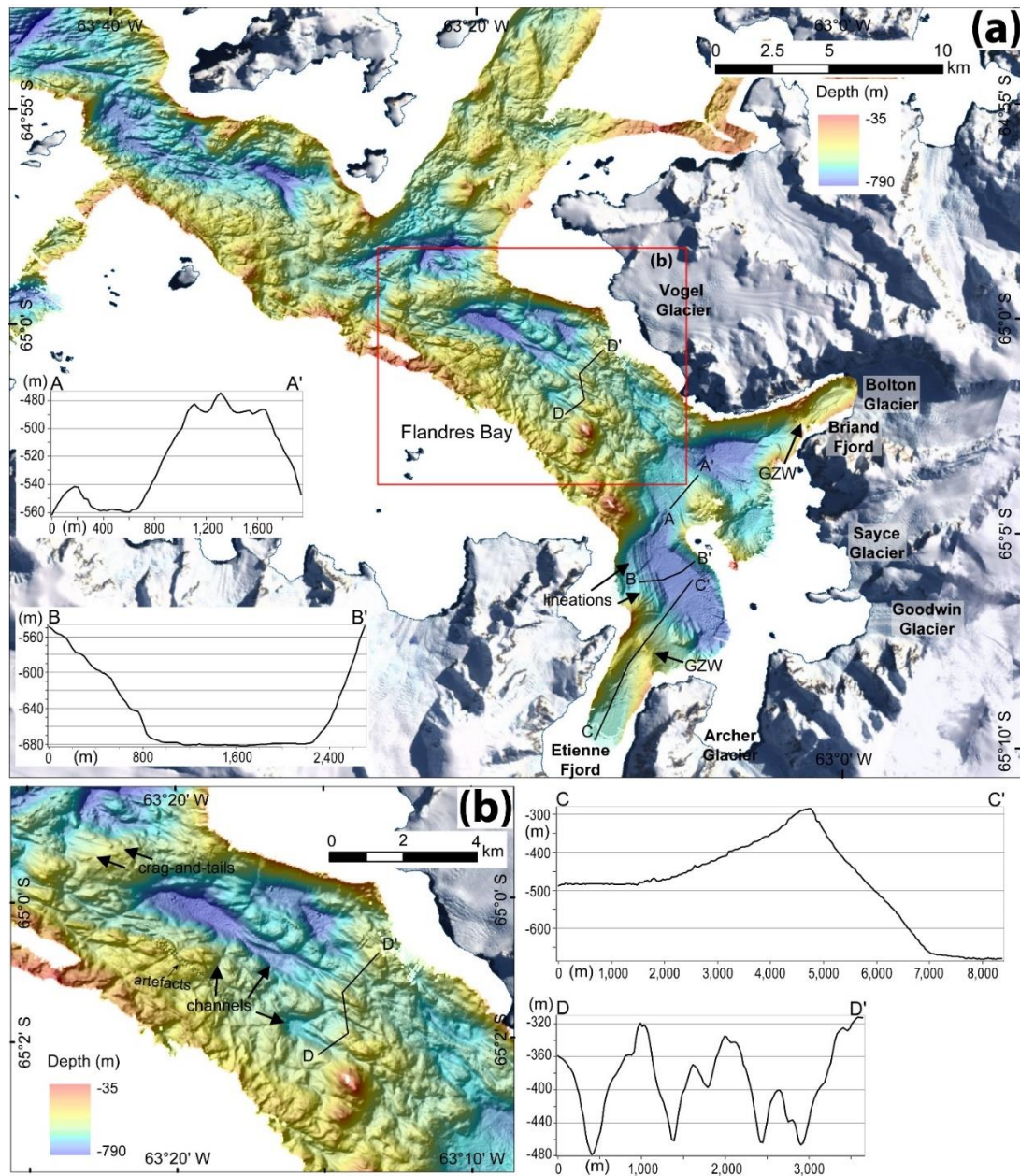
167
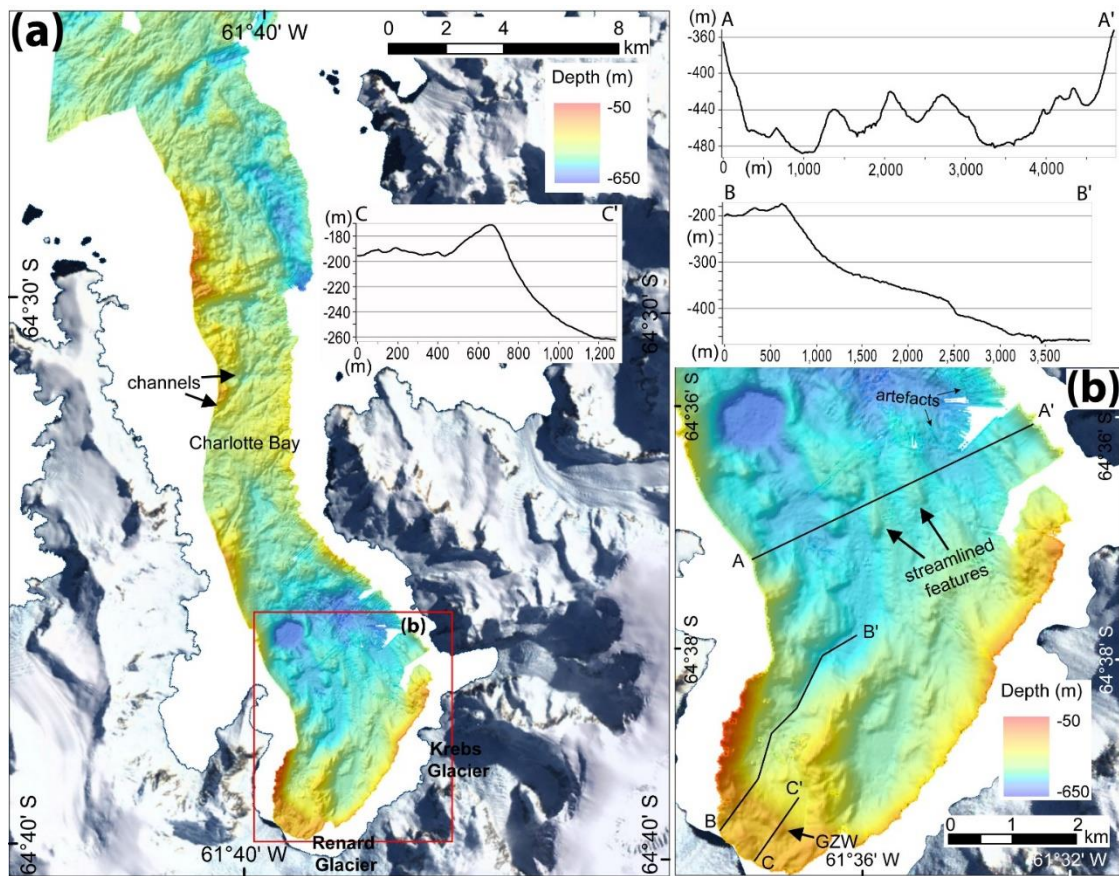
Figure B.3 Multibeam bathymetry map of Charlotte Bay. Vertical exaggeration is 5x in (a) and (b). Interpretation of seafloor features in Figure B.1.

Figure B.4 Multibeam bathymetry map of (a) Andvord Bay, (b) Lester Cove, and (c) Moser Glacier Cove. Vertical exaggeration is 5x in all images. Interpretation of seafloor features in Figure B.1.

Figure B.5 Multibeam bathymetry map of Hughes Bay, (b) Cierva Cove, and (c) Brialmont Cove. Vertical exaggeration is 3x in (a), and 5x in (b) and (c). Interpretation of seafloor features in Figure B.1.

170

Figure B.6 Multibeam bathymetry map of Flandres Bay, Briand Fjord, and Etienne Fjord. Vertical exaggeration is 5x in (a) and (b). Interpretation of seafloor features in Figure B.1.
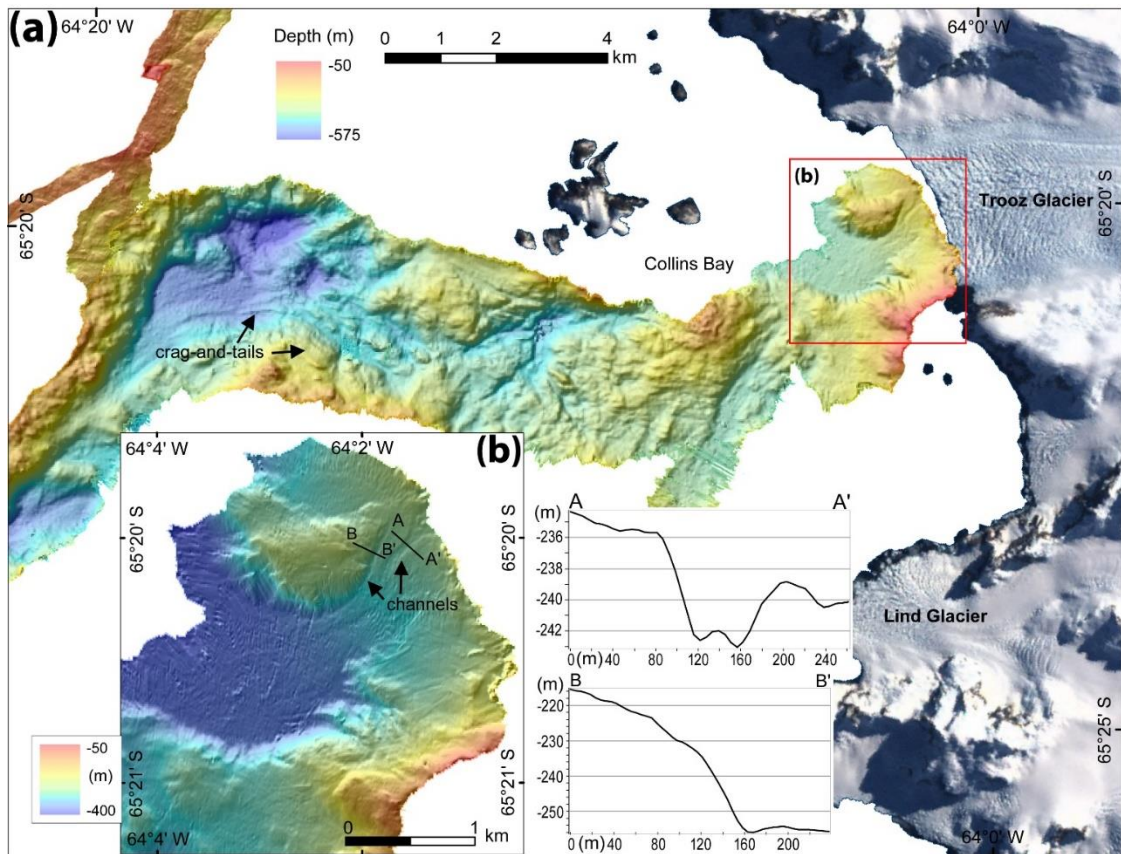
Figure B.7 Multibeam bathymetry map of Collins Bay. Vertical exaggeration is 3x in (a) and 2x in (b). Interpretation of seafloor features in Figure B.1.

APPENDIX C - Supplementary Material for Chapter 4

Sediment cores from Flandres, Collins, and Beascochea bays
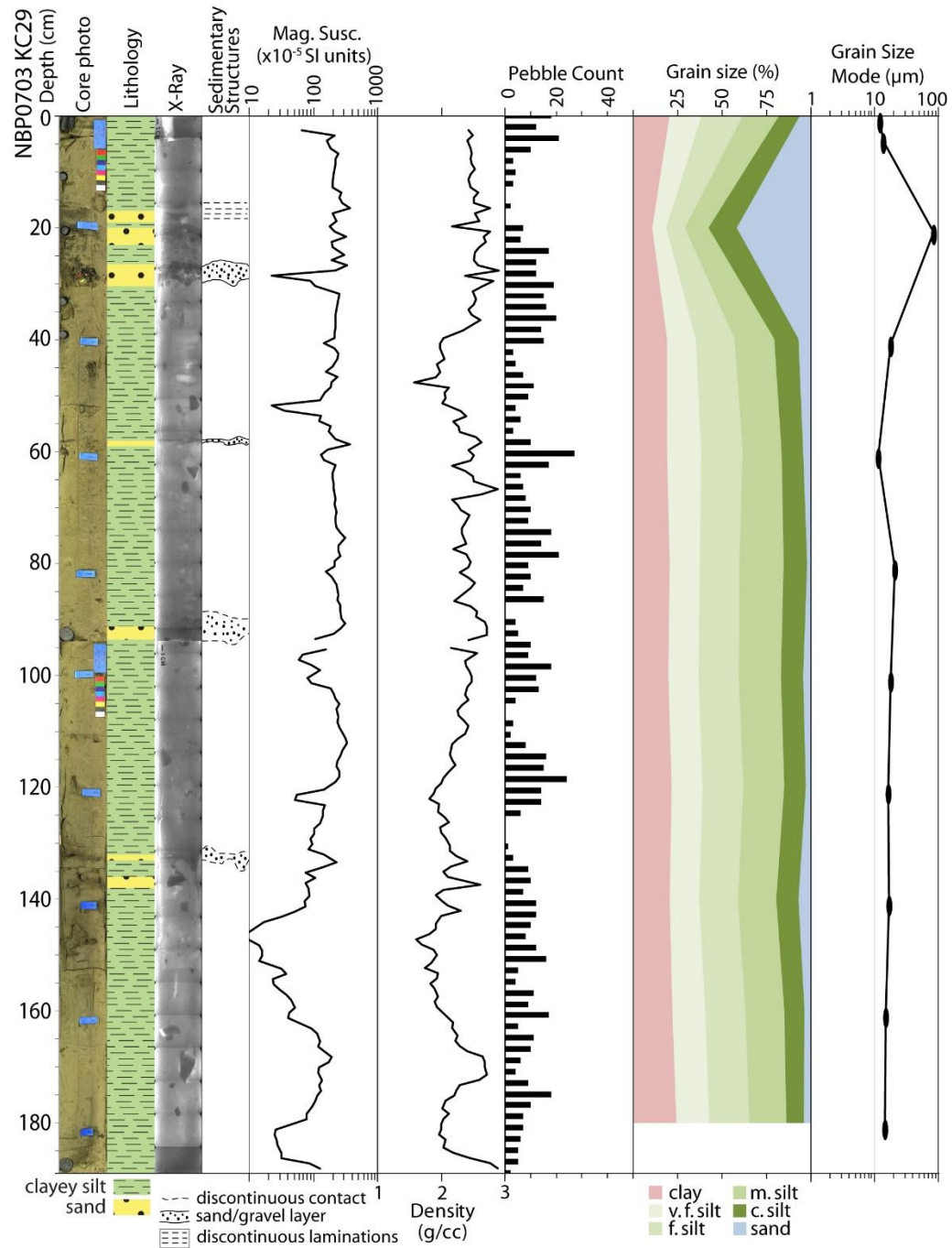
Figure C.1 Core NBP0703 KC29 from inner Flandres Bay. Location of core found in Figure 4.2.
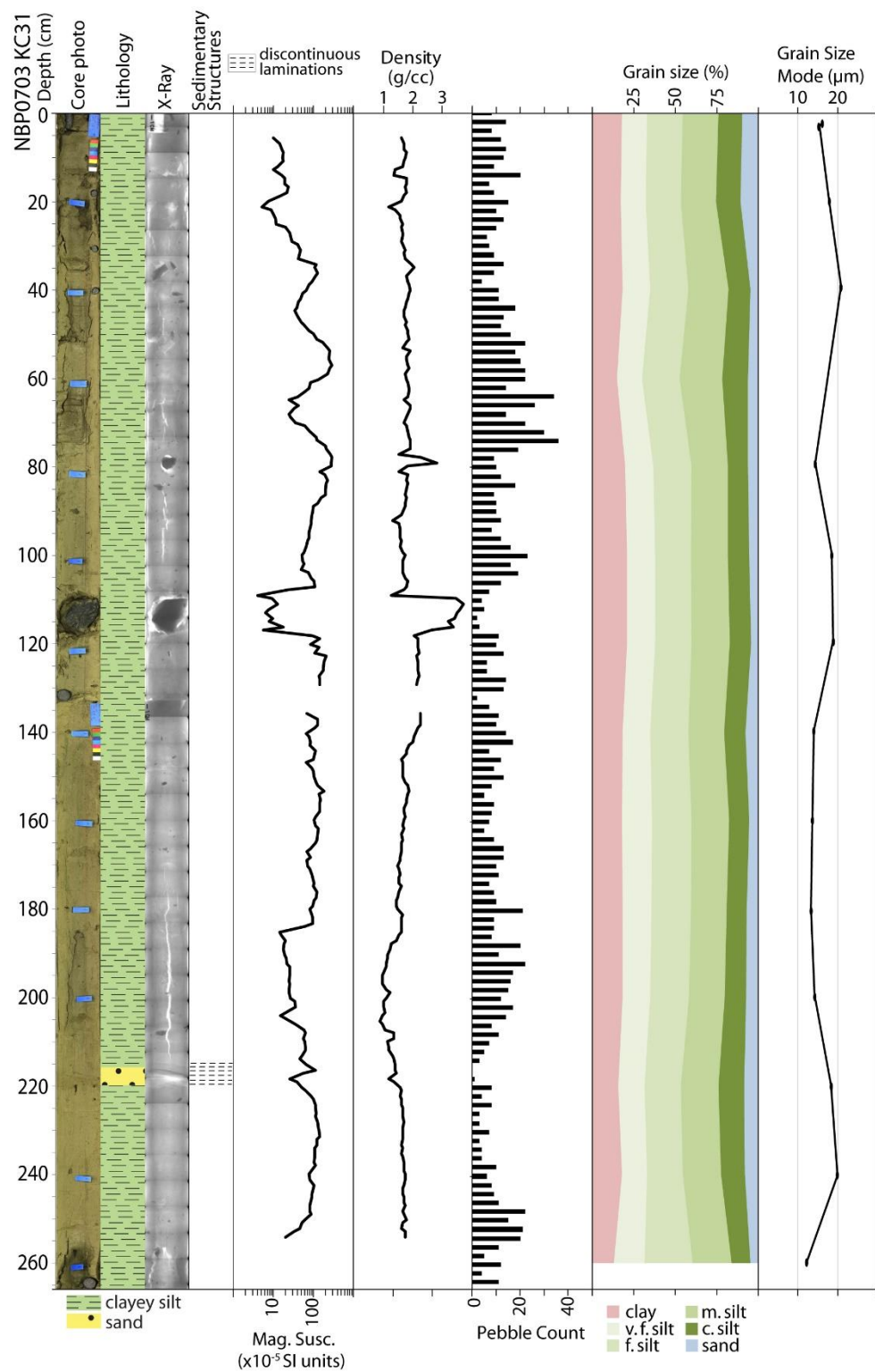
Figure C.2 Core NBP0703 KC31 from outer Flandres Bay. Location of core found in Figure 4.2.
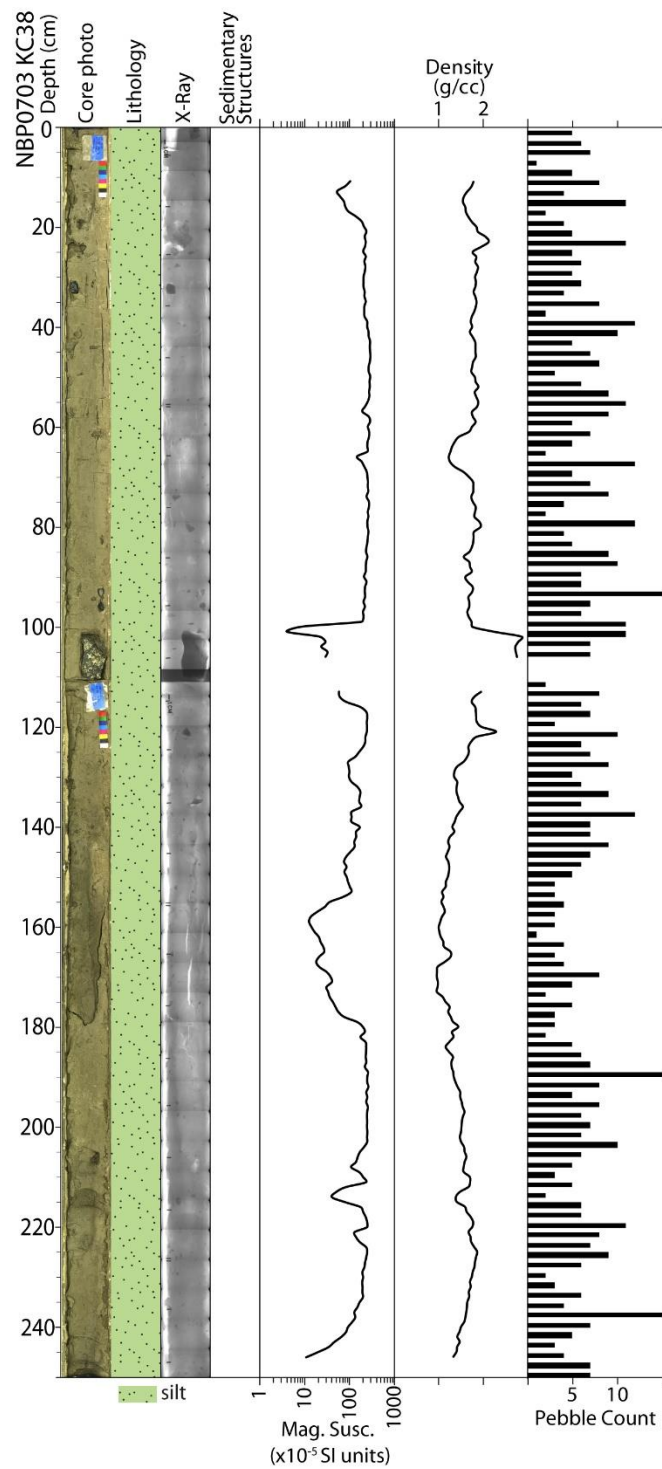
Figure C.3 Core NBP0703 KC38 from outer Collins Bay. No sedimentary structures found in KC38. Location of core found in Figure 4.3.
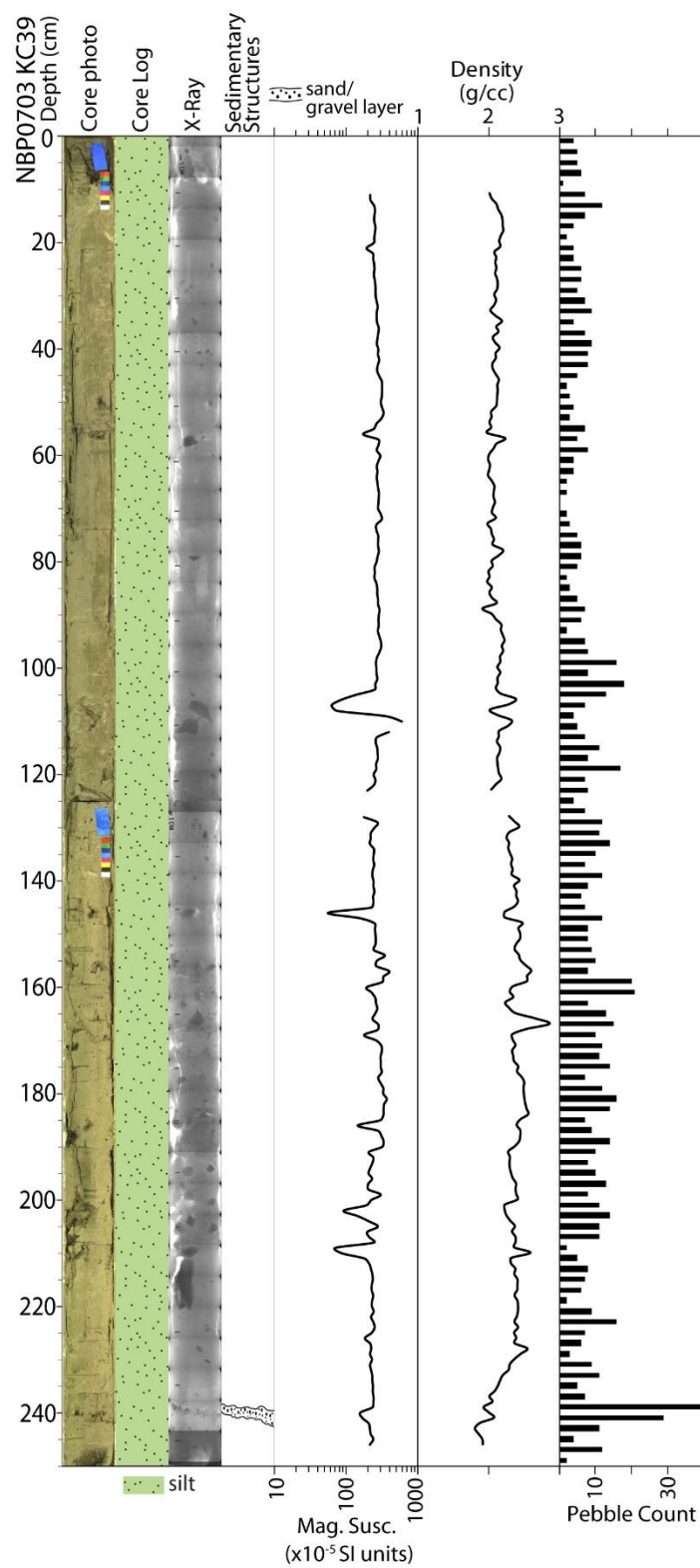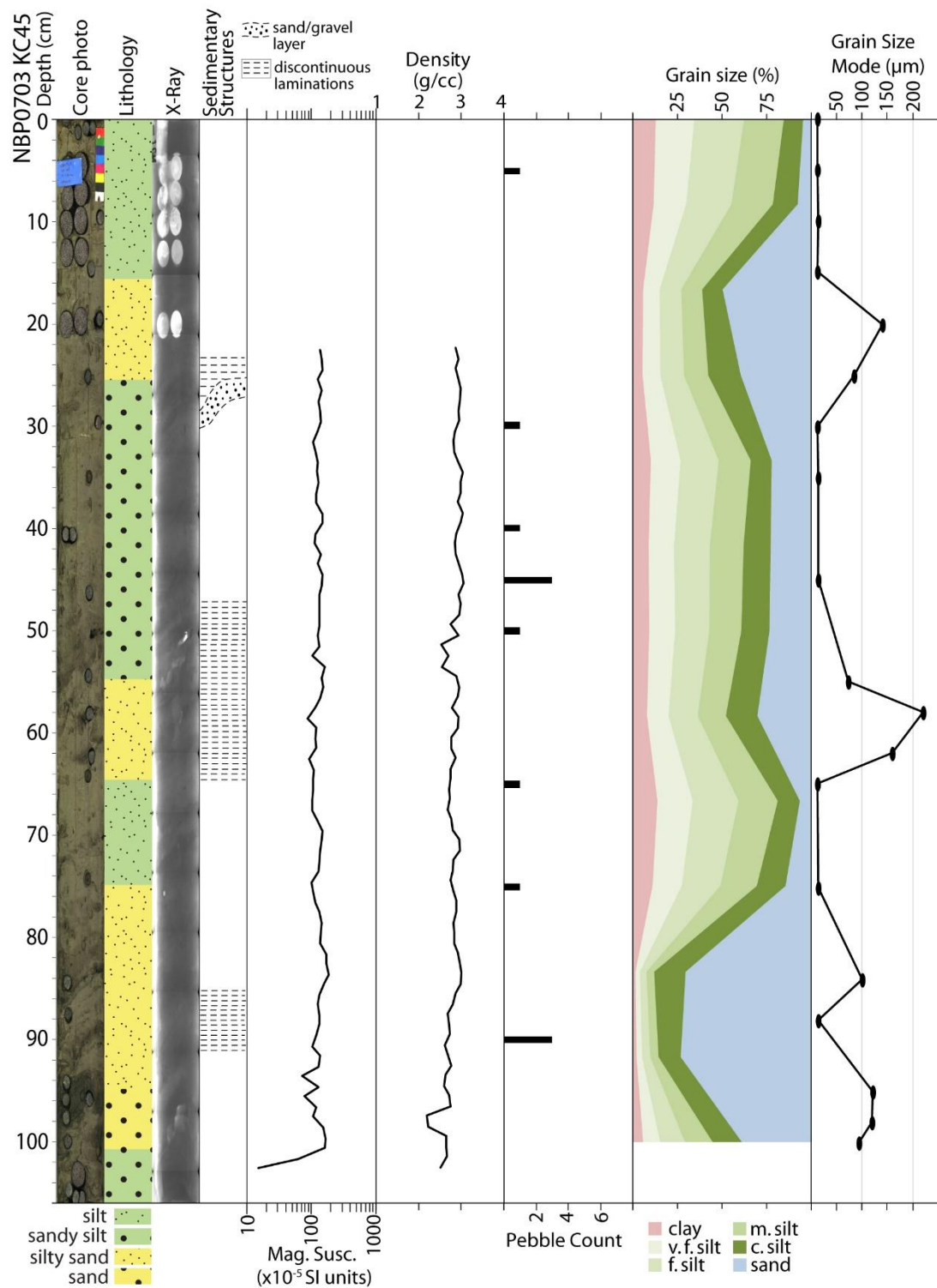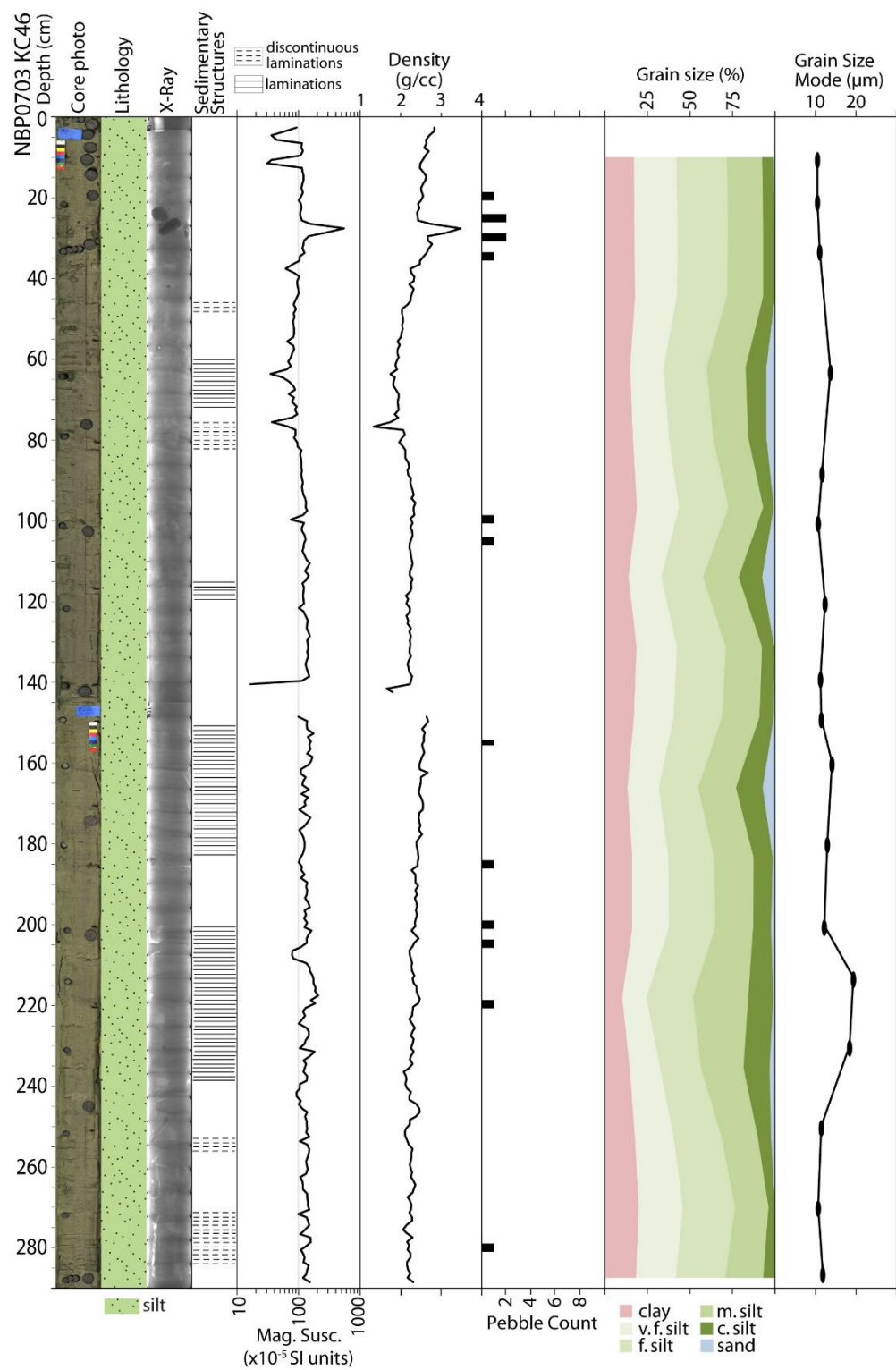
Figure C.4 Core NBP0703 KC39 from outer Collins Bay. Location of core found in Figure 4.3.
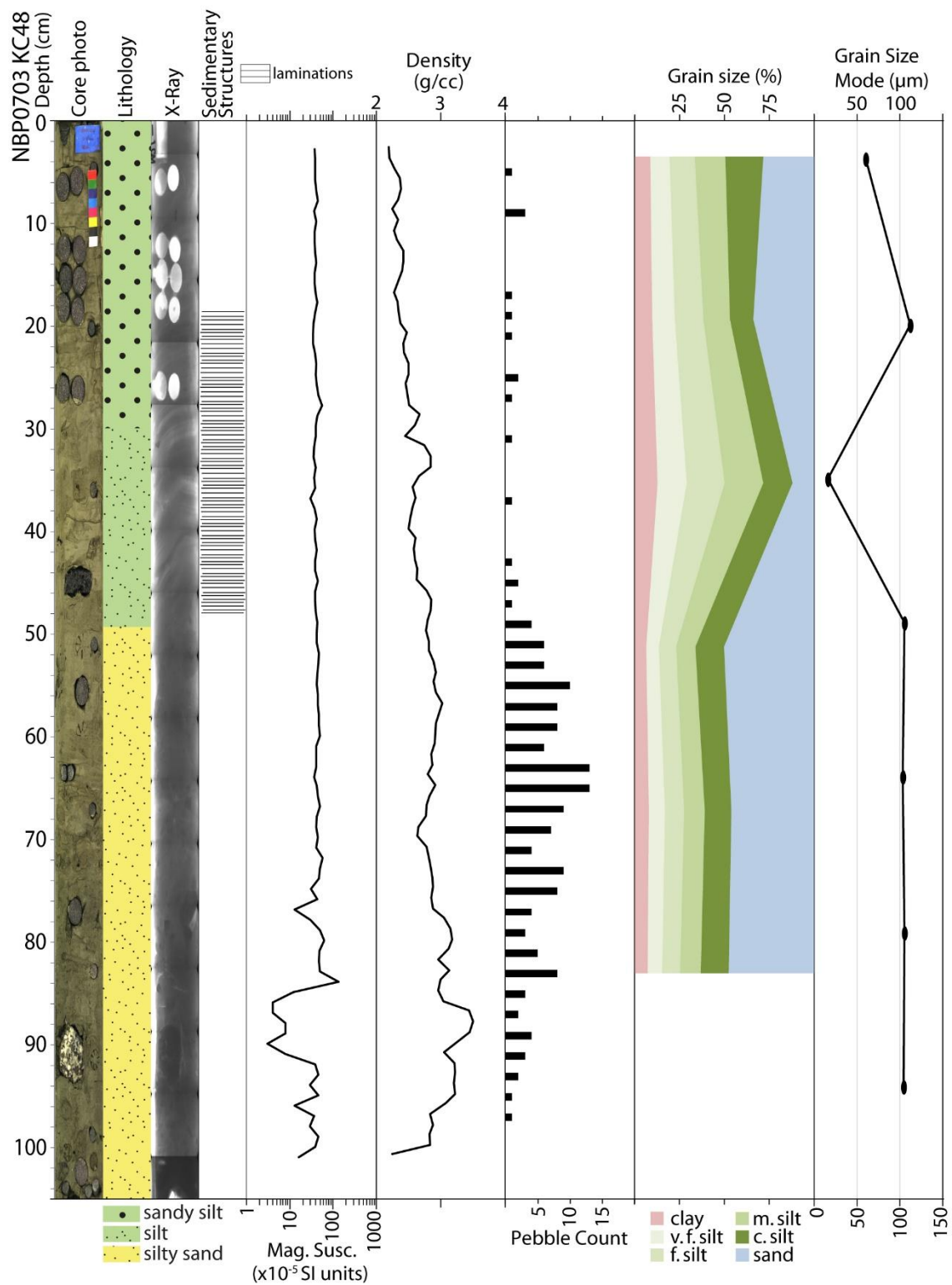
176
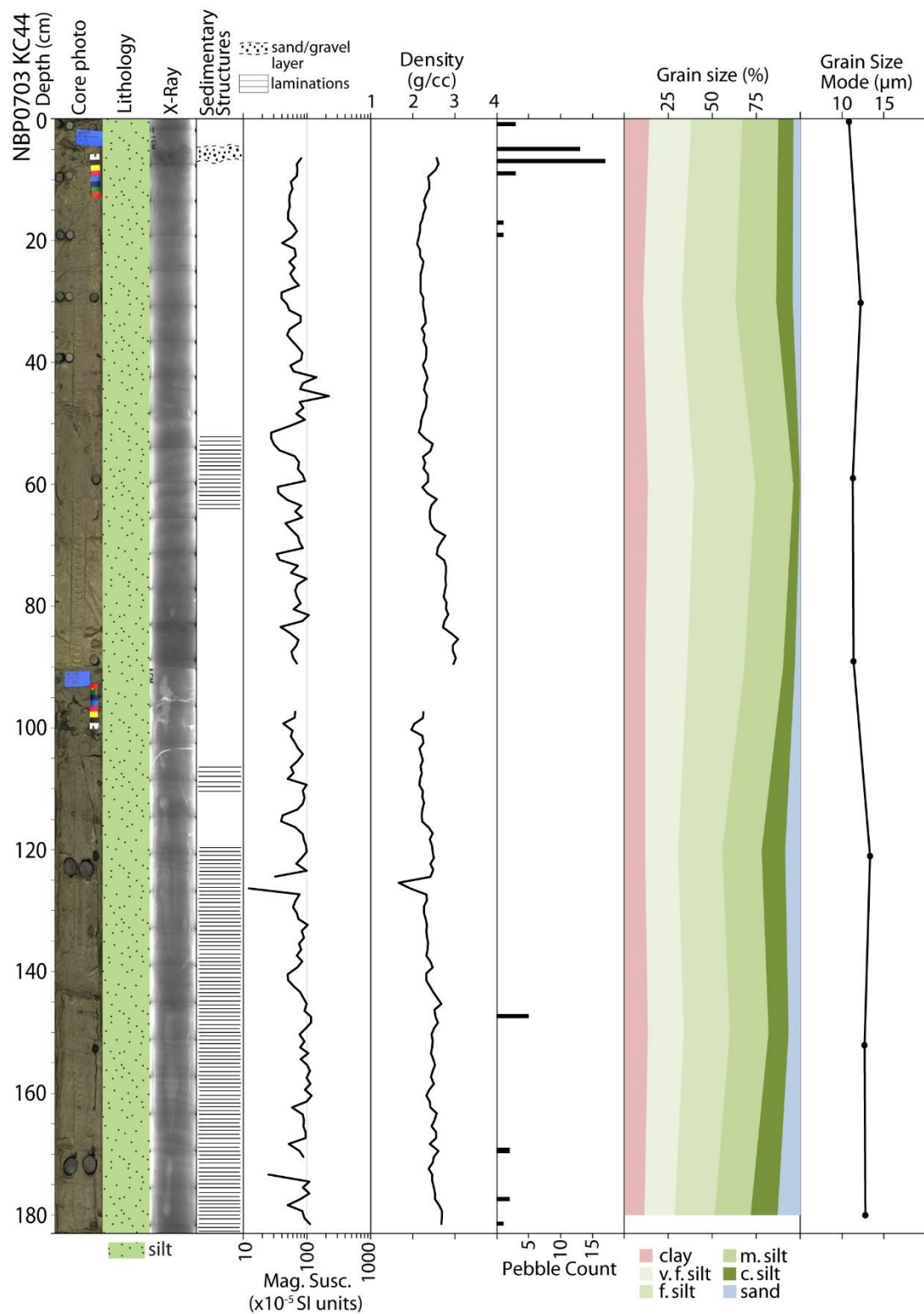
Figure C.5 Core NBP0703 KC44 from inner Beascochea Bay. Location of core found in Figure 4.3.
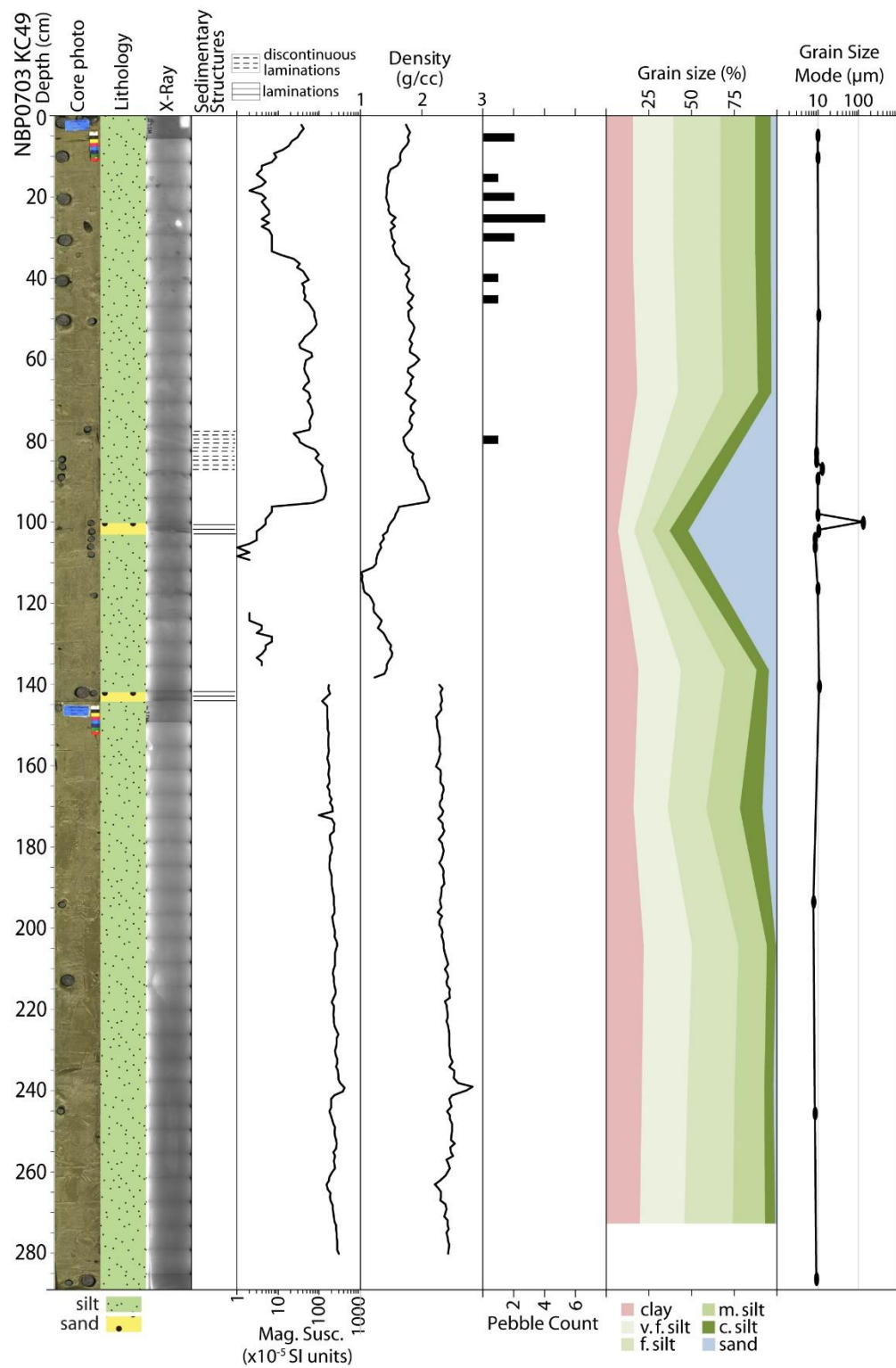
Figure C.6 Core NBP0703 KC45 from inner Beascochea Bay. Location of core found in Figure 4.3.

Figure C.7 Core NBP0703 KC46 from the middle are of Beascochea Bay. Location of core found in Figure 4.3.

Figure C.8 Core NBP0703 KC48 from inner Beascochea Bay. Location of core found in Figure 4.3.

Figure C.9 Core NBP0703 KC48 from outer Beascochea Bay. Location of core found in Figure 4.3.